THE MODIFICATION OF BIO-BASED POLYESTERS WITH ADDTITIVES BY MEANS OF SOLUTION CASTING AND EXTRUSION

by

APISATA HOLT

(Under the Direction of Jason Locklin)

ABSTRACT

Recently, the development of bio-based polymers has attracted considerable attention, due to their composability or biological degradability. In this study, poly(lactic acid) (PLA) and poly(hydroxyalkanoate) (PHA) were modified with three functional additives for improving their thermal, mechanical, and rheological properties for industrial application. A plasticizer, a processing aid, and a nucleating agent used as additives were blended with PLA or PHA in various concentrations using a solution casting technique or a melt blending process. Poly(butylene glutarate) (PBG) was explored due to its potential to be used as a plasticizer and processing aid for PLA and PHA, respectively. The nucleation effect of poly(3-hydroxybutyrate) (PHB) was investigated on PHA. Differential scanning calorimetry (DSC), tensile testing, dynamic mechanical analysis (DMA), and melt flow index (MFI) were used to determined thermal, mechanical, and rheological properties of these blends. Atomic force microscopy (AFM), scanning electron microscope (SEM), and polarized optical microscope (POM) were used to determine the morphology of the blends. The rates of composting biodegradation for the selected blends were evaluated in a respirometer under aerobic conditions at 58 °C. The results suggested that

PBG is a useful plasticizer for PLA and an effective processing aid for PHA. PBG improved the % elongation at break and accelerated the rate of degradation of PLA. Besides the melt fracture on the surface of extruded PHA can be eliminated by adding PBG to the blend in a commercial extruder. It was found that PHB is an effective nucleating agent for PHA, and since PHB is a biologically degradable material, blending of PHB with PHA is still route to an environmentally friendly product.

INDEX WORDS: Poly(lactic acid), Poly(hydroxyalkanoates), Poly(butylene glutarate), Plasticizer, Processing aid, Nucleating Agent, Composting Biodegradable

THE MODIFICATION OF BIO-BASED POLYESTERS WITH ADDTITIVES BY MEANS OF SOLUTION CASTING AND EXTRUSION

by

APISATA HOLT

BS, Kasetsart University, Thailand, 2003

Ph.D., Kasetsart University, Thailand, 2009

A Dissertation Submitted to the Graduate Faculty of The University of Georgia in Partial Fulfillment of the Requirements for the Degree

DOCTOR OF PHILOSOPHY

ATHENS, GEORGIA

2021

THE MODIFICATION OF BIO-BASED POLYESTERS WITH ADDTITIVES BY MEANS OF SOLUTION CASTING AND EXTRUSION

by

APISATA HOLT

Major Professor:	Jason Locklin
Committee:	I. Jonathan Amster
	Jin Xie

Electronic Version Approved:

Ron Walcott
Dean of the Graduate School
The University of Georgia
May 2021

DEDICATION

This dissertation is dedicated to my family for their unconditional love throughout my life. Thank you for believing, understanding, and being patient with me in this journey.

ACKNOWLEDGEMENTS

This journey would not have been possible without the support of my mentors, friends, and family. First, I would like to thank Dr. Jon Amster who introduced me to the graduate school and gave me many opportunities to be a part of the UGA chemistry department. Also, Dr. Jeffrey Urbauer who helped me with the graduate school application. Thank you, Dr. Jin Xie, for introducing me to nanobiotechnology. You expand my understanding about medical perspectives and inspire me to envision what could be possible in the future. Next, I would like to thank my PI, Dr. Jason Locklin for allowing me to be a part of his lab as a graduate student. I thank you for your time, support, and for all of the opportunities I was given during this journey. You are my role model for hard work and demonstrating dedication to research. Your advice and mentorship have shaped and inspired me to be a better scholar and chemist. In addition, I would like to thank Dr. Daniel Carraway, the RWDC team, and the New Material Institute team for the many opportunities to collaborate on such interesting and impactful projects.

To my lab mates, I would like to thank all my friends in Locklin' s lab, Danimer's lab, Riverbend's lab, and the Chemistry department's lab. Thank you for sharing your knowledge, techniques, and UGA's state-of-the-art equipment. You are wonderful people, and I am lucky to know you all.

Finally, my biggest thanks to my husband for all the support you have shown me. Thanks for being persistent and so patience with me. I am looking forward to spending more time with you after my graduation.

TABLE OF CONTENTS

Page

LIST OF TABLES

Page

LIST OF FIGURES

Page

LIST OF SCHEMES

Page

CHAPTER 1

INTRODUCTION AND LITERATURE REVIEW

Introduction of Bio-based Aliphatic Polyesters

Plastics are widely used and an important part of everyday life. Conventional production of plastics worldwide consumes over 250 million metric tons of fossil fuels each year.[1] These petroleum-derived plastics have high carbon footprint and take a long time to degrade. The increasing accumulation of plastic wastes in the environment lead to imbalanced and damaged ecological system adversely affects wildlife and humans. A great number of bio-based polymers have been developed due to the desire and need to replace fossil fuel-based polymers. Bio-based polymers have a smaller carbon footprint and play significant role to reduce carbon dioxide emission because they derive from renewable biological resources such as starch, cellulose, and lignin.

Recently, the development of bio-based aliphatic polyesters has attracted considerable attention due to their degradability.[2-4] Bio-based aliphatic polyesters can be classified based on their synthesis process. This chapter discusses the bio-based aliphatic polyesters that synthesized from the monomers that obtained from renewable resources such as poly(lactic acid) (PLA), and the polyesters that produced by microorganism through fermentation process such as poly(hydroxyalkanoates) (PHAs). Figure 1.1 shows the structures of these polyesters.

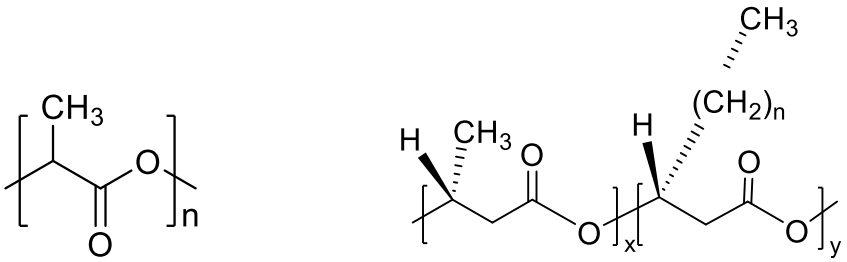

Poly(lactic acid), PLA Poly(hydroxyalkanoate), PHA

Figure 1.1 General structures of aliphatic polyesters

Poly(lactic acid), PLA

The synthetic routes to obtain PLA are performed by direct condensation polymerization of lactic acid or ring opening polymerization of lactide. The polycondensation does not provide sufficiently high molecular weight due to the negatively influences of esterification equilibrium reaction and the difficulty in removing water as byproducts. Therefore, common pathway to obtain high molecular weight is through ring opening polymerization.[5] Two isomers of lactic acid, L (+) and D (-) can be derived from the fermentation of renewable agricultural sources. These two lactic acids also can convert to lactide, a cyclic dimer, by removing water under mild conditions and without solvent.[6] With different content of the two isomers, several distinct forms of PLA can be PDLA, PLLA and PDLLA. Scheme 1.1 shows polymerization of PLA from L-lactic acid and D-lactic acid.

Scheme 1.1 Polymerization scheme of PLA from L-lactic acid and D-lactic acid.

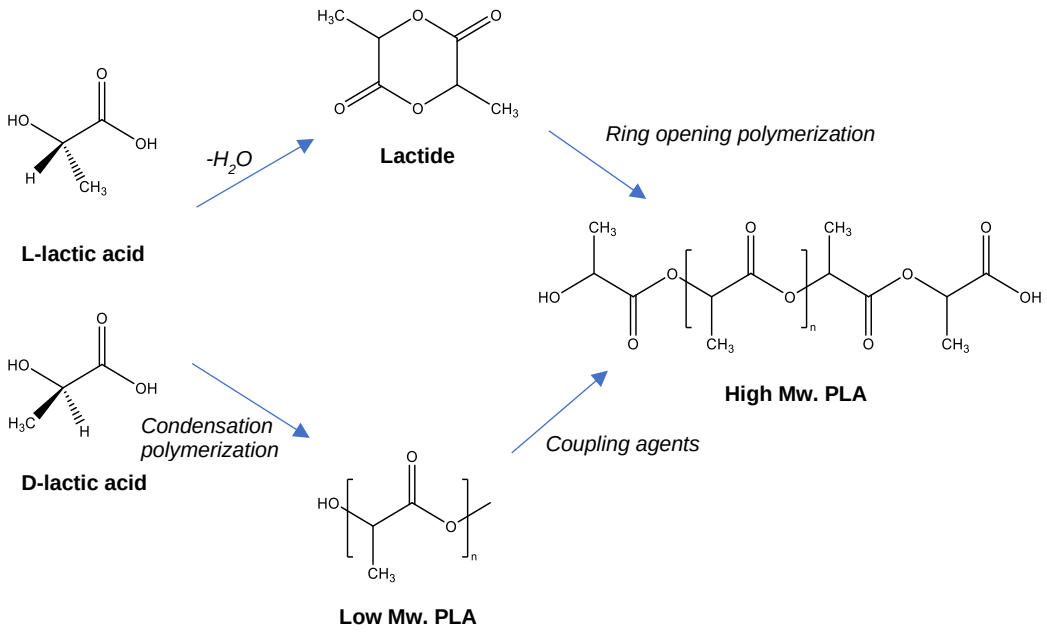

The ratio of the optically active configuration influences the crystalline, thermal, and mechanical properties. PLA can be semi-crystalline or entirely amorphous depending on the content of two lactides (L and D). Due to the imperfection introduced by D-lactic acid, semi-crystalline PLA contains more than 93% of L-lactic acid while entirely amorphous PLA contains 50% - 93% of L-lactic acid.[7] Crystallinity influences thermal and mechanical properties of PLA. Typically, the glass transition temperature (T_g) of PLA ranges from 50-80 °C and the melting transition (T_m) range from 130-180 °C depending on their crystallinity and molecular weight. In term of mechanical properties, PLA has properties similar to poly (ethylene terephthalate) or PET. Its tensile strength and elastic modulus are about 50-70 MPa and 3GPa, respectively.[8] However, PLA is rigid and very brittle below its T_g with less than 10% elongation at break. The crystallization kinetic of

PLA is also found to be relatively slow and decrease as the purity of L-lactic acid decrease. PLA brittleness and slow crystallization rate can be disadvantage and limit the possibility to extend its applications in industrial unless PLA is suitably modified.

PLA is one of the promising candidates as alternative of petrochemical polymers because it is commercially available, composting biodegradable, nontoxic, and biocompatibility. NatureWorks LLC is the major producer of PLA, which is marketed under the brand name Ingeo.[9] PLA is an aliphatic polyester that can be degraded by simply hydrolysis of the backbone ester bonds into nontoxic matters. The products of PLA degradation are lactic acid and oligomers that can be consumed by microorganisms and then produce carbon dioxide (CO_2), water (H_2O) and solid biomass.[10] Since the final products of PLA degradation mainly consist of CO_2 and H_2O which are considered non-toxic, the US food and Drug Administration (FDA) has approved PLA for biomedical applications.[11] With these promising properties, PLA is considered as a suitable alternative material for medical and packaging applications.

The hydrolysis process of the PLA depends on various factors including the morphology, degree of crystallinity, molecular weight, presence of additives, and conditions in the degradation environment such as pH, humidity and temperature.[12] As temperature is increased, the degradation time is shorten. PLA is degraded in human body at temperature 37 °C in 2-3 years but can be degraded under commercial composting condition where the temperature can go up to 70 °C in 75-80 days.[13] The degradation of PLA in water at a temperature of 20 °C remains almost stable[14] as well as the degradation of PLA in soil is slow and take a long time to begin[15, 16]. Slow rate of degradation of PLA is obvious disadvantages when considering the practical requirements in packaging

applications. PLA as currently produced does not meet the specific requirement such as toughness, fast crystallization, and quick decomposition in landfill. Therefore, modifying PLA for achieve all the desired properties need to be made in order to extend its applications in several industrials' domains.

Poly(hydroxyalkanoates), PHAs

Poly(hydroxyalkanoates) (PHAs) are a family of aliphatic polyesters synthesized by a variety of microorganisms. They have attracted extensive attention as natural biodegradable plastics and potential alternatives to replace fossil-based plastics. PHAs shows biological degradability in all aerobic and anaerobic environments and can be used to make completely compostable, and soil and marine biodegradable products.[17] PHAs have been classified based on the monomer composition in their structures including short chain length (SCL) and medium chain length (MCL). The SCL-PHAs have a total number of carbon atom in monomer unit between 3 to 5 carbon atoms, while the MCL-PHAs have subunits containing 6 to 14 carbon atoms.[18] There are around 150 different PHA monomers have been report and this number continues to increase with the new types of PHA.[19] The thermal and mechanical properties of PHAs depend on polymer composition and comonomer content.

Poly(hydroxybutyrate) (PHB) is one of the most studied PHAs and belongs to SCL. This homopolymer containing 4 carbon subunits of 3-hydroxybutyrate has properties that are similar to the petroleum polymers polypropylene (PP).[19] PHB is highly crystalline and has T_m is around 175 °C. The applications of PHB are limited because PHB has large spherulites and exhibits secondary crystallization which occurs during storage time at room

temperature causes brittleness and poor mechanical properties. In addition, PHB has poor thermal stability with very narrow processing window. Its thermal decomposition temperature is similar to its T_m. At temperature above T_m, sever degradation by random chain scission reaction through β-elimination can be induced into various oligomers and crotonic acid. As a result, a drastic decrease in molecular weight occurs.

It is known that PHA containing comonomer such as 3-hydroxyhexanoate (Hx) has lower crystallinity and lower T_m than PHB homopolymer. Moreover, it has been shown that the introduction of Hx monomer unit has improved the mechanical properties of PHB. Doi et al. have reported a decrease of the crystallinity from 60 to 26%, a decrease of melting temperature from 177 °C to 120 °C, and an increase of the elongation at break from 5 to 850% as the Hx unit content increase from 0 to 17%.[20] The resultant copolymerized PHB with Hx is called Poly[(3-hydroxybutyrate)-co-(3-hydroxyhexanoate)] or PHBHx. The chemical structures of PHB and PHBHx are shown in Figure 1.2.

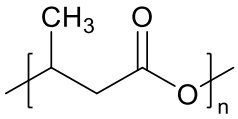

Poly(hydroxybutyrate), PHB

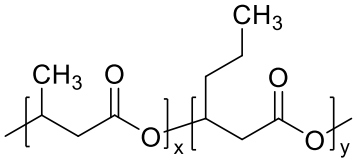

Poly[(3-hydroxybutyrate)-co-(3 hydroxyhexanoate)], PHBHx

Figure 1.2. Chemical structures of PHB and PHBHx.

With the increasing content of Hx, the side chain of Hx unit expands and acts as crystalline defects, thus lowering the melting temperature. As a result, T_m can be adjusted

by changing the ratios of the Hx comonomer, consequently broadening temperature window in melting process. Despite the better mechanical properties and melt processability, PHBHx copolymer has a critical drawback in crystallization rate. The rate of crystallization of PHBHx is too slow and shows much lower than crystallization rate of PHB. These characteristics make it difficult to use PHBHx to make products via extrusion and injection molding. The rate of crystallization is an important parameter for industrial process. Polymers that have a slow crystallization rate tends to stay soft, tacky and stick to itself making it difficult to achieve rapid mold release. A consequence of this is that injection molding cycle times are extended. In general, crystallization rate can be increased by acceleration the nucleation process. Nucleating additives are typically used in industry for speeding up this process. This poor processability is one of the major drawbacks of the PHBHx.[21] It is known that unmodified PHBHx cannot be extruded, or injection molded with economic cycle times. Therefore, it is important to find suitable nucleating agents that can achieve a desire rate of crystallization.

Strategies Towards to Improve Polyester Properties

Bio-based aliphatic polyesters such as PLA and PHAs are rarely used without tailoring their properties. With the purpose of functional improvement, polyesters are usually modified by either copolymerization or physical blending. Blending is more practical, convenient, and cost effective to obtain achieved properties than copolymerization.[22] Polymers are usually mixed with various additives. The type and amount of these additives will be properly selected in order to enhance performance characterization of polymers. This section will describe three types of additives:

plasticizers, processing aids, and nucleating agents. Two different methods used for the preparation of polymer blends such as solution casting and melt blending are also presented.

1. Plasticizers

Plasticizers are additives that are added to polymers to make them softer and more flexible. Typically, plasticizers are added by two purposes: 1) to aid processing and 2) to modify the properties of the final product. Introduction plasticizers into polymers as a processing aid help to lower the processing temperature, reduce the melt viscosity, and decrease shear rate causing better flow and less heat generation during the process. As a modified final product, plasticizers increase flexibility, elongation and toughness (impact strength) by lowering polymer T_g. [23, 24]

There are two kinds of plasticizers, internal and external plasticizers. Internal plasticizers are chemically modifying the polymers as an integral part of the polymer chain. It involves copolymerization into the polymer structure or reacts with the original polymers[25]. By making polymer structure less order, internal plasticizers generally have bulky substituents. These bulky groups provide more space for polymer chains to move resulting more difficult for the chains to come closely together. On the other hand, external plasticizers are substances that added to polymers and interact with polymer chains without involving chemical reaction. The external plasticization can generally be achieved by adding low molecular weight, relatively non-volatile organic compound to polymers. External plasticizers are commonly used for commercial applications due to it is very convenient to select the particular substance from a variety of plasticizers and vary the amounts of plasticizers for tunable to attain desired processability and product properties.[26,

[27] Since external plasticizers are not chemically bound to original polymer, they are easily lost by extraction, migration or evaporation in certain condition. For applications, the plasticizers loss can lead to functional failures such as brittleness in the unplasticized state and contaminate the surrounding medium.

The use of plasticizers for the manufacture of plastic products is not a new practice.[27] The selection of a plasticizer for production is generally limited by the required safety, environmental favorability, chemical and physical property that dictate their miscibility, processing temperature and required flexibility towards the target application.[28] More than 300 different types of plasticizers are manufactured world-wide.[29] Phthalates, commonly known as 'ester plasticizers' have been widely used since the 1920s.[29] However, the use of phthalates have become controversial with concerns of their effects on human health and on the environment.[28] Since phthalates are semi-volatile organic compounds, and are not chemically bound to the polymer matrix, they ultimately leach out of the polymers overtime and end up in the environment. Several studies have suggested that phthalates disrupt the hormone system and cause reproductive problems in mammals.[30]

Global demand for all plasticizers will increase to about 9.75 million tons by 2024.[31] As the bio-based plastic industry continues to grow, the demand for bio-based plasticizers will certainly go in the same direction. There is increased interest in the use of bio-based plasticizers due to the advantages of renewability, degradability, and low-toxicity. Therefore, it become challenges and opportunities for research into these bio-based non-toxic plasticizers.

2. Processing aids

Processing aids are additives used for increasing the processing efficiency. In extrusion process, it is well known that high molecular weight polymers exhibit flow instabilities at high production rate. Consequently, the extrudate distortions or melt fracture are observed, rendering a poor product quality. Processing aids are used for instability elimination which target at slip promotion and leads to lower stress and pressure in the extruder. Processing aids act as lubricants which can lower melt viscosity or prevent polymers from sticking to metal surfaces. Fluoropolymer, stearates, and polymer blends are common processing additives using in the extrusion of molten polymers.[32] Fluoropolymers are traditional used as processing aids in the commercial extruder for polypropylene (PP), linear low density polyethylene (LLDPE), and high density polyethylene (HDPE).[32] Stearate can promote slip and aid in the reduction of instabilities of PP.[33] Other polymers such as polyethylene glycol (PEG) was found to enhance the improvement in the processability of polyethylene/polypropylene.[34]

The effect of processing aids on the elimination of flow instabilities may result from two factors. First, the viscosity of processing aids is lower than that of polymers. Consequently, they tend to segregate or migrate in interface between the metal die wall and the polymer melt. Secondly, the adhesion of processing aids to metal surface is higher than the adhesion of polymer to metal surface. Thus, the processing aids will come to contact with the metal die wall surface during the extrusion process. The metal die wall becomes coated with a very thin layer of processing aid and causes slippage. The slip of polymer molecules is also influenced by a number of factors such as temperature, pressure, molecular weight, and immiscible blends.[35]

3. Nucleating agents

Crystallization of polymer occurs upon cooling from melting. This crystallization process involved two processes attributed to primary and secondary crystallization.[36] Primary crystallization is related to the formation of nuclei site form the melt state (nucleation) and spherulite growth. Secondary crystallization occurs when spherulites impinging on each other at which point the growth ceases. Crystallization rate of polymers can be increased by accelerating the nucleation process. Nucleating agents are widely used in semi-crystalline polymers to increase the rate of crystallization. The addition of nucleating agents into polymers involves the addition of a foreign materials or impurities which presents a new surface and promotes the heterogeneous nucleation process. In this case, heterogeneous nucleation uses foreign pre-existing surfaces to reduce the free-energy barrier for the formation of nucleation.[37]

The nucleating agents can be mainly divided into three kinds: inorganic additives, organic additives, and polymers.[38] Inorganic compound such as talc, silica, titanium dioxide, and boron nitride have found to be nucleating agents. The nucleation effect of these mineral additives highly depends on concentration, surface, particle size, and distribution.[39] In this case, they are typically insoluble in the melt and their melting point is well above melting point of polymers matrix. On the other hand, organic additives especially salts dissolve in the polymer melt and react with polymer chains. Sodium benzoate is the most common commercially organic salt. It induces chain scission and produce ionic chain which subsequently precipitate into ionic cluster and form the nuclei. Another type of nucleating agent is a group of ion-containing polymers called ionomers.

They have a negatively charged acid groups which have been partially neutralized with sodium ions.[40] These ionomers aggregate in the melt and acts as heterogeneous species.[41]

It was found that surface-induced epitaxial crystallization of polymers plays an important role in heterogeneous nucleation. Epitaxial crystallization was considered the growth of one crystalline phase (guest crystal) on the surface of a crystal of another phase (host crystal) in one or more strictly defined crystallographic orientation.[42] Most polymers were shown to have epitaxial interaction between polymers and their nucleating agents.[43] Epitaxial crystallization can occur due to such good lattice matching between nucleating agents and polymers. In the case of talc, it has been known to nucleate many aliphatic polyesters such as poly(ethylene terephthalate)[44] and poly(hydroxybutyrate-co-hydroxyhexanoate) through an epitaxial mechanism. By using the concept of epitaxy, suitable nucleating agent can be searched and selected for the polymer. The overall efficiency nucleating agent not only be attributed to the dispersion quality but to the lattice matching between nucleating agents and polymers.

4. Polymer Blending

Polymer blending is an effective, simple, and versatile method to develop the new materials.[45] Instead of synthesizing new polymers, existing two or more polymers and/or copolymers combine by mixing together. Polymer blend can be obtained by two ways, solution casting and melt compounding. The first way is to dissolve two polymers in the same common solvent, and subsequently letting the solvent evaporate. This method works fine in the small lab scale. However, in the industrial scale, this method could be expensive,

and effects on environment. The using of extra solvent, and the evaporation of solvent to the air are not suitable for making polymer blends in large amounts.

The second way is to mix polymers together in an extruder where temperature is high enough to melt the polymers without causing degradation. This method does not require using any solvent. The basic components of the extruder composed of four main parts: feeder, screw, barrel, and die exit shown in Figure 1.3. In this polymer processing, screw rotation speed, melt temperature, and retention time are the important variables which can affect product quality such as surface finish, mechanical properties, and thermal degradation. Therefore, it is a challenging task to find the appropriate condition while mixing polymers together with the extruder. In order to avoid the thermal degradation of polymers during extrusion, many researchers suggested to dry them prior to the melt processing. Also, the melt temperature in the extruder must be kept at a low level in order to minimize the degradation.[46]

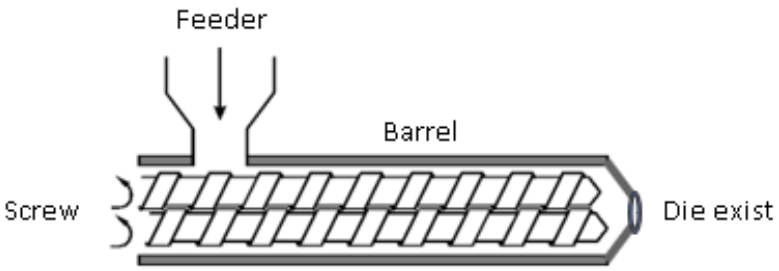

Figure 1.3. The basic components of an extruder

Objectives and Dissertation Outline

The overall objectives of this dissertation are as follows: 1) explore the structures and properties of the polymerization of glutaric acid and butanediol. 2) modify PLA by blending with poly(butylene glutarate) (PBG) as a bio-based plasticizer to create a product more suitable for commercial applications. 3) study the PBG as a bio-based processing aid for PHBHx in hot-melt extruder. 4) investigate PHB as a nucleating agent for PHBHx. The rest of this dissertation is organized into four chapters.

Chapter 2 of this dissertation discussed the use of PBG as a plasticizer to improve PLA ductility and accelerate composting biodegradation rate of PLA. PBG was synthesized through polycondensation reaction between 1,4-butanediol and glutaric acid. The preparation of the films of various PLA/PBG blends by solution casting and hot pressing was also described. Mechanical properties of the blends between PLA and PBG were compared to PLA and PBS blends. Degradation studies were carried out using respirometry under aerobic conditions at 58 °C for 90 days.

Chapter 3 describes the use of PBG as a processing aid for PHBHx in hot-melt extrusion. The appropriate condition was explored to extrude PHBHx. Various compositions of PHBHx/PBG blends were prepared at different weight ratios. The effects of PBG on melt viscosity, flowability, and viscoelastic properties were investigated. Moreover, the thermal and mechanical properties, and phase morphology of the PHBHx/PBG blends were characterized. The processability of selected PHBHx/PBG blend was evaluated by determining the melt flow instabilities.

Chapter 4 of this dissertation investigates the use of PHB as a nucleating agent for improvement crystallization rate of PHBHx. PHBHx was blended with PHB at various ratio in hot melt extruder. The crystallization kinetics of PHBHx/PHB were studied under the isothermal and non-isothermal crystallization process. Melting behavior of the neat PHBHx and PHBHx/PBH blends were determine by using modulated differential scanning calorimetry (MDSC). Composting biodegradation were measured by gaseous carbon loss under aerobic conditions.

Finally, chapter 5 summarized the chapter of this dissertation and offers an outlook and future work that could extend from the present research.

References

1. Gerngross, T. U.; Slater, S. C., How green are green plastics? *Sci. Am.* **2000,** *283* (2), 37-41.

2. Ishida, N.; Saitoh, S.; Ohnishi, T.; Tokuhiro, K.; Nagamori, E.; Kitamoto, K.; Takahashi, H., Metabolic engineering of Saccharomyces cerevisiae for efficient production of pure L-(+)-lactic acid. *Appl. Biochem. Biotechnol.* **2006,** *131* (1-3), 795-807.

3. Cheng, Y.; Deng, S.; Chen, P.; Ruan, R., Polylactic acid (PLA) synthesis and modifications: a review. *Front. Chem. China* **2009,** *4* (3), 259-264.

4. Södergård, A.; Stolt, M., Properties of lactic acid based polymers and their correlation with composition. *Prog. Polym. Sci.* **2002,** *27* (6), 1123-1163.

5. Hu, Y.; Daoud, W. A.; Cheuk, K. K. L.; Lin, C. S. K., Newly Developed Techniques on Polycondensation, Ring-Opening Polymerization and Polymer Modification: Focus on Poly(Lactic Acid). *Materials (Basel)* **2016,** *9* (3), 133.

6. Jamshidian, M.; Tehrany, E. A.; Imran, M.; Jacquot, M.; Desobry, S., Poly-Lactic Acid: Production, Applications, Nanocomposites, and Release Studies. *Compr. Rev. Food Sci. Food Saf.* **2010,** *9* (5), 552-571.

7. Garlotta, D., A Literature Review of Poly(Lactic Acid). *J. Polym. Environ.* **2001,** *9* (2), 63-84.

8. Farah, S.; Anderson, D. G.; Langer, R., Physical and mechanical properties of PLA, and their functions in widespread applications — A comprehensive review. *Adv. Drug Delivery Rev.* **2016,** *107*, 367-392.

9. Castro-Aguirre, E.; Iñiguez-Franco, F.; Samsudin, H.; Fang, X.; Auras, R., Poly(lactic acid)—Mass production, processing, industrial applications, and end of life. *Adv. Drug Delivery Rev.* **2016,** *107*, 333-366.

10. Höglund, A.; Hakkarainen, M.; Edlund, U.; Albertsson, A. C., Surface modification changes the degradation process and degradation product pattern of polylactide. *Langmuir : the ACS journal of surfaces and colloids* **2010,** *26* (1), 378-83.

11. Abd Alsaheb, R. A.; Aladdin, A.; Othman, N. Z.; Abd Malek, R.; Leng, O. M.; Aziz, R.; El Enshasy, H. A., Recent applications of polylactic acid in pharmaceutical and medical industries. *J. Chem. Pharm. Res.* **2015,** *7*, 51-63.

12. Benali, S.; Aouadi, S.; Dechief, A.-L.; Murariu, M.; Dubois, P., Key factors for tuning hydrolytic degradation of polylactide/zinc oxide nanocomposites. *Nanocomposites* **2015,** *1* (1), 51-61.

13. Muthu, S. S., *Sustainable Fibres and Textiles*. Woodhead Publishing: Cambridge, 2017.

14. Vert, M., Aliphatic Polyesters: Great Degradable Polymers That Cannot Do Everything. *Biomacromolecules* **2005,** *6* (2), 538-546.

15. Urayama, H.; Kanamori, T.; Kimura, Y., Properties and Biodegradability of Polymer Blends of Poly(L-lactide)s with Different Optical Purity of the Lactate Units. **2002,** *287* (2), 116-121.

16. Ohkita, T.; Lee, S.-H., Thermal degradation and biodegradability of poly (lactic acid)/corn starch biocomposites. **2006,** *100* (4), 3009-3017.

17. Meereboer, K. W.; Misra, M.; Mohanty, A. K., Review of recent advances in the biodegradability of polyhydroxyalkanoate (PHA) bioplastics and their composites. *Green Chem.* **2020,** *22* (17), 5519-5558.

18. Steinbüchel, A.; Lütke-Eversloh, T., Metabolic engineering and pathway construction for biotechnological production of relevant polyhydroxyalkanoates in microorganisms. *Biochem. Eng. J.* **2003,** *16* (2), 81-96.

19. Tan, G.-Y. A.; Chen, C.-L.; Li, L.; Ge, L.; Wang, L.; Razaad, I. M. N.; Li, Y.; Zhao, L.; Mo, Y.; Wang, J.-Y., Start a Research on Biopolymer Polyhydroxyalkanoate (PHA): A Review. **2014,** *6* (3), 706-754.

20. Doi, Y.; Kitamura, S.; Abe, H., Microbial Synthesis and Characterization of Poly(3-hydroxybutyrate-co-3-hydroxyhexanoate). *Macromolecules* **1995,** *28* (14), 4822-4828.

21. Dong, T.; Mori, T.; Aoyama, T.; Inoue, Y., Rapid crystallization of poly(3-hydroxybutyrate-co-3-hydroxyhexanoate) copolymer accelerated by cyclodextrin-complex as nucleating agent. *Carbohydr. Polym.* **2010,** *80* (2), 387-393.

22. Tokiwa, Y.; Calabia, B. P.; Ugwu, C. U.; Aiba, S. J. I. j. o. m. s., Biodegradability of plastics. *Int. J. Mol. Sci.* **2009,** *10* (9), 3722-3742.

23. Sears, J. K.; Darby, J. R., *Mechanism of plasticizer action*. Wiley-Interscience,: New York, 1982; p 35-77.

24. Han, J. H., *Innovations in food packaging*. Elsevier: London, UK, 2005.

25. Frados, J., *Plastics engineering handbook of the Society of the Plastics Industry, inc*. 1976.

26. Sothornvit, R.; Krochta, J. M., 23 - Plasticizers in edible films and coatings. In *Innovations in Food Packaging*, Han, J. H., Ed. Academic Press: London, 2005; pp 403-433.

27. Vieira, M. G. A.; da Silva, M. A.; dos Santos, L. O.; Beppu, M. M., Natural-based plasticizers and biopolymer films: A review. *Eur. Polym. J.* **2011,** *47* (3), 254-263.

28. Ljungberg, N.; Wesslén, B., Tributyl citrate oligomers as plasticizers for poly (lactic acid): thermo-mechanical film properties and aging. *Polymer* **2003,** *44* (25), 7679-7688.

29. Daniels, P. H., A brief overview of theories of PVC plasticization and methods used to evaluate PVC-plasticizer interaction. *J. Vinyl Addit. Technol.* **2009,** *15* (4), 219-223.

30. Mathieu-Denoncourt, J.; Wallace, S. J.; de Solla, S. R.; Langlois, V. S., Plasticizer endocrine disruption: Highlighting developmental and reproductive effects in mammals and non-mammalian aquatic species. *Gen. Comp. Endocrinol.* **2015,** *219*, 74-88.

31. Global demand for plasticizers continues to rise. *Additives for Polymers* **2017,** *2017* (10), 10-11.

32. Achilleos, E. C.; Georgiou, G.; Hatzikiriakos, S. G., Role of Processing Aids in the Extrusion of Molten Polymers. *J. Vinyl Addit. Technol.* **2002,** *8* (1), 7-24.

33. Russell, C. A., Effect of stearate processing aids upon polypropylene stability. *Polym. Eng. Sci.* **1965,** *5* (2), 84-89.

34. Xie, M.; Liu, X.; Li, H., Influence of poly(ethylene glycol)-containing additives on extrusion of ultrahigh molecular weight polyethylene/polypropylene blend. *J. Appl. Polym. Sci.* **2006,** *100* (2), 1282-1288.

35. Hatzikiriakos, S. G., Slip mechanisms in complex fluid flows. *Soft Matter* **2015,** *11* (40), 7851-7856.

36. Seven, K. M.; Cogen, J. M.; Gilchrist, J. F., Nucleating agents for high-density polyethylene-A review. *Polym. Eng. Sci.* **2016,** *56* (5), 541-554.

37. Wunderlich, B., *Macromolecular Physics V2*. Elsevier: 2012; Vol. 2.

38. Jiang, X. L.; Luo, S. J.; Sun, K.; Chen, X., Effect of nucleating agents on crystallization kinetics of PET. *eXPRESS Polym. Lett.* **2007,** *1*, 245-251.

39. Deshmukh, K.; Kangda, A. R.; Mahajan, S. P.; Chopra, S.; Kumar, A.; Peshwe, D. R., INFLUENCE OF TALC PARTICLE SIZE ON NUCLEATING EFFICIENCY OF COMMERCIAL ISOTACTIC POLYPROPYENE (iPP). *Journal of Research in Engineering and Applied Sciences* **2018,** *3* (1), 1-5.

40. Scheirs, J., Additives for the Modification of Poly(Ethylene Terephthalate) to Produce Engineering-Grade Polymers. In *Modern Polyesters: Chemistry and Technology of Polyesters and Copolyesters*, 2004; pp 495-540.

41. Bazuin, C. G.; Eisenberg, A., Modification of polymer properties through ion incorporation. *Ind. Eng. Chem. Prod. Res. Dev.* **1981,** *20* (2), 271-286.

42. Lotz, B.; Wittmann, J. C., Epitaxial crystallization of isotactic and syndiotactic polypropylene. In *Polypropylene: An A-Z reference*, Karger-Kocsis, J., Ed. Springer Netherlands: Dordrecht, 1999; pp 215-220.

43. Wittmann, J. C.; Lotz, B., Epitaxial crystallization of polymers on organic and polymeric substrates. *Prog. Polym. Sci.* **1990,** *15* (6), 909-948.

44. Haubruge, H. G.; Daussin, R.; Jonas, A. M.; Legras, R.; Wittmann, J. C.; Lotz, B., Epitaxial Nucleation of Poly(ethylene terephthalate) by Talc: Structure at the Lattice and Lamellar Scales. *Macromolecules* **2003,** *36* (12), 4452-4456.

45. Koning, C.; Van Duin, M.; Pagnoulle, C.; Jerome, R., Strategies for compatibilization of polymer blends. *Prog. Polym. Sci.* **1998,** *23* (4), 707-757.

46. Taubner, V.; Shishoo, R., Influence of processing parameters on the degradation of poly(L-lactide) during extrusion. *Prog. Polym. Sci.* **2001,** *79* (12), 2128-2135.

CHAPTER 2

BLENDS OF POLY(BUTYLENE GLUTARATE) AND POLY(LACTIC ACID) WITH ENHANCED DUCTILITY AND COMPOSTING PERFORMANCE[1]

[1]Reprinted with permission from Holt, A.; Ke, Y.; Bramhall, J. A.; Crane, G.; Grubbs, J. B.; White, E. M.; Horn, J.; Locklin, J. *ACS Appl. Polym. Mater.* **2021,** *3* (3), 1652-1663. Copyright (2021) American Chemical Society. Reprinted with permission from publisher.

Abstract

Blends of poly(lactide) (PLA) with poly(butylene glutarate) (PBG) have been investigated with a focus on the improvement of PLA brittleness and an enhancement of the degradation rate under industrial composting conditions. PBG was synthesized by melt polycondensation between 1,4-butanediol (C4) and glutaric acid (C5). The effect of the odd carbon atom number in the dicarboxylic acid monomer caused a decrease in melting temperature (T_m) and crystalline content, and subsequently an increase in composting degradation rate. Films of PLA blended with various compositions of PBG were prepared by solution casting and hot pressing. Physical, mechanical, and viscoelastic behavior along with morphology of the blends were investigated using a variety of techniques. All PLA/PBG blends showed a decrease in both glass transition temperature (T_g) and tensile strength, but showed an increase in the % elongation at break. The composting degradability of PBG and selected PLA/PBG blends were investigated using respirometry. Considering all the analyses performed, adding PBG to PLA improved the brittleness of PLA and accelerated the rate of degradation in industrial composting. PLA/PBG blends exhibited higher ductility than blends of PLA with poly(butylene succinate), a polymer commonly compounded with PLA in many thermoplastic applications. The compatibility of PBG in a PLA matrix was dependent on the concentration of PBG in PLA matrix, with phase separation evident above 3 wt %.

Introduction

In recent years, the development of bio-based polyesters have attracted considerable attention due to monomer sourcing from renewable resources (and thus CO_2 sequestration), along with selective abiotic and biotic degradation under certain environmental conditions.[1, 2] Among these polyesters, poly(lactide) (PLA) is one of the most well-studied thermoplastics and a commercial alternative for some conventional petroleum-based polymers.[3, 4] PLA is an aliphatic polyester, its monomer lactide is produced through the fermentation of renewable resources, and its composting degradation products are water and carbon dioxide when carried out in aerobic conditions at temperatures at or above the glass transition temperature. PLA is used in many market sectors for both disposable and durable goods including packaging, textile, automotive, additive manufacturing, and medical applications. PLA exhibits good mechanical properties as well as easy processability.[5, 6] Its tensile strength and tensile modulus are similar to poly(ethylene terephthalate) (PET).[7-9] PLA can be conventionally processed using extrusion, injection molding, blow molding, and also fiber spinning.

The well-known drawbacks of PLA such as brittleness, low heat deflection temperature, poor impact resistance, and slow degradation rate at end-of-life are major disadvantages for commercial applications in the single-use item and packaging industries.[10, 11] Current research on PLA modification has been focused on improving the mechanical and thermal properties by either copolymerization or physical blending, with compounding being the more practical and cost effective method to obtain the desired properties.[12] PLA blends with nanocomposites and nanofibrils have also been explored to overcome the brittleness of PLA. There have been several studies aimed at controlling the

phase morphology of these reenforcing nanocomposites such as adding PBS and PBAT nanofibrils in the PLA matrix.[13, 14] Moreover, Certain small-molecule plasticizers such as citrate esters,[15] triacetine,[16] and epoxidized soybean oil,[17] or other polymers such as polyethylene glycol,[18, 19] poly(caprolactone),[20] poly(butylene succinate),[21] and poly(butyleneadipate-co-terephthalate)[22] have been observed to be effective additives at improving flexibility and toughness. The role of these additives is to enhance the mobility of polymer chains as well as increasing elongation at break of the polymer.[23]

Organic plasticizers with low molecular weight and high to moderate vapor pressure have the tendency to volatilize during extrusion or eventually migrate from the polymer matrix of the formed article under certain conditions. The loss of plasticizers can lead to functional failures and contaminate the surrounding medium which limits their use in areas like food packaging and biomedical applications. Polymeric plasticizers have been used to hinder plasticizer migration due to their high molecular weight, better water resistance, excellent oil and solvent extraction and longer service life.[24] More specifically, many polyesters also have the characteristics of low toxicity and safety.[25] It is reported that blending PLA with ductile polyesters that exhibits lower glass transition temperature (T_g) such as poly(butylene succinate) (PBS) can improve PLA brittleness.[21] PBS is an aliphatic polyester synthesized by melt polycondensation of 1,4-butanediol (C4) and succinic acid (C6). It is semi-crystalline with a glass transition temperature (T_g) of about -30°C and a melting temperature (T_m) around 114°C. As a soft component in binary PLA/PBS blends, it is reported that PBS acts as a stress concentrator preventing brittle failure and enabling ductile yield.[26] The elongation at break of PLA/PBS blends increases gradually with

increasing PBS content. However, without the use of reactive extrusion,[27] the brittleness of PLA does not significantly improve until the PBS content is very high, at 80-90wt%.[28, 29]

In term of degradation in aerobic conditions, polyesters such as PLA and PBS degrade through a two-step process.[30, 31] In the first step, hydrolytic degradation occurs under an appropriate temperature and moisture environment resulting in substantial decrease in molecular weight. Then, enzymatic degradation by certain microorganisms can metabolize these lower molecular weight (monomeric and possibly oligomeric) components to biomass, carbon dioxide and water. The hydrolysis process of the PLA and PBS depends on various factors including the morphology, degree of crystallinity, presence of additives, and conditions in the degradation environment such as pH, humidity, and temperature.[32] Importantly, water absorptivity plays a significant role in hydrolysis process. The degradation of PLA in soil is slow partly because of its hydrophobicity, where water is unable to easily penetrate the PLA matrix.[33] The degradation of PLA in industrial compost is much faster than in soil conditions since the temperature of the inoculum can rise above or around the T_g. The elevated temperature environments (~50-60 °C) in industrial compost helps to increase chain mobility in the amorphous phase, with a subsequent increase in the diffusion rate of water.[34] The addition of PBS to PLA has also resulted in accelerated hydrolytic degradation. It has been reported that the relatively higher hydrophilic character of PBS compared to PLA and immiscible PBS particles enhance the hydrophilicity and introduce gaps/voids in blends, providing channels for water penetration.[27, 35]

Poly(butylene glutarate) (PBG) is also an aliphatic polyester, but synthesized from 1,4-butanediol (C4) and glutaric acid (C5). The chain length of diacids and the even-odd

effect on the chemical structure of the aliphatic polyesters ultimately determine their thermal properties and crystallinity.[36] From a materials point-of-view, the effect of an odd numbered diacid can influence the number of hydrogen bonds per gram of polymer, leading to a decrease in T_m and percent crystallinity. Polyesters made from even-even carbon monomers (such as PBS) display relatively high T_m and crystallinity, and the degree of crystallinity of the polyester plays an important role in the degradation process. Low crystallinity with a higher fraction of amorphous phase is usually more easily degraded by hydrolysis due to faster rate of water diffusion.[37] Nowadays, odd or even diacids and diols monomers can be produced on a large scale from renewable plant-resources such as corn starch and sugar cane.[38, 39] The fermentation technology alternative to petroleum-derived products is made possible in the biosynthetic routes of succinic acid[38] and more recently glutaric acid.[40, 41] The potential for bio-based production to replace petroleum-based production of these monomers has attracted lots of attention because it is a sensible approach for achieving economic and environmental sustainability.[42]

In view of thermal properties and degradation rate, the use of PBG can offer several advantages such as improving brittleness and increasing degradation rate to PLA blends. In this work, the odd-even aliphatic polyester PBG was first synthesized through polycondensation/transesterification and fully characterized in terms of thermal and degradation properties. Next, blends of PLA and PBG were prepared with various compositions via solution casting, and the influence of PBG on the thermal, mechanical, and morphological properties of the PLA blends was investigated. The impact of PBG on composting biodegradation was also examined. The result from this study will offer not only an alternative to petroleum-based additives, but improvements in both mechanical

properties and rate of degradation at much lower blend ratios than other aliphatic polyesters.

Experimental Section

1. Materials

PLA (Ingeo 3251D, Nature Works, LLC.) was obtained in resin form from Danimer Scientific. The T_g was approximately 60°C and the T_m was approximately 170°C. According to the manufacturer's data sheet, the exact proportion of D, L stereoisomer level of monomer was not specified. PBS (FZ91PM) in pellet form was supplied by PTT MCC Biochem Co., Ltd (Thailand). It has a T_g about -30°C and the T_m about 114°C. Glutaric acid and Zirconium (IV) butoxide ($Zr(OBu)_4$) were purchased from Sigma-Aldrich. 1,4 butanediol was purchased from Alfa Aesar and HPLC grade chloroform ($CHCl_3$) was purchased from JT Baker, U.S.A. Sigmacell cellulose (type 101) used as received in powder form was purchased from Sigma-Aldrich. This cellulose powder was used as a positive control to monitor microbial activities based on ASTM standard D5338-15 for composting biodegradation test.[43]

2. PBG synthesis and characterization

PBG was prepared by copolymerization of glutaric acid and 1,4 butanediol through a two-step procedure using a rotary evaporator equipped with a condensation-collecting flask, a silicon oil bath, a nitrogen inlet, and a vacuum system controller. The molar ratio of diacid to diol was 1:1.01, and the catalyst was 0.08wt% of the total monomers.

Briefly, 210 g (1589 mmol) of glutaric acid and 145 g (1609 mmol) of 1,4 butanediol were added together into a 500 mL round bottle flask. The monomer mixture was heated to 150°C for 1 hour (agitated at 25 rpm) under a constant stream of nitrogen at

atmospheric pressure in order to completely melt the monomers and remove all oxygen. After this time, the agitation and temperature of the mixture was raised to 50 rpm and 165°C, respectively. The vacuum pressure was gradually reduced from atmospheric pressure to 100 torr over a period of 3 hours to prevent excessive foaming and avoid monomer evaporation during polymerization. The water byproduct was collected and removed from the reaction vessel.

Next, the reaction pressure was slowly reduced to 1 torr and the reaction mixture was continuously agitated for 16 hours. Subsequently, the number of carboxylic acid end groups (acid number) were determined by standard titration in dioxolane with potassium hydroxide and phenolphthalein indicator (see the Supporting Information). When the acid number (AN) of the product was lower than 30, $Zr(OBu)_4$ (0.3 ml, 0.78 mmol) was added as catalyst and continued to react for additional 12 hours to obtain a product of high molecular weight. The final product was cooled to room temperature and freeze dried for 24 hours.

The structure of PBG was determined by proton nuclear magnetic resonance (^1H NMR) in $CDCl_3$ (Varian Inova 600 MHz spectrometer). The molecular weight and polydispersity index (PDI) of PBG samples were measured at 40°C by gel permeation chromatography (GPC). The GPC system included an automatic sampler (Shimadzu, SIL-20A), two pumps (Shimadzu, LC-20AD), a column oven (Shimadzu, CTO-20A), an ultraviolet detector (Shimadzu, SPD-20 A), and a refractive index detector (Shimadzu, RID-10A). $CHCl_3$ was used as the mobile phase at a flow rate of 1.0 mL/min and molecular weight is reported relative to polystyrene standards. Thermogravimetric analysis (TGA) was performed on a Discovery TGA (TA Instruments) to obtain the decomposition

temperature of PBG by heating from 30°C to 500°C at a rate of 3°C/min under nitrogen atmosphere. Thermal properties and degradability of PBG were investigated by using differential scanning calorimetry (DSC) on a DSC 250 (TA Instruments) and a 12-channel respirometer (ECHO instruments).

3. Preparation of the blends

Films of PLA/PBG blends and PLA/PBS blends were prepared by solution casting at various compositions. The composition ratios of the PBG and PBS in the blends were 0, 1, 3, 5, 10 and 15wt%. PLA and PBG (or PBS) (approximately 2 g total polymer) were dissolved into 15 mL of $CHCl_3$. The mixtures were stirred at 350 rpm for 12 hours before casting in a clean glass petri dish (10 cm in diameter). The solvent was allowed to evaporate for 24 hours at room temperature. The cast films were then removed from the petri dish and air dried at room temperature for 12 hours.

In order to make uniform films with thickness 100 ± 5 µm, a hydraulic press with heated platens (Carver, 4386) was used at 175°C. The cast films were first placed between the platens without any pressure for 3 minutes, then the films were pressed for 1 minute at 500 psi. The specimens were removed from the press and cooled at room temperature (approximately 1 minute). The final film thickness was measured with digital calipers. All films were stored in a desiccator for further analysis.

4. Characterization of the blends

4.1 Differential scanning calorimetry (DSC)

DSC measurements were performed on a DSC 250 (TA Instruments) under nitrogen atmosphere. Specimen weighing approximately 5 to 6 mg were heated at a rate of 10°C/min from 25° to 200°C and held isothermally at 200°C for 1 minute to eliminate

thermal history. They were then cooled to -80°C at 10°C/min and held isothermally for 1 minute before a second heating step. The glass transition temperature (T_g), cold crystallization temperature (T_{cc}), and melting temperature (T_m) of the PLA blends were determined using the second heating curve.

4.2 Dynamic mechanical analysis (DMA)

DMA was conducted on a DMA Q800 (TA Instruments). All films were cut into rectangular shapes using a punch (25 mm x 5.3mm) from 100 ± 5 μm thick films. The specimens were gripped by tension clamps with a clamp compliance of about 4 in.lb. DMA multifrequency strain analysis with oscillations of 20 μm amplitude at 1 Hz was conducted. The temperature was ramped from 30°C to 120°C at 3°C/min. The storage modulus, loss modulus, and tan δ were analyzed.

4.3 Tensile test

The tensile properties of the neat PLA and the blends were measured using a tensile tester (Shimadzu, AGS-X series). Films were cut into dog-bone shapes using a die-cutter (Qualitest, ASTM-D1708-96-MET). All specimens were tested at room temperature with a cross-head speed of 5 mm/min.

4.4 Atomic Force Microscopy (AFM) and Atomic Force Microscopy-Infrared Spectroscopy (AFM-IR)

PLA and polymer blend morphologies were examined by PeakForce Quantitative Nanomechanical Property Mapping (PF-QNM) on a Bruker Multimode Atomic Force Microscope. Image processing and data analysis were performed with the NanoScope Analysis software. Thin films of PLA and the blends were prepared by spin coating onto silicon wafers coated with native oxide (UniversityWafer, Inc). The silicon wafers were

cut into 2 cm × 2 cm squares and sonicated for 5 minutes with hexane, isopropyl alcohol, acetone, and water, followed by drying with a stream of nitrogen. The mixtures of polymer with various blend ratios (1-15%wt PBG) were dissolved in $CHCl_3$ to produce 20mg/mL solution. Thin films were then fabricated at room temperature with a spin speed of 1500 rpm using 200 µL of the mixture. Film thickness was measured using spectroscopic ellipsometry (J.A. Woollam, M-2000V).

The AFM-IR measurements were carried on a NanoIR3 system (Bruker) in contact mode. The AFM-IR images were recorded with a contact mode tip (Anasys Instruments Inc) which has a resonance frequency of 13 ± 4 kHz and a spring constant of 0.07-0.4 N/m. The AFM height images were acquired simultaneously with IR maps at ambient conditions. IR maps at 1730 cm^{-1} and 1760 cm^{-1} wavenumbers were obtained to study the phase separated morphology of the films. These single IR radiation images were recorded with a scan rate of 0.5 Hz and resolution of 512 × 256 pixels.

4.5 Scanning electron microscope (SEM)

Phase morphology of the fracture surface of the tensile bar was investigated using a FEI Teneo field emission-SEM at an accelerating voltage of 5kV with a spot size of 7. Specimen were cut from the fracture surface of the tensile bar, fixed on pucks with conductive tape such that the cross section could be observed. The three-dimensional image of sample geometry fixed on the puck is illustrated in Figure A.1. The fracture surfaces were sputter coated with a gold/palladium coating using a LEICA EM ACE200 high vacuum sputter coater. The thickness of Au/Pd layer was 6 nm.

4.6 Composting biodegradation test

All composting biodegradation tests were divided into two sets of experiments based on two different objectives. The degradation studies of PBS and PBG were first conducted in order to assess the effects of the even or odd carbon monomers on the rate of degradation. Next, the degradation studies of PLA and selected PLA blended with 15wt% of PBG were performed to determine the effect of PBG on PLA degradation. Each experimental set was carried out in a 12-channel respirometer (ECHO instruments) under aerobic conditions at 58 °C for 90 days. The air was pumped into each reactor channel with a flow rate of 180 mL/min. The amounts CO_2 emission from the outlet gas were analyzed every 2 hours using a built-in gas sensor.

Two sets of compost inoculum were collected from industrial-scale compost facility located at the University of Georgia, Athens, GA. These two compost sets were about 4-5 months old derived from composting the organic fraction of green waste, forest residue, food waste, and livestock manure. The temperature in the composting pile (50 cm depth) while collecting was 51°C for the first set and 53 °C for the second set. Both sets of compost were sieved using a 4.75 mm screen (Sieve No.4) to discard any large items such as stone, wood, and glass. The properties of fine and homogeneous compost such as pH, volatiles and total solids were measured by pH probe and thermogravimetric analysis. Carbon and nitrogen content of the two compost sets and samples were measured using the method described in Kristen (Table A.1).[44]

Approximately 250 g of fine and homogeneous compost inoculum was introduced into 12 reactors. In each experimental set, samples were run in three replicates composed of 5 g of two test materials, 5 g of cellulose (positive reference), and blank (control) which

is compost inoculum only. For the first degradation experiment, synthesized PBG was cut into small pieces and sieved using Sieve No. 4. PBS was dissolved in $CHCl_3$ and precipitated in methanol and sieved using Sieve No. 4. For the second degradation experiment, both PLA and 15wt% PBG/PLA films were cut into a size of 25 x 25 mm. In both experiments, cellulose was used as received in powder form.

The compost inoculum in all reactors was stirred weekly to prevent clumping and provide even distribution of moisture. Water was added into the reactors as necessary in order to maintain constant moisture level and prevent drying of the compost inoculum. The actual carbon dioxide (CO_2) emission from each sample was measured and calculated by subtracting from the average CO_2 production from the blank. The composting biodegradability was calculated from the ratio of actual CO_2 emission to the theoretical amount of the evolved CO_2 in each test period according to the testing method from ASTM standard D5338-15.[43] For a better understanding of the degradation kinetics, the data were fitted to a Modified Gompertz model which was developed to describe the cumulative CO_2 generation curve from each reactor.[45-48] The methods calculating biogas production, , and Modified Gompertz model fitting are presented in the Supporting Information.

Results and Discussion

1. Synthesis and characterization of PBG

PBG was synthesized following the two-step melt polymerization process of glutaric acid and 1,4 butanediol (Scheme 1). In the beginning, esterification reactions between acid and alcohol dominate and generate *low molecular weight oligomers.* In this stage, the viscosity of the melt is low enough that phase equilibrium can be achieved with a good agitation.[49] The reaction mixture was heated to 165°C and mixed at 50 rpm under

reduce pressure of 100 torr for 3 hours until no more water was removed from the reaction mixture. The viscosity of the polymer melt increased with reaction time, and the removal of the small molecules becomes more difficult, limited by mass transfer.[50] The vacuum pressure was lowered further (1 torr) and heated for an additional 16 hours. The number average molecular weight (Mn), weight average molecular weight (Mw), and polydispersity index (PDI) of PBG at this stage was 7,384 g/mol, 11,308 g/mol, and 1.53, respectively. In the second step, transesterification was carried out using a Lewis acid catalyst, ($Zr(OBu)_4$), for an additional 12 hours to yield higher molecular weight polymer (Mn = 24,229 g/mol, Mw = 40,560 g/mol, and PDI =1.67).

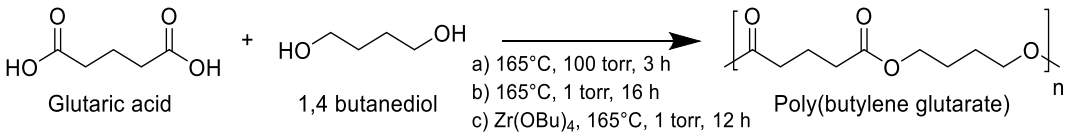

Scheme 2. 1. Synthetic scheme for the formation of PBG by polycondensation of glutaric acid and 1,4 butanediol.

^{1}H NMR analysis was performed to verify the chemical structure of PBG (Figure A.2), where the butylene sub-unit resonance signals of the *A* and *B* protons were observed at 4.10 ppm and 1.70 ppm, respectively. The signal of a and b protons from the glutarate sub-unit are located at 2.37 ppm and 1.94 ppm. The thermal decomposition of PBG was determined by the percentage of the mass loss versus temperature using TGA. From the thermogram curve (Figure A.3), the degradation temperature of PBG was approximately 372°C measured by onset extrapolation. The thermal properties of PBG are shown in Figure A.4. From the DSC curve, the T_g and T_m of PBG is -60°C and 38 °C, respectively.

It is noted that the T_m of PBG is significantly lower than that of PBS (~114°C), which limits its application as a stand-alone thermoplastic.

Next, PBG was compared to PBS to evaluate the effects of the odd or even carbon monomers on the rate of degradation. The compost inoculum that was used in this experiment had pH of 8.2, total solid of 54.2 % of the wet solid, and volatile solid of 17.0% of the wet solid. The total carbon to nitrogen ratio (C/N) of the compost inoculum was 15.3. The carbon and nitrogen content of PBG were C = 60.1% and N = 0.02% and PBS were C = 59.7% and N = 0.02%, respectively. Each sample was run in triplicate. Figure 2.1 shows the respirometry data. In an operation time of 30 days, the cellulose positive control reached 72.1 % biodegradation on average. PBG and PBS achieved 77.7% and 45.1% biodegradation under the same period of evaluation. The % relative composting biodegradation of PBG and PBS was 107.7 and 62.5 when normalized against cellulose. All data for % composting biodegradation and % relative composting biodegradation after 60 days and 90 days are reported in Table A.2.

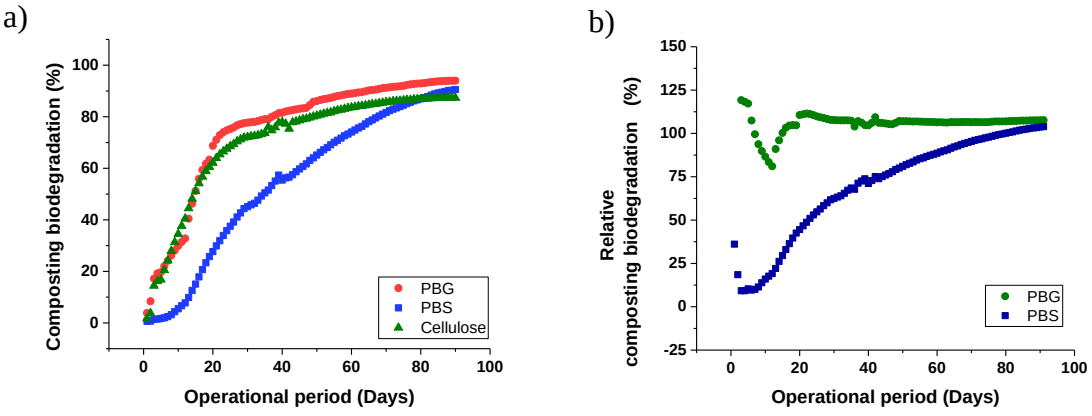

Figure 2.1. Composting biodegradation of PBG and PBS under ASTM D5338. (a) composting biodegradation (b) relative composting biodegradation.

The result of the biodegradation experiments demonstrates that PBG degraded faster than PBS and cellulose under the conditions of ASTM D5338 which simulate industrial composting. The replacement of succinic acid (C4) by glutaric acid (C5) significantly decreases the T_m from 114°C to 38°C, which increases the degradation rate from 60 days to 24 days. This observation could be described to the fact that odd or even number of carbon atom monomers and orientation of dipole alignment in these two polyesters (PBG and PBS) influence crystal structure.[36, 51-53] In polyesters with an even number of carbon atoms between carbonyl groups contains close layers of dipoles of opposite direction. This has the effect of canceling the local polarization. In polyesters with an odd number of carbon atoms between carbonyl groups, all the dipoles are arranged in an identical direction, which repel each other, decreasing the overall stability.[53] Scheme 2 illustrates the arrangement of the polar layers for PBS and PBG.[53, 54] The overall effect of odd carbon numbers is a decrease in crystallinity and T_m. In this regard, the crystallinity and T_m of polyesters has a strong effect on the abiotic (hydrolytic) and biotic degradation rate. The lower T_m of PBG is excellent for composting biodegradation, since the elevated temperature during composting routinely exceeds 50°C.

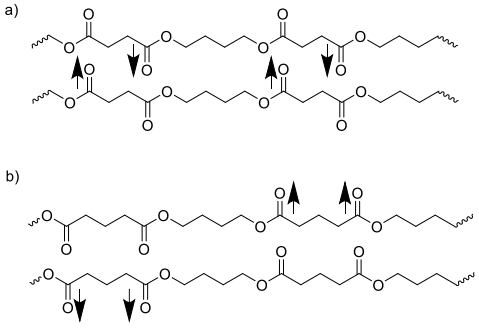

Scheme 2. 2. Schematic illustration of the arrangement of the polar layers for PBS (a) and PBG (b). The arrows indicate the direction of polarization.

2. Thermal properties of PLA/PBG blends

Figure 2.2 shows the second heating DSC thermograms of neat PLA, PBG and subsequent blends. The first heating and cooling curves are presented in Figure A.5 and A.6. All DSC curves in Figure 2.2 displayed three thermal transitions: T_m, T_g, and T_{cc}. The detailed results of DSC are summarized in Table A.3, as these thermal transitions can be used to differentiate the miscibility of the blends. A miscible blend is characterized by a single thermal transition while an immiscible blend is characterized by multiples thermal transitions for each polymer. PLA/PBG blends showed a single T_m below an addition level of 3wt% of PBG. However, for higher concentrations of PBG, two independent melting transitions for PLA and PBG are observed, which is evidence for phase separation in PBG loading above 3wt%.

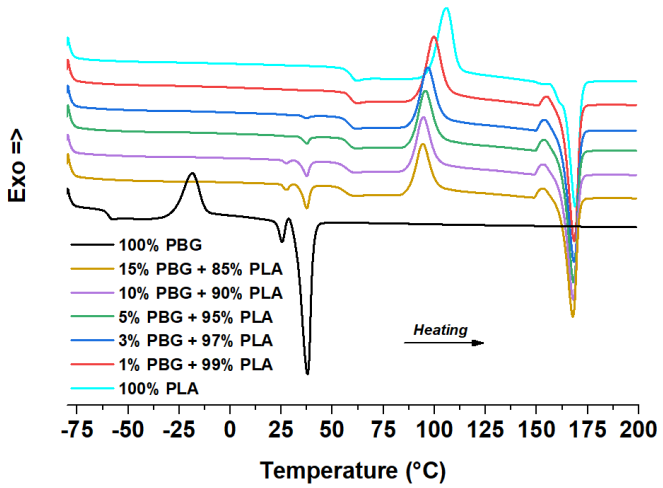

Figure 2.2. DSC thermograms of second heating cycle of PLA and PLA/PBG blends.

From the DSC scans shown in Figure 2.2, PLA has a T_g at 58 °C, T_{cc} at 106 °C and T_m at 169 °C. The blends containing PBG showed a lower T_g with increasing PBG content. The T_g decreased from 58 °C (neat PLA) to 55 °C (PLA/15wt% PBG). This indicates that

the mobility of PLA chains is slightly enhanced due to the presence of PBG. It is apparent that the addition of PBG also affects T_{cc}. The T_{cc} observed in PLA at 106 °C was decreased to 94 °C with the addition of 15wt% of PBG, consistent with the lowering of the T_g. The increased chain mobility likely enhances the ability of PLA to cold crystallize at lower temperatures.[18] This result is similar to other plasticized PLA reports with citrate ester plasticizers,[55] ester oligomers,[56] and epoxidized soybean oil.[17] The crystallinity of PLA (X_C%) was calculated from DSC curves using the following equation:

$$X_C\% = (\Delta H_m - \Delta H_{cc} / \Delta H^0_m * X_{PLA}) \times 100 \quad (1)$$

where ΔH_m was the enthalpy of melting, ΔH_{cc} was the enthalpy of cold crystallization, and X_{PLA} was the weight fraction of PLA in the blends. ΔH^0_m was the melting enthalpy of 100% crystalline PLA, which is 93 J/g.[57] From Table A.3, the degree of crystallinity increased when the PBG content was increased. The crystallinity in neat PLA was 3.1% and increased to 7.5% with the addition of 15wt% PBG. The degree of crystallinity of PLA/PBG blends was higher than the PLA again likely due to the increased chain mobility.

3. Viscoelastic behavior of PLA/PBG blends

Figure A.7 shows the storage modulus (E'), loss modulus (E") and tan delta (tan δ) as a function of temperature, as measured by dynamic mechanical analysis (DMA). In Figure A.7, the E' of all samples decreased with increasing temperature below 60°C. There was a significant drop of E' in the regions between 50-60 °C as the material enters the glass transition, indicating an increase in the mobility of the polymer. Between 60-90 °C, the E' curves displayed a short plateau that starts to rise around 90 °C due to the onset of cold crystallization.[17, 58, 59] When comparing PLA and PLA/PBG blends, the E' of the PLA/PBG

blends exhibited lower values, decreasing with increasing PBG content from 2984 MPa (neat PLA) to 2311 MPa (PLA/15%wt PBG). In addition, the T_g observed by DMA decreases with increasing PBG content. The T_g of PLA was 52.3°C, and 15wt % of PBG decreased the T_g to 46.2°C, consistent with that observed from DSC.

The E" curves are displayed in Figure A.7, which demonstrate that the peak intensity of E" in the PLA/PBG blends is lower than neat PLA. The peak intensity of E'' is related to the melt viscosity of a polymer,[60] and the shifting of the E" peak can be associated with a decreased melt viscosity in the blends. It was observed that the E" for neat PLA is 533.6 MPa and decreased to 372.7 MPa for PLA/15wt% PBG. The tan δ also shifts to lower temperature with increasing PBG content in the blends. All of the DMA data is summarized in Table 2.1.

Table 2.1. DMA data of PLA/ PBG blends.

Sample	PLA/PBG content (wt%)	Storage Modulus (MPa)	T_g (°C)	Loss Modulus (at the beginning) (MPa)	Loss Modulus (Top peak) (MPa)	Tan Delta (Top peak)
1	100/0	2984	52.3	81.3	533.6	2.4
2	99/1	2968	50.2	78.3	473.2	2.5
3	97/3	2913	49.3	75.7	518.9	2.3
4	95/5	2847	48.8	78.1	489.4	2.4
5	90/10	2547	47.6	76.5	431.3	2.4
6	85/15	2311	46.2	78.6	372.7	2.2

4. Miscibility of PLA/PBG blends

The AFM topography of different blend compositions in which the amount of PBG was varied between 1wt % and 15wt% are shown in Figure 2.3. Micro-voids were readily observed when PLA was blended with PBG above 3wt%. This is also evidence of phase separation and corroborates the observations from DSC, where multiple thermal transitions were observed. Since the solubility of the two components in the solution are different and the interfacial adhesion between PBG and PLA is relatively poor, PBG aggregated and formed micro-voids in the PLA matrix during the film forming process.[61, 62] The average height and diameter of the holes increased with increasing amount of PBG. Table A.4 reports the film thickness, height, and diameters of the voids.

To confirm the morphological observations, AFM-IR was used to identify and map polymer components in the blends. Figure A.8 shows AFM height images and IR mapping images of PLA with 15%wt PBG taken at 1730 cm^{-1} and 1760 cm^{-1} which can be assigned to the carbonyl stretching vibration band of PBG and PLA components, respectively (Figure A.9). As seen in these IR mapping images, the IR absorption at 1730 cm^{-1} is dominant in the micro-voids, whereas it is weak in the ridge areas. In contrast, the ridge regions show a high IR absorption at 1760 cm^{-1} due to the high density of carbonyl groups of PLA. This result further suggests that PLA and PBG are immiscible.

Like all other polymer classes, PLA blended with other polymers are either partially miscible or immiscible, and their mechanical properties depends strongly on this miscibility.[63, 64] PLA/PBS blends also demonstrate an immiscible phase structure which resulted in an unsatisfactory toughening effect.[27] The main challenge with immiscible polymer blends is improving the adhesion between the blended components or reducing

the dispersed phase domain size. For this reason, compatibilizers are typically added to improve the properties of the blend. Compatibilization of polymer blends were not attempted in this study, but likely can be used to further improve the miscibility (and subsequent toughness) in these composites.

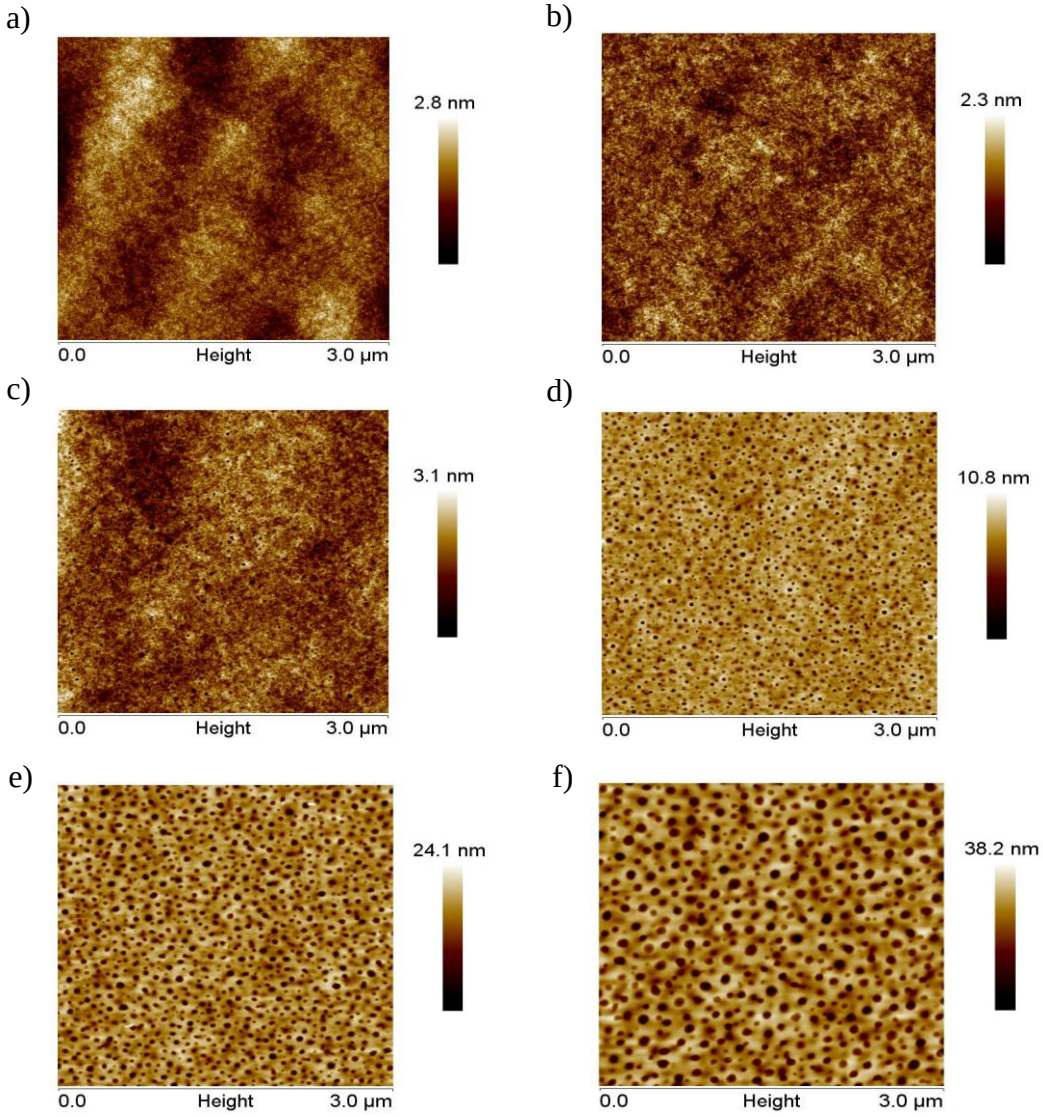

Figure 2.3. AFM height images of a spin-coated films of the PLA and PLA/PBG blends (a) neat PLA, (b) 1% PBG + 99% PLA, (c) 3% PBG + 97% PLA, (d) 5% PBG + 95% PLA, (e) 10% PBG + 90% PLA, and (f) 15% PBG + 85% PLA.

5. Tensile properties of PLA/PBG blends

Tensile strength, tensile modulus, and % elongation at break of pure PLA, various PLA/PBG blends and various PLA/PBS blends are shown in Table A.5. A typical stress-strain curve for the blends is also shown in Figure 2.4. The inclusion of PBG in PLA decreases the tensile strength and tensile modulus but increases the % elongation at break. The tensile modulus of neat PLA exhibited the highest value (3.4 GPa) compared to the blends. The elongation at break of PLA/PBG increased from 2.5 % to 21.6 % with 15wt% of PBG. The increase in ductility suggests that the PLA/PBG blends become more flexible with increasing PBG content.

The same trends in tensile strength, tensile modulus, and % elongation at break were also observed in the PLA/PBS blends. According to our observations, a higher concentration of PBS in the PLA matrix is necessary to achieve the same improvement in toughness. The addition of 5% and 15% of PBS into PLA matrix improved the % elongation at break by 5.0% and 13.2%, respectively. These results suggested that the brittleness of PLA can be adjusted by blending with PBS. Interestingly, PLA/PBG blends exhibit higher ductility than PLA/PBS blends under the same loadings. The PLA/PBG blend had a 14.9% elongation at break with only 5% of PBG, while the PLA/PBS blend had a similar elongation at break (13.2%) at a loading of 15% PBS.

Regarding the *stress-strain curve,* the deformation and fracture behavior of the neat PLA can be considered as the resistance to stretching of polymer chain networks. By adding PBG, the mobility of PLA chains is enhanced and the resistance to stretching decreases, resulting in a reduced tensile modulus and tensile strength. Moreover, there is recognizable yielding behavior and strain softening of all PLA/PBG blends. Stain softening

is a gradual decline of stress at increasing strain which is primarily a consequence of brittleness and heterogeneity of the material.[65]

During the tensile testing, PLA/PBG blends exhibited a stress-whitening effect,[66] whereas PLA/PBS did not (Figures A.10-A.11). This crazing occurred when the samples were deformed, decreasing their transparency and becoming opaque in appearance. The micro-voids[67] that were observed with AFM are likely responsible for the initiation of this "whitening" effect. Under enough mechanical loading, the tensile stress applied is concentrated at the interface of the micro-voids and as a result, the micro-voids increase in size and allow for the alignment of micro-fibrils between voids. The aligned structure enables the fibrils to carry the applied stress until breaking. The extensive stress is dissipated by crazing and postpones the ultimate failure of the material.[11] To explore the toughness mechanism, SEM was used to study the fracture surface of the specimens.

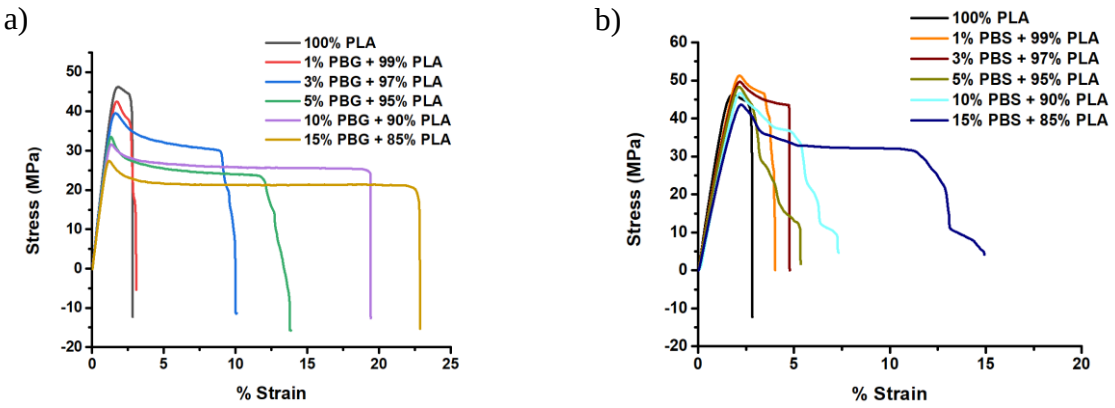

Figure 2.4. Stress-strain curves for (a). PLA/PBG blends and (b). PLA/PBS blends.

6. Morphology of PLA/PBG blends

Figure 2.5 (and also A.12) shows the SEM images of the tensile test fracture surface of the PLA/PBG blends. The fracture surface of neat PLA is very smooth and uniform, as expected with no phase separation. The fracture surface of the blends appears rougher and the formation of micro-voids with increasing PBG content are obvious. The void size continues to grow with stress loading during the tensile test. This visible increase in void formation correlates well with the AFM analysis. As the PBG content increases, the appearance of more voids is observed due to an increase in phase separation. The increase in void size with increasing PBG content also correlates well with the tensile testing data. Samples that have higher PBG loading demonstrate longer elongation at break due to void growth and alignment of microfibrils. The average void size for blends with 1%, 3%, 5%, 10%, and 15% PBG were 0.5-1μm, 1-2μm, 2-3μm, 3.5-4.5 μm, and 7-8 μm respectively. This increase in void size coupled with an increased elongation at break confirms that as the void grows, it allows for the alignment of microfibrils which results in greater stress dissipation and better toughness.

7. Aerobic composting biodegradability of PLA/PBG blends

The composting biodegradability of PLA and PLA-based blends were investigated by respirometry to determine the influence of PBG on PLA degradation. In general, it is our observation that the blending of polymers influences the overall degradation behavior of the blend, and typically differs from the degradation rate of the neat components alone. The interaction among different species in the blends and overall morphology influence the diffusion rate of water and subsequent hydrolytic reactions during degradation.[68] Because of space limitations in the respirometer and the best performance of toughness,

the blend of 15% PBG and 85% PLA was selected for respirometry evaluation. The carbon and nitrogen contents of PLA were 52.5% and 0.03% and the blend were 53.3% and 0.01%, respectively. The compost inoculum that used in this experiment had pH of 8.0, total solid of 51.7wt% of the wet solid, and volatile solid of 17.7wt% of the wet solid. The total carbon to nitrogen ratio (C/N) of the compost inoculum was 19.2.

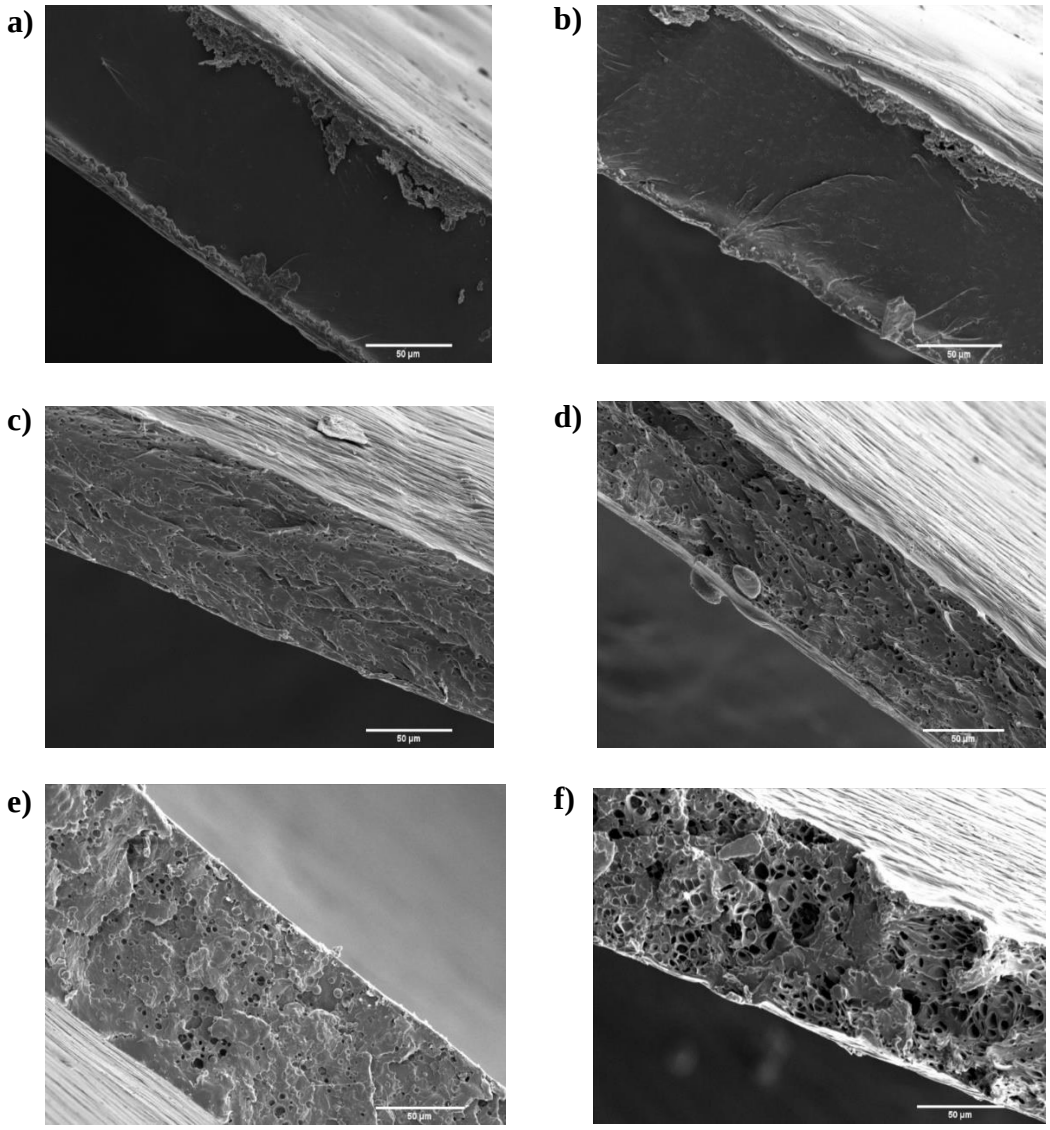

Figure 2.5. SEM cross-section images of tensile bar fracture surface of PLA and PLA/PBG blends (a) neat PLA, (b) 1% PBG + 99% PLA, (c) 3% PBG + 97% PLA, (d) 5% PBG + 95% PLA, (e) 10% PBG + 90% PLA, (f) 15% PBG + 85% PLA.

All the emitted CO_2 was monitored and quantified during the composting degradation test. The percent of composting biodegradation can be calculated by dividing the actual CO_2 emission from the samples by the theoretical CO_2 emission from the samples and multiplying by 100. After 90 days under a controlled composting aerobic condition in a respirometer operated at 58 °C, the composting biodegradation of PLA was 40.2% PLA and the blend reached 54.5% (Figure 2.6a). The relative composting biodegradation of PLA and the blend was 66.1% and 89.6%, respectively (Figure 2.6b). The results showed that the composting biodegradation of this blend degraded faster than the neat PLA and it passed the threshold limit requirement for biodegradation imposed by the ASTM standard D6400-12,[69] which states that the biodegradability must reach at least 90% relative to cellulose within 180 days.

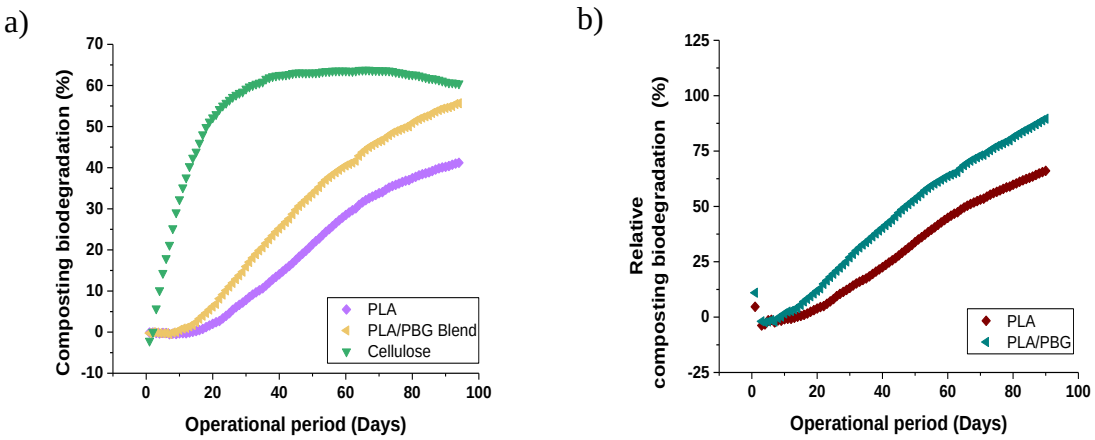

Figure 2.6. Degradability of cellulose (reference material), PLA and PLA blended with 15% PBG (a) composting biodegradation (b) relative composting biodegradation.

Modified Gompertz model

By using the modified Gompertz model to fit sample CO_2 production, the composting biodegradation of each test specimen can compare quantitatively through two different composting experiments. This compost inoculum was sourced from the same industrial composting facility and from comparable 4-5 months old compost. The PBG and PBS were studied against the "Cellulose 1" positive control while the PLA and PLA/PBG blend were examined against the "Cellulose 2" positive control in a later experiment. The difference in CO_2 production between the blank controls and any test material reveals the amount of gaseous carbon loss from each sample as shown in Figure 2.7.

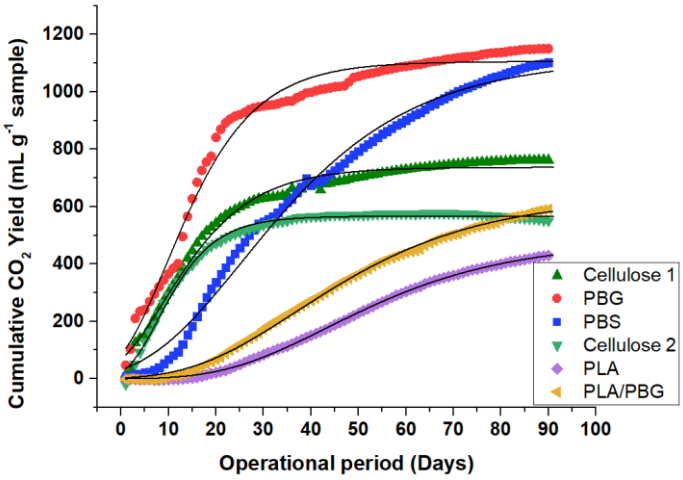

Figure 2.7. Gaseous Carbon Loss from Samples. The cumulative CO_2 production is plotted for each operational day for the two respirometry experiments. Note that "Cellulose 1" is the positive control for the PBG and PBS composting experiment and "Cellulose 2" is the positive control for the PLA and PLA/PBG blend composting experiment. Dotted lines represent the modified Gompertz models according to the corresponding parameters in Table 2.2.

Notably, the cumulative yield of the cellulose controls in the PBG and PBS respirometry experiments displayed higher cumulative CO_2 yield than the cellulose controls in the PLA and PLA/PBG blend respirometry experiment. This observation also helps describe the activity of the compost inoculum, whereby the inoculum in the PBG and PBS testing likely had higher overall activity on the cellulose control and the test samples when compared to the separate PLA and PLA/PBG blend respirometry experiments. The maximum CO_2 potential (P_m) was 737.1 and 566.5 mL $CO_2 \cdot g^{-1}$ sample for Cellulose 1 and Cellulose 2 positive controls, respectively, verifying the higher inoculum activity of the first composting experiment.

Modified Gompertz kinetic parameters and absolute biodegradation of PBG, PBS, PLA and 15% PBG + 85% PLA are shown in Table 2.2. PBG returned the fastest rate of biodegradation (39.7 mL $CO_2 \cdot d^{-1}$), even faster than the cellulose controls in the respirometry experiments. By extension, the PBG/PLA blend also yielded a faster rate of biodegradation (10.7 mL $CO_2 \cdot d^{-1}$) than the PLA alone (8.2 mL $CO_2 \cdot d^{-1}$). The increase in the rate of biodegradation and the decrease in the hydrolysis lag phase time observed in the PLA/PBG blend when compared to the PLA suggests that the PLA/PBG blend will have better industrial composting outcomes than PLA.

Table 2.2. Modified Gompertz Model Parameters of CO_2 Production and Gaseous Carbon Loss from Samples.

Parameters	Cellulose 1	PBG	PBS	Cellulose 2	PLA	85% PLA+ 15% PBG
P_m *(mL* $CO_2 \cdot g^{-1}$ *sample)*	737.1	1106.0	1115.0	566.5	481.6	635.4
R_m *(mL* $CO_2 \cdot d^{-1}$*)*	26.2	39.7	20.3	31.1	8.2	10.7
λ (day)	-1.3	-0.5	5.4	1.2	21.7	15.0
CO_2 yield (mL $CO_2 \cdot g^{-1}$ *sample)*	762.8	1151.4	1104.8	547.0	439.8	603.4
Absolute biodegradation (%)	87.4[†]	94.1[†]	90.8[†]	60.5[*]	41.2[*]	55.7[*]
Biodegradation relative to Cellulose (%)	N/A	107.6[†]	103.9[†]	N/A[*]	66.1[*]	89.6[*]

[†]Biodegradation values determined after 90 days of testing against Cellulose 1.
[*]Biodegradation values determined after 90 days of testing against Cellulose 2.

During the initial degradation period, there was a very short lag-phase period. The lag phase time for Cellulose and PBG returned negative values of -1.3 and -0.5 days, respectively. This occurs in situations where bio-products (CO_2 was monitored in this experiment) are generated almost instantaneously without a lag period.[70] This is not

surprising for the cellulose control considering the compost inoculum is primarily composed of lignocellulosic biomass where endogenous cellulase enzymes are abundant; however, the PBG also returned a negative lag phase time, suggesting this polymer is readily deconstructed instantaneously in thermophilic composting inoculum. The instantaneous biodegradation of PBG is likely associated with both abiotic and enzymatic hydrolysis processes to afford the fast metabolism of the carbon into CO_2.

Conclusions

In this work, PBG was successfully synthesized through a melt polycondensation reaction and can be sourced using 100% bio-based monomers. PBG is readily compostable and blending PBG with PLA improves the PLA brittleness without *compromising its* degradability. Thermal properties of PBG demonstrate a lower T_g and T_m when compared to PBS due to the odd carbon atom in the diacid repeat unit, which ultimately increases the degradation rate of PBG. Blends of PLA and PBG were prepared with various compositions via solution casting and were fully characterized by thermal and mechanical testing along with AFM and SEM. Blends of PBG exhibit phase separation above 3% and enhance the mobility of PLA chains in the matrix. The tensile toughness of the blends is increased without compromising the tensile strength or modulus of PLA. The composting biodegradation also showed the PBG/PLA blend had faster degradation rate than the neat PLA during the testing period. Further work on copolymer compatibilizers is ongoing, which aim at enhancing the adhesion strength between the two components and manipulating the phase domain size, which will allow further tuning of the ultimate mechanical properties and rates of composting biodegradation.

References

1. Ishida, N.; Saitoh, S.; Ohnishi, T.; Tokuhiro, K.; Nagamori, E.; Kitamoto, K.; Takahashi, H., Metabolic engineering of Saccharomyces cerevisiae for efficient production of pure L-(+)-lactic acid. *Appl. Biochem. Biotechnol.* **2006,** *131* (1-3), 795-807.

2. Cheng, Y.; Deng, S.; Chen, P.; Ruan, R., Polylactic acid (PLA) synthesis and modifications: A review. *Front. Chem. China* **2009,** *4* (3), 259-264.

3. Auras, R.; Harte, B.; Selke, S., An overview of polylactides as packaging materials. *Macromol. Biosci.* **2004,** *4* (9), 835-64.

4. Garlotta, D., A Literature Review of Poly(Lactic Acid). *J. Polym. Environ.* **2001,** *9* (2), 63-84.

5. Lim, L.-T.; Auras, R.; Rubino, M., Processing technologies for poly (lactic acid). *Prog. Polym. Sci.* **2008,** *33* (8), 820-852.

6. Williams, C. K.; Hillmyer, M. A., Polymers from Renewable Resources: A Perspective for a Special Issue of Polymer Reviews. *Polymer Reviews* **2008,** *48* (1), 1-10.

7. Li, H.; Huneault, M. A., Effect of nucleation and plasticization on the crystallization of poly (lactic acid). *Polymer* **2007,** *48* (23), 6855-6866.

8. Huneault, M. A.; Li, H., Morphology and properties of compatibilized polylactide/thermoplastic starch blends. *Polymer* **2007,** *48* (1), 270-280.

9. Grijpma, D. W.; Nijenhuis, A. J.; Van Wijk, P. G. T.; Pennings, A. J., High impact strength as-polymerized PLLA. *Polym. Bull.* **1992,** *29*, 571-578.

10. Liu, H.; Zhang, J., Research progress in toughening modification of poly (lactic acid). *J. Polym. Sci., Part B: Polym. Phys.* **2011,** *49* (15), 1051-1083.

11. Kfoury, G.; Raquez, J.; Hassouna, F.; Odent, J.; Toniazzo, V.; Ruch, D.; Dubois, P., Recent advances in high performance poly (lactide): from "green" plasticization to super-tough materials via (reactive) compounding. *Front. Chem.* **2013,** *1* (32), 1-46.

12. Tokiwa, Y.; Calabia, B. P.; Ugwu, C. U.; Aiba, S., Biodegradability of Plastics. *Int. J. Mol. Sci.* **2009,** *10* (9), 3722-3742.

13. Xie, L.; Xu, H.; Niu, B.; Ji, X.; Chen, J.; Li, Z. M.; Hsiao, B. S.; Zhong, G. J., Unprecedented Access to Strong and Ductile Poly(lactic acid) by Introducing In Situ Nanofibrillar Poly(butylene succinate) for Green Packaging. *Biomacromolecules* **2014,** *15* (11), 4054-4064.

14. Hosseinnezhad, R.; Vozniak, I.; Morawiec, J.; Galeski, A.; Dutkiewicz, S., In situ generation of sustainable PLA-based nanocomposites by shear induced crystallization of nanofibrillar inclusions. *RSC Adv.* **2019,** *9* (52), 30370-30380.

15. Labrecque, L.; Kumar, R.; Dave, V.; Gross, R.; McCarthy, S., Citrate Esters as Plasticizers for poly (lactic acid). *J. Appl. Polym. Sci.* **1997,** *66* (8), 1507-1513.

16. Ljungberg, N.; Wesslén, B., The Effects of Plasticizers on the Dynamic Mechanical and Thermal Properties of poly(lactic acid). *J. Appl. Polym. Sci.* **2002,** *86* (5), 1227-1234.

17. Ali, F.; Chang, Y.; Kang, S.; Yoon, J., Thermal, mechanical and rheological properties of poly (lactic acid)/epoxidized soybean oil blends. *Polym. Bull.* **2009,** *62*, 91-98.

18. Kulinski, Z.; Piorkowska, E., Crystallization, structure and properties of plasticized poly (L-lactide). *Polymer* **2005,** *46* (23), 10290-10300.

19. Sheth, M.; Kumar, R. A.; Davé, V.; Gross, R. A.; McCarthy, S. P., Biodegradable Polymer Blends of Poly (lactic acid) and Poly (ethylene glycol). *J. Appl. Polym. Sci.* **1997,** *66* (8), 1495-1505.

20. Zhang, L.; Xiong, C.; Deng, X., Biodegradable Polyester Blends for Biomedical Application. *J. Appl. Polym. Sci.* **1995,** *56* (1), 103-112.

21. Park, J. W.; Im, S. S., Phase Behavior and Morphology in Blends of poly (L-lactic acid) and Poly (butylene succinate). *J. Appl. Polym. Sci.* **2002,** *86* (3), 647-655.

22. Jiang, L.; Wolcott, M. P.; Zhang, J., Study of Biodegradable Polylactide/Poly(butylene adipate-co-terephthalate) blends. *Biomacromolecules* **2006,** *7* (1), 199-207.

23. Vieira, M. G. A.; da Silva, M. A.; dos Santos, L. O.; Beppu, M. M., Natural-based plasticizers and biopolymer films: A review. *Eur. Polym. J.* **2011,** *47* (3), 254-263.

24. An, Y.; Ding, Y.; Tan, J.; Yang, W., Influences of Polyester Plasticizers on the Properties of Oil Resistance Flexible Poly (vinyl chloride) and Powder Nitrile Butadiene Rubber Blends. *Adv. Sci. Lett.* **2011,** *4* (3), 875-879.

25. Jia, P.; Xia, H.; Tang, K.; Zhou, Y., Plasticizers Derived from Biomass Resources: A Short Review. *Polymers* **2018,** *10* (12), 1303.

26. Wang, R.; Wang, S.; Zhang, Y.; Wan, C.; Ma, P., Toughening Modification of PLLA/PBS Blends via in Situ Compatibilization. *Polym. Eng. Sci.* **2009,** *49* (1), 26-33.

27. Su, S.; Kopitzky, R.; Tolga, S.; Kabasci, S., Polylactide (PLA) and Its Blends with Poly(butylene succinate) (PBS): A Brief Review. *Polymers* **2019,** *11* (7), 1193.

28. Bhatia, A.; Gupta, R. K.; Bhattacharya, S. N.; Choi, H. J., Compatibility of biodegradable poly (lactic acid)(PLA) and poly (butylene succinate)(PBS) blends for packaging application. *Korea-Australia Rheology Journal* **2007,** *19* (3), 125-131.

29. Hassan, E.; Wei, Y.; Jiao, H.; Muhuo, Y. J. J. o. f. B.; Informatics, Dynamic Mechanical Properties and Thermal Stability of Poly (lactic acid) and Poly (butylene succinate) blends Composites. *J. Fiber Bioeng. Inform.* **2013,** *6* (1), 85-94.

30. Wcisłek, A.; Sonseca Olalla, A.; McClain, A.; Piegat, A.; Sobolewski, P.; Puskas, J.; El Fray, M., Enzymatic Degradation of Poly (butylene succinate) Copolyesters Synthesized with the Use of Candida antarctica Lipase B. *Polymers* **2018,** *10* (6), 688.

31. Muthuraj, R.; Misra, M.; Mohanty, A. K., Hydrolytic degradation of biodegradable polyesters under simulated environmental conditions. *J. Appl. Polym. Sci.* **2015,** *132* (27), 42189.

32. Benali, S.; Aouadi, S.; Dechief, A.; Murariu, M.; Dubois, P., Key factors for tuning hydrolytic degradation of polylactide/zinc oxide nanocomposites. *Nanocomposites* **2015,** *1* (1), 51-61.

33. Haider, T. P.; Völker, C.; Kramm, J.; Landfester, K.; Wurm, F. R., Plastics of the Future? The Impact of Biodegradable Polymers on the Environment and on Society. *Angew. Chem., Int. Ed.* **2019,** *58* (1), 50-62.

34. Siparsky, G. L.; Voorhees, K. J.; Dorgan, J. R.; Schilling, K., Water Transport in Polylactic Acid (PLA), PLA/Polycaprolactone Copolymers, and PLA/Polyethylene Glycol Blends. *J. Environ. Polym. Degrad.* **1997,** *5* (3), 125-136.

35. Wang, Y.; Xiao, Y.; Duan, J.; Yang, J.; Wang, Y.; Zhang, C., Accelerated hydrolytic degradation of poly(lactic acid) achieved by adding poly(butylene succinate). *Polym. Bull.* **2016,** *73*, 1067-1083.

36. Bunn, C. W., The Melting Points of Chain Polymers. *J. Polym. Sci.* **1955,** *16* (82), 323-343.

37. Woodard, L. N.; Grunlan, M. A., Hydrolytic Degradation and Erosion of Polyester Biomaterials. *ACS Macro Lett.* **2018,** *7* (8), 976-982.

38. Jansen, M. L.; van Gulik, W. M., Towards large scale fermentative production of succinic acid. *Curr. Opin. Biotechnol.* **2014,** *30*, 190-197.

39. Stadler, B. M.; Wulf, C.; Werner, T.; Tin, S.; de Vries, J. G., Catalytic Approaches to Monomers for Polymers Based on Renewables. *ACS Catal.* **2019,** *9* (9), 8012-8067.

40. Li, W.; Ma, L.; Shen, X.; Wang, J.; Feng, Q.; Liu, L.; Zheng, G.; Yan, Y.; Sun, X.; Yuan, Q., Targeting metabolic driving and intermediate influx in lysine catabolism for high-level glutarate production. *Nat. Commun.* **2019,** *10*, 3337.

41. Wang, J.; Wu, Y.; Sun, X.; Yuan, Q.; Yan, Y., De Novo Biosynthesis of Glutarate via α-Keto Acid Carbon Chain Extension and Decarboxylation Pathway in Escherichia coli. *ACS Synth. Biol.* **2017,** *6* (10), 1922-1930.

42. Isikgor, F. H.; Becer, C. R., Lignocellulosic biomass: a sustainable platform for the production of bio-based chemicals and polymers. *Polym. Chem.* **2015,** *6* (25), 4497-4559.

43. D5338-15, Standard Test Method for Determining Aerobic Biodegradation of Plastic Materials Under Controlled Composting Conditions, Incorporating Thermophilic Temperatures. ASTM: 2015.

44. Kirsten, W. J., Automatic Methods for the Simultaneous Determination of Carbon, Hydrogen, Nitrogen, and Sulfur, and for Sulfur Alone in Organic and Inorganic materials. *Analytical Chemistry* **1979,** *51* (8), 1173-1179.

45. Wang, S.; Lydon, K. A.; White, E. M.; Grubbs, J. B.; Lipp, E. K.; Locklin, J.; Jambeck, J. R., Biodegradation of Poly(3-hydroxybutyrate-co-3-hydroxyhexanoate) Plastic under Anaerobic Sludge and Aerobic Seawater Conditions: Gas Evolution and Microbial Diversity. *Environ. Sci. Technol.* **2018,** *52* (10), 5700-5709.

46. Yoon, Y.; Kim, S.; Oh, S.; Kim, C., Potential of anaerobic digestion for material recovery and energy production in waste biomass from a poultry slaughterhouse. *Waste Management* **2014,** *34* (1), 204-209.

47. Costa, J. C.; Barbosa, S. G.; Alves, M. M.; Sousa, D. Z., Thermochemical pre-and biological co-treatments to improve hydrolysis and methane production from poultry litter. *Bioresour. Technol.* **2012,** *111*, 141-147.

48. Zwietering, M. H.; Jongenburger, I.; Rombouts, F. M.; van 't Riet, K., Modeling of the Bacterial Growth Curve. *Appl. Environ. Microbiol.* **1990,** *56* (6), 1875-1881.

49. Nisoli, A.; Doherty, M. F.; Malone, M. F., Feasible Regions for Step-Growth Melt Polycondensation Systems. *Ind. Eng. Chem. Res.* **2004,** *43* (2), 428-440.

50. Gupta, S. K.; Kumar, A., *Reaction Engineering of Step Growth Polymerization*. Plenum Press: New York, 1987.

51. Bhaumik, D.; Mark, J. E., Odd-even variations in the melting points of some ethylene polyesters. *Makromol. Chem.* **1986,** *187* (5), 1329-1334.

52. Rickert, S. E.; Baer, E.; Wittmann, J. C.; Kovacs, A. J., Epitaxial Crystallization of Polyesters on Inorganic and Organic Substrates. *J. Polym. Sci., Polym. Phys. Ed.* **1978,** *16* (5), 895-906.

53. Stempfle, F.; Ortmann, P.; Mecking, S., Long-Chain Aliphatic Polymers To Bridge the Gap between Semicrystalline Polyolefins and Traditional Polycondensates. *Chem. Rev.* **2016,** *116* (7), 4597-4641.

54. Korshak, V. V.; Vinogradova, S. V., *Polyesters*. Pergamon Press: New York, 1965.

55. Maiza, M.; Benaniba, M. T.; Quintard, G.; Massardier-Nageotte, V., Biobased additive plasticizing Polylactic acid (PLA). *Polímeros* **2015,** *25* (6), 581-590.

56. Cicogna, F.; Coiai, S.; De Monte, C.; Spiniello, R.; Fiori, S.; Franceschi, M.; Braca, F.; Cinelli, P.; Fehri, S. M. K.; Lazzeri, A.; Oberhauser, W.; Passaglia, E., Poly(lactic acid) plasticized with low-molecular-weight polyesters: structural, thermal and biodegradability features. *Polym. Int.* **2017,** *66* (6), 761-769.

57. Fischer, E. W.; Sterzel, H. J.; Wegner, G., Investigation of the structure of solution grown crystals of lactide copolymers by means of chemical reactions. *Kolloid-Zeitschrift und Zeitschrift für Polymere* **1973,** *251*, 980-990.

58. Kamthai, S.; Magaraphan, R. In *Thermal and mechanical properties of polylactic acid (PLA) and bagasse carboxymethyl cellulose (CMCB) composite by adding isosorbide diesters*, AIP Conf. Proc. , Jana, S. C., Ed. 2015; p 060006.

59. Shi, X.; Zhang, G.; Phuong, T. V.; Lazzeri, A., Synergistic Effects of Nucleating Agents and Plasticizers on the Crystallization Behavior of Poly(lactic acid). *Molecules* **2015,** *20* (1), 1579-1593.

60. Silverajah, V. S. G.; Ibrahim, N. A.; Yunus, W. M. Z. W.; Hassan, H. A.; Buong, W. C., A Comparative Study on the Mechanical, Thermal and Morphological Characterization of Poly(lactic acid)/Epoxidized Palm Oil Blend. *Int. J. Mol. Sci.* **2012,** *13* (5), 5878-98.

61. Dalnoki-Veress, K.; Forrest, J. A.; Stevens, J. R.; Dutcher, J. R., Phase separation morphology of spin-coated polymer blend thin films. *Phys. A* **1997,** *239* (1-3), 87-94.

62. Heriot, S. Y.; Jones, R. A. L., An interfacial instability in a transient wetting layer leads to lateral phase separation in thin spin-cast polymer-blend films. *Nat. Mater.* **2005,** *4* (10), 782-786.

63. Krause, S., Polymer Compatibility. *J. Macromol. Sci. , Rev. Macromol. Chem.* **1972,** *7* (2), 251-314.

64. Sangeetha, V. H.; Deka, H.; Varghese, T. O.; Nayak, S. K., State of the Art and Future Prospectives of poly (Lactic acid) Based Blends and Composites. *Polym. Compos.* **2018,** *39* (1), 81-101.

65. Vignjevic, R.; Djordjevic, N.; Vuyst, T. D.; Gemkow, S., Modelling of strain softening materials based on equivalent damage force. *Computer Methods in Applied Mechanics and Engineering* **2018,** *335*, 52-68.

66. Wang, P.; Hutchings, I. M.; Duncan, S. J.; Jenkins, L.; Woo, E., Strain whitening of a thermoplastic olefin material. *J. Mater. Sci.* **2006,** *41* (15), 4847-4859.

67. Bagheri, R.; Pearson, R. A., The use of microvoids to toughen polymers. *Polymer* **1995,** *36* (25), 4883-4885.

68. La Mantia, F. P.; Morreale, M.; Botta, L.; Mistretta, M. C.; Ceraulo, M.; Scaffaro, R., Degradation of polymer blends: A brief review. *Polym. Degrad. Stab.* **2017,** *145*, 79-92.

69. D6400-12, Standard Specification for Labeling of Plastics Designed to be Aerobically Composted in Municipal or Industrial Facilities. ASTM: 2012.

70. Shen, J.; Zhu, J., Development of General Gompertz Models and Their Simplified Two-Parameter Forms Based on Specific Microbial Growth Rate for Microbial Growth, Bio-Products and Substrate Consumption. *Advances in Biotechnology & Microbiology* **2017,** *4* (3), 0064-0074.

CHAPTER 3

POLY(BUTYLENE GLUTARATE) AS A PROCESSSING AID FOR HOT-MELT EXTRUSION OF POLY(HYDROXYALKANOATE)[2]

[2] Holt, A. and Locklin, J. To be submitted to *Journal of Applied Polymer Science.*

Abstract

Poly(butylene glutarate), PBG was first used as a novel processing aid for poly(hydroxyalkanoate), PHA in hot-melt extrusion. Various compositions of PHA/PBG blends were prepared at weight ratios of 100/0, 95/5, 90/10, 85/15, and 80/20. The rheological, thermal, mechanical, and morphological properties were investigated by means of rheological test, melt flow index (MFI), dynamic mechanical analysis (DMA), differential scanning calorimetry (DSC), tensile test, and atomic force microscopy-infrared spectroscopy (AFM-IR). It was found that the presence of PBG reduced the melt viscosity but increased the flowability of PHA. By the incorporation of PBG, the storage modulus, loss modulus, and glass transition temperature (Tg) decreased with the increasing PBG content. These results are attributed to the increase of molecular chain mobility of PHA and therefore reduce its viscosity. In addition, morphology of the blends showed an immiscible two-phase system with PBG dispersed in the PHA matrix. Compared with neat PHA, the concentration with 5 wt % PBG increased the % elongation at break about 155.1%. However, the % elongation at break of the PHA/PBG blends was decreased as the loading of PBG further increased above 5 wt %. As the results, the concentration of 10 wt % PBG has been considered as a better balance performance between mechanical and rheological properties. This optimum addition level of 10 wt % was selected to evaluate the processability in the commercial scale extruder compared with the neat PHA. Due to the processing aid effect by PBG, it has demonstrated that the extrusion pressure and melt fracture were eliminated during the extrusion process.

Introduction

Hot-melt extrusion is one of the most widely used processing techniques in the plastic industries.[1] Many commercial polymers such as polyolefins, polyamides, and polyesters undergo a processing step from a reactor tank to an extruder in order to produce final products. Currently, more than half of all plastic products, including plastic bags, sheets, and pipes, are manufactured by this process.[2] In the extrusion process, raw materials which can be solid, or liquid are first fed through a feeder or an injection pump into a barrel. With a rotating screw under elevated temperature inside the barrel, polymers are melted, mixed, and formed into uniformly molten polymer. Finally, the molten materials exist the extruder through a die and form into products of different shapes. Extrusion system is an efficient technology offering a continuous process and inexpensive way for the processing of polymers.[3] With this processing technique, consistent products can be manufactured at high output rates with low cost. Extrusion also provides a more environmentally friendly process as the products are produced in solvent-free conditions.[4]

In extrusion processes, extrudate distortion known as melt fracture is one of the common problems when extruding plastics.[5] During extrusion, molten polymers are forced to extrude through the barrel and die at high flow rate for the efficiency of production process. At this high flow rate, melt polymers are subjected to high shear stresses and exhibit flow instabilities causing the extrudate surface becomes visibly rough leads to unacceptable products which made them worthless.[6] Processing aids are often added during the extrusion to improve the processability. The role of processing aids enables high molecular weight polymers to be processed at high shear rate without melt fracture. The addition of processing aids results in good-quality product that are produce at higher output

rate.[7] Fluoropolymer, stearates, and polymer blends are common processing additives using in the extrusion of molten polymers.[8]

Owing to current environmental issues and public awareness of eco-friendly alternatives, the use of bio-based or biodegradable plastics has become an attempt to replace petroleum-based plastics.[9, 10] The development of bio-based or biodegradable processing aids can play a crucial role in helping to reduce the dependence on fossil-based resources and offer fully environmentally friendly when blends with other bio-based or biodegradable materials. Poly(butylene glutarate) (PBG) is an aliphatic polyester containing odd-even carbon monomers of glutaric acid and butanediol. These low-cost monomers can be derived from renewable agricultural resources. The thermal properties of bio-based PBG showed significantly low glass transition temperature, T_g (-60°C) and low melting temperature, T_m (38°C). Moreover, composting biodegradation of PBG is comparable to cellulose. Within 90 days in a respirometer operated at 58°C, PBG and cellulose have achieved 94.0% and 87.4% biodegradation.[11] As an additive, PBG has been used for poly(lactic acid) in toughness improvement and acceleration of composting biodegradation. The addition of PBG resulted in decrease in T_g and increase of % elongation at break due to an increase in the PLA chain mobility.[11]

Along with environmental concerns, several studies have shown that poly(hydroxyalkanoate) (PHA) is one of the most promising material that can replace non-biodegradable synthetic plastics.[12, 13] PHA obtained by bacterial synthesis shows biodegradable behaviors in all aerobic and anaerobic environments and can be used to make completely compostable, and soil and marine biodegradable products.[14] Currently, most of industrial efforts aimed at extrusion the PHA into commercial products on

industrial scale. By blending with additives or other polymers, thermal and mechanical properties of PHA and be modified and thereby improved for various applications.[15, 16]

Based on the properties of PBG that is eco-friendly and has low softening temperature, it is reasonable to expect that PBG can be used as a good plasticizer or processing aid for PHA. In this work, we reported the first investigation on the performance of PBG as an effective additive for PHA in the hot-melt extruder. With the aim to be able to extrude the PHA for industrial applications, the appropriate extrusion condition of PHA was first examined. The effects of the extrusion conditions caused by thermo-mechanical degradation were determined by molecular weight measurements using gel permeation chromatography (GPC). Then, the effects of PBG on melt viscosity, flowability, and viscoelastic properties were investigated by rheological test, melt flow index (MFI), and dynamic mechanical analysis (DMA).

Moreover, the thermal and mechanical properties, and phase morphology of the PHA/PBG blends were characterized by differential scanning calorimetry (DSC), tensile test, and atomic force microscopy-infrared spectroscopy (AFM-IR). All the analyses were performed to assess the suitability concentration of PBG for using in the commercial scale extruder. Finally, the processability of selected PHA/PBG blend was evaluated and the effect of PBG on the instability (melt fracture) elimination was also discussed. The results of this study will provide industrial product development perspectives for PHA.

Experimental Section

1. Materials

PHA in powder form with comonomer unit of 3-hydroxyhexanoate (Hx) molar fraction of 5.6% were provided by RWDC. The number average molecular weight (M_n),

weight average molecular weight (M_w) and polydispersity index (PDI) are 429.7 kg/mol, 744.0 kg/mol, and 1.7, respectively. The PBG used in this study was synthesized through a melt polycondensation reaction according to the method reported in the literature.[11] The M_n, M_w and PDI are 28.9 kg/mol , 53.3 kg/mol, 1.8, respectively. All chemicals were used without further purification for the blends. HPLC grade chloroform ($CHCl_3$) was purchased from JT Baker, U.S.A. Silicon wafers used as substrates were purchased from UniversityWafer Inc.

2. Sample preparations

2.1. Processing Condition

PHA is highly moisture sensitive and can be naturally degraded by the simple hydrolysis of ester bonds in the presence of water. Thus, prior to the blending process, the PHA was dried in a vacuum oven at 60 °C for 48 h. PHA is also prone to degrade when exposes to high processing temperature and to relevant mechanical stresses. Therefore, it is important to check first and find the appropriate extrusion condition. The effects of thermo-mechanical degradation during extrusion were investigated by varying the screw speeds (30, 60, 100 rpm) and varying barrel temperatures (150, 160, 170, 180 °C). The total input of material approximately 7 g was melt processed using a laboratory scale twin-screw extruder (MiniLab II HaakeTM Rheomex CTW 5) with a residence time of 6 min. Molecular weight variations as consequence of temperature and screw speed profiles were monitored to provide evidence of degradation.

2.2 Preparation of PHA and PBG blends for characterizations

PBG was added at five concentrations, 0, 5, 10, 15, 20 wt %, based on 100 parts of PHA. The extrusion procedure was conducted according to the screw speed and

temperature profiles suggested based on above finding in Minilab micro-compounder which are 30 rpm and 150 °C. This Minilab micro-compounder allows the preparation of small batches of 7g. After the mixing step, the tensile and DMA specimens were prepared by means of an injection molding machine (HAAKE MiniJet II). The temperature of the heated cylinder was 155 °C and the mold was heated to 40 °C. A pressure of 650 bars was used for the injection for 5 seconds and a post-pressure of 400 bar was used for 2 seconds. The dimensions of the dog-bone bars complied with the standard ASTM D638 type V,[17] while dimensions of DMA bars were 60 mm x 11 mm x 3mm.

2.3 Preparation of PHA and PBG blend to verify the processability.

The blend of PHA with 10% PBG was selected to evaluate the processability in the commercial scale extruder compared with the neat PHA. In this blending process, melt-extrusion of 300 g was carried on a twin-screw extruder MIC18PH/6L-35D (Leistritz) with a screw diameter of 18 mm and an L/D ratio of 40:1. The screw speed during processing was 50 rpm, and the temperature profile from feed zone to die zone was the following: Z1= 157 °C, Z2 = 157 °C, Z3 = 150 °C, Z4 = 150 °C, Z5 = 150 °C, Z6 = 140 °C, Z7= 120 °C. The extrudate was quenched in a water bath at 55 °C after exiting from the extruder and allowed to rest at room temperature before it entered the winding machine.

3. Characterizations

3.1 Gel Permeation Chromatography (GPC)

The molecular weight and molecular weight distribution of samples were determined by using a OMNISEC RESOLVE (Malvern) equipped with refractometer, right angle and low angle light scattering detector (RALS/LALS), and viscometer. GPC columns packed with porous poly (styrene-co-divinylbenzene) particles regulated at a

temperature of 35 °C. HPLC grade chloroform was used as the eluent and permeated through the columns at the flow rate of 1 mL/min. Filtered sample solution at concentrations of 1 mg/mL was injected into the system. The data collected were processed and analyzed using OMISEC- v11.10 software.

3.2 Rheological test

Rheological test was performed at 150 °C and screw speeds between 25 to 250 rpm in a lab-scale co-rotating twin screws extruder with a backflow channel (MiniLab II HaakeTM Rheomex CTW 5). The samples approximately 5 g were processed in recirculating mode for 6 min before measuring the viscosity. The rheological test itself is done and controlled by the HAAKE PolySoft OS Software. The backflow channel in the MiniLab is constructed as a rheological slit capillary with two pressure sensors. The rheological information about the viscosity of the samples can be calculated according to the Equation S3.

3.3 Melt flow index (MFI)

MFI is the mass flow rate expressed in gram mass per 10 minutes. MFI of PHA blended with PBG were measured using MP1200 (Tinius Olsen). The sample of 4 g was heated for 5 minutes in the barrel and extruded through the die under a constant load 2.16 kg at 165 °C. A 100 g rod was used as a plunger and the results of MFI were averaged from three replicate measurements.

3.4 Dynamic Mechanical Analysis (DMA)

DMA of the PHA-based blends were investigated using a DMA Q800 (TA Instruments). Rectangular specimens of about 1 x 10 mm (thickness x width) were used for analysis. All samples were gripped by tension clamps with a clamp compliance of 6

in.lb. The oscillatory frequency of the dynamic test was 1 Hz. The temperature was raised at rate 3 °C/min in the range of -25 °C to 125 °C.

3.5 Differential Scanning Calorimetry (DSC)

Thermal analysis was performed using DSC 250 (TA Instruments) under a nitrogen flow. The weight of sample was about 5-6 mg. All samples were heated to 180 °C at a rate of 10 °C/min and held for 1 min to eliminate thermal history. Then, they were cooling to -80 °C at a cooling rate of 10 °C/min to investigate the crystallization peaks. After holding at -80 °C for 1 min, the sample were reheated again to 180 °C to obtain T_g and T_m values.

3.6 Atomic Force Microscopy-Infrared Spectroscopy (AFM-IR)

The AFM-IR data in this study were obtained by using a NanoIR3 system (Bruker). Contact mode with an AFM tip (Anasys Instruments Inc) which has a resonance frequency of 13 ± 4 kHz and a spring constant of 0.07-0.4 N/m were used for scanning. The scan rate was 0.25 Hz, and the scan size was 2.5 x 2.5 µm. The height images were acquired simultaneously with IR maps at ambient conditions. IR maps at 1730 cm^{-1} and 1170 cm^{-1} wavenumbers were obtained to study the phase separated morphology of the films. The film samples for AFM-IR were prepared by spin coating onto silicon wafers coated with native oxide (UniversityWafer, Inc). PHA/PBG with various blend ratios (0-20%wt PBG) was dissolved in $CHCl_3$ overnight to make 10 mg/mL solution. The spin coating was carried out by using 200 µL of the solution at 2000 rpm at room temperature on the clean silicon wafers (2.5 cm × 2.5 cm). Film thickness was measured using spectroscopic ellipsometry (J.A. Woollam, M-2000V).

3.7 Tensile test

The tensile properties of the neat PHA and the blends were measured using a tensile testing (Shimadzu, AGS-X series). The type V dog-bone specimens were prepared from injection molding according to ASTM D638 which have an overall length of 63.5 mm, width of 3.18 mm, and thickness of 3.20 mm.[17] All specimens were tested at room temperature with a crosshead speed of 5 mm/min and a 7.62-mm gauge length. Results from three specimens were average.

Results and Discussion

1. Finding the extrusion condition/Survey of Processing Methods for PHA.

As starting point, the goal of this experiment was to identify the appropriate extrusion condition of PHA by quantifying degradation from molecular weight measurements. Various extrusion screw speeds and temperatures were investigated as an extrusion time of 6 min. The decrease of molecular weight caused by thermo-mechanical degradation are shown in Table 3.1. At temperature 150°C, by increasing the screw speed from 30 to 100 rpm, the decrease of weight average molecular weight (M_w) from 600.7 g/mol down to 481,666 g/mol. The assessment of the impact of the temperature also investigated and it showed that the increase of temperature has triggered a drastic degradation of the PHA chains as evidenced by the decrease of Mw. The use of the highest processing temperature at 180°C resulted in a significant decrease to 245.9 g/mol. From these results, in order to preserve the Mw, screw speed and temperature were set to 30 rpm and 150°C as this condition could be used to process PHA without a significant reduction of M_w.

Table 3.1. Effects of the extrusion temperatures and screw speeds on the PHA weight average molecular weight (M_w), number average molecular weight (M_n), and polydispersity index (M_w/M_n)

Sample	Temperature (°C)	Screw speed (rpm)	M_n (kg/mol)	M_w (g/mol)	M_w/M_n
1	150	30	338.0	600.7	1.8
2	150	60	275.3	546.6	2.0
3	150	100	340.8	481.7	1.4
4	160	30	288.8	522.1	1.8
5	170	30	184.1	364.2	2.0
6	180	30	86.7	245.9	2.6

2. Relative melt viscosity

Measuring the rheological data can be conducted directly in the lab-scale extruder. The MiniLab determined the viscosity by using the backflow channel as a slit capillary. Shear rate (γ), shear stress (τ), and relative melt viscosity (η) were calculated by equation A1. The η values versus shear rates curves at 150°C were shown in Figure 3.1. It was observed that the values of η decreased with increasing shear rate. This shear thinning behavior is a common property of polymer melts under shear flow.[18] From Figure 3.1, it is clear that the addition of PBG has a significant effect on the viscosity of PHA. Compared with that of neat PHA, the values of η decreased in all sets of blends. It is obvious that these values systematically dropped with the increase of PBG content. At

highest PBG concentration (20 wt %), the η values were below 600 Pa.s at 150°C. The results from this rheology study gave credence to the use of PBG as a processing aid for PHA.

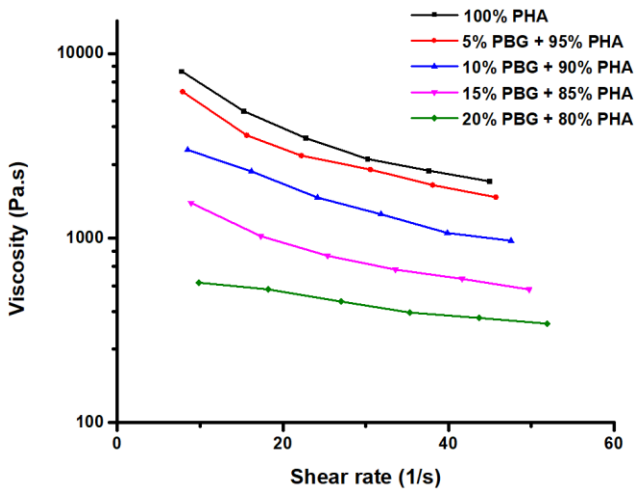

Figure 3.1. The rheological plot of PHA/PBG blends at 150C: (a) 95% PHA+ 5% PBG, (b) 90% PHA+ 10% PBG, (c) 85% PHA+ 15% PBG, (b) 80% PHA+ 20% PBG.

3. Flow properties of PHA/PBG blends

MFI is used to determine the flow properties of melt polymers at limited intervals of time. It refers to the number of grams of melt polymer that are pushed out of the die within 10 minutes under the load. Table 3.2 shows the effects of adding PBG at 5,10, 15 and 20 wt % in PHA on the MFI. It was observed that the values of MFI for all samples were higher than those of neat PHA. Evidently, the value of MFI increased with increasing PBG content. The effect of rising MFI is related to the higher mobility of the polymer chains. This result is caused by the interaction between the PBG and PHA matrix, which reduce the viscosity of PHA to be more mobile. The MFI data correlates well with the rheological analysis.

Table 3.2. Effect of PBG contents on MFI in the blends.

Samples	Melt Flow Index (g/10 minutes)
100% PHA	1.4
95% PHA + 5% PBG	1.6
90% PHA + 10% PBG	2.0
85% PHA + 15% PBG	3.1
80% PHA + 20% PBG	6.4

4. Viscoelastic properties

DMA analysis was used to investigate the viscoelastic properties and transition of the blends. The curves of the storage modulus (E'), loss modulus (E"), and tan delta (tan δ) as a function of temperature are given in Figure B.1. The lower E' of all blended PHA with PBG compared to neat PHA can be seen in Table 3.3. which indicated the increase in the flexibility of PHA imparted by the PBG. With increasing PBG loading up to 20 wt %, the value of E' showed a noticeable decrease from 4823 MPa to 2710 MPa. When the temperature elevated above 0°C, E' of all samples decreased very sharply as entering to the glassy region. The glass transition temperatures (T_g) are given in Table 3.1 and showed that measured values decreased from 3.8°C to -1.3°C. As observed, the peak intensity of E'' decreased significantly with increasing PBG content, from 501.3 MPa for neat PHA to 175.3 MPa for 20 wt % PBG loading. The drop in E'' was due to a decrease in melt viscosity. Besides, the tan δ peak shifted to lower temperature with increasing PBG content

in the blends. The shifts in T_g and decreases in E' were associated with the increased mobility of PHA polymer chain. From these results, it was proven that an increase in the amount of PBG from 5% -20% had increase the mobility of PHA polymer chain by acting as a good processing aid.

Table 3.3. DMA data of PHA/ PBG blends.

Sample	PHA/PBG content (wt %)	Storage Modulus (MPa)	T_g (°C)	Loss Modulus (Top peak) (MPa)	Tan Delta (Top peak)
1	100/0	4823	3.8	501.3	0.2
2	95/5	4095	3.3	342.0	0.1
3	90/10	3884	2.1	295.0	0.1
4	85/15	3748	0.5	286.7	0.1
5	80/20	2710	-1.3	175.3	0.1

5. Thermal properties

The DSC analysis was conducted to determine the exothermic crystallization process and endothermic melting process of PHA/PBG blends. Table B.2 summarizes the main thermal parameters such as T_c, T_g, and T_m corresponding to the DSC thermograms shown in Figure 3.2. As shown in Figure 3.2a, the crystallization peak of pure PHA was detected at 79.2°C. After addition of PBG into PHA, sharp narrow crystallization peaks were detected at around 87-89 °C. These crystallization peaks have shifted to a higher

temperature indicated that the presence of PBG enhanced the crystallization rate of PHA. This means that PBG can act as heterogeneous nucleation seeds for PHA. It is important to note that when PBG loading increase above 10 wt %, a small exotherm can be found at -16.5 °C which related to the crystallization peak of PBG.

Figure 3.2b showed endothermic thermograms that were detected from the second heating. This DSC curves showed that all the blends had multiples thermal transitions, suggesting that the blends were immiscible. The heating curves of each blend had two T_m, where their values are close to that of pure components of blends. The blends containing PBG showed a lower T_g with increasing PBG content. The T_g decreased from 2.7 °C (neat PHA) to 0.5 °C (PHA/20 wt% PBG). This indicates that the mobility of PHA chains is enhanced due to the presence of PBG.

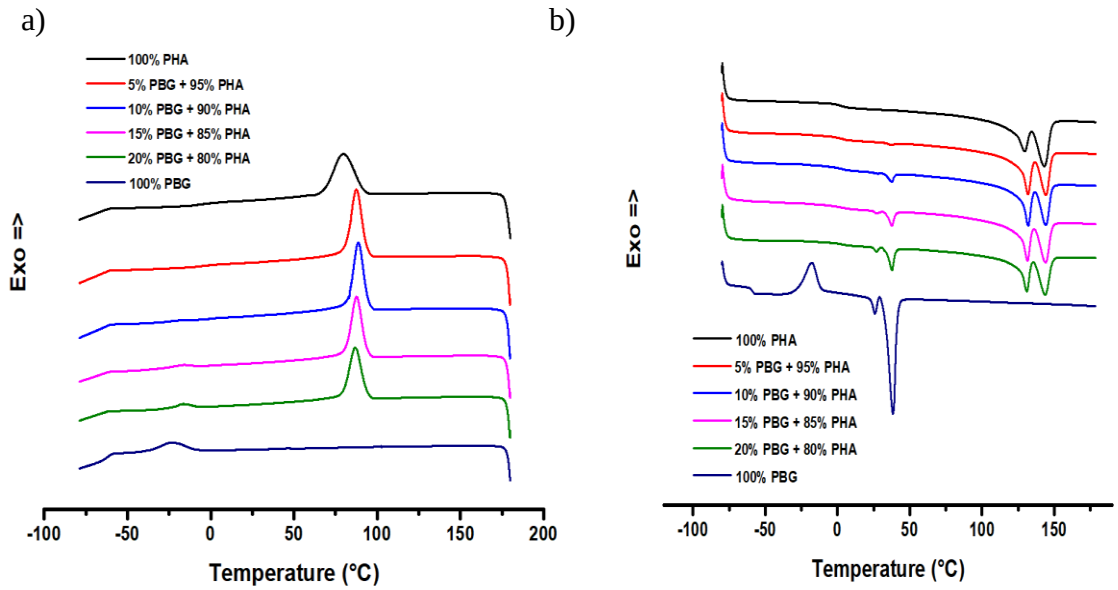

Figure 3.2. DSC cooling scan (a) and DSC second heating scan (b) of PA and PLA/PBG blends.

6. Phase morphology

AFM height images were investigated for the different weight ratios between PHA and PBG (100/0, 95/5, 90/10, 85/15, and 80/20). Their results are presented in Figure 3 and their spin-coated films thickness is reported in Table 3.4. It can be seen that the neat PHA shows a relatively smooth surface morphology compared to the blends. By addition of PBG, the micro-structured two-phase morphology was observed, which indicated that PHA/PBG blends are not miscible. It appears that PBG dispersed in the PHA matrix and formed micro-voids. Figure B.2-B.3 shows IR mapping images of PHA with 15 wt % PBG taken at 1730 cm^{-1} and IR mapping images of PHA with 20 wt % PBG taken at 1170 cm^{-1} This absorption wavenumber is dominant in the micro-voids, indicating the presence of PBG.

In the PHA/PBG blends, PBG tended to segregate from PHA matrix, and distributed in the form of small discrete droplets which can be observed as micro-voids. Because the PBG is immiscible in PHA and its viscosity is much lower that that of PHA, PBG will act as a lubricant to induce interphase slippage of the blends. As stressed by Rosenbaum et al. (1995) a potential polymer to work as a processing aid for the extrusion of another polymer should first be immiscible and have an interfacial tension with the polymer under flow smaller than the interfacial tension of the polymer under flow with the wall.[19] This mean that PBG might migrate towards the die wall surface and coat it during extrusion due to the higher affinity of PBG with the metal wall and to minimize viscous dissipation.

Figure B.4. shows the coating thickness appeared in the extruder wall after cooling the extruder at 80 °C. As expected, the deposition of PBG/PHA on the extruder wall increased with increasing PBG content. The 20 wt % PBG blended with 80 wt% PHA had the maximum coating surface compared to other blends. The neat PHA and the blend of 5 wt % PBG did not exhibit any coating area on the extruder wall. From these observations, the films that accumulated on the extruder wall confirmed that PBG coating occurred during the extrusion.

Table 3.4. Film thickness of PHA/PBG at various PBG content.

Samples	Film Thickness (nm)
100% PHA,	185.8
5% PBG + 95% PHA,	176.1
10% PBG + 90% PHA,	179.9
15%PBG + 85% PHA,	167.8
20% PBG + 80% PHA.	167.1

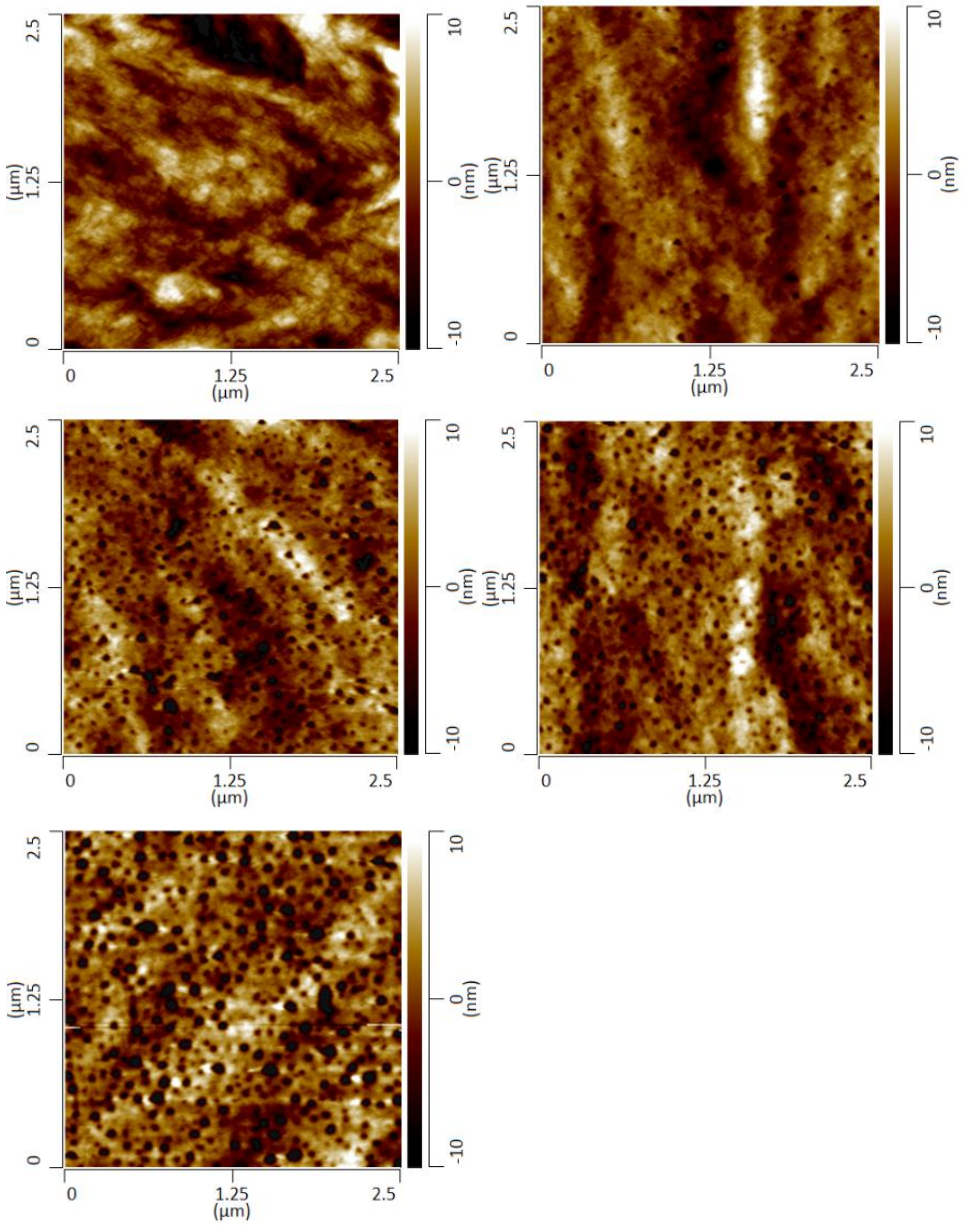

Figure 3.3. Contact-mode AFM height images of (a) 100% PHA, (b) 5% PBG + 95% PHA, (c) 10% PBG + 90% PHA, (d) 15%PBG + 85% PHA, (e) 20% PBG + 80% PHA.

7. Mechanical properties

The effect of PBG content on the mechanical properties of PHA are depicted in Figure 3.4. Stress-strain curves of the PHA/PBG blends were plotted in Figure B.5, and the extracted parameters were summarized in Table B.2. With the increasing addition of PBG, the tensile strength of samples decreased systematically from 32.7 MPa to 20.5 MPa, while tensile modulus declined slightly from 0.9 to 0.7 GPa. When the content of PBG was 5 wt %, the % elongation at break of the blends was enhanced up from 17.8 % to 41.5%. This result indicated that the ductility was improved suggesting that the loading of PBG was beneficial to improving tensile toughness. However, it could be seen form Table B.2 that further addition of PBG resulted in a reduction of the % elongation at break. When the concentration of PBG was 10%, a decrease of % elongation at break was observed with 39.6%. When PBG loading increase to 15% or above, the blends were very brittle and the % elongation at break were lower compared to the neat PHA.

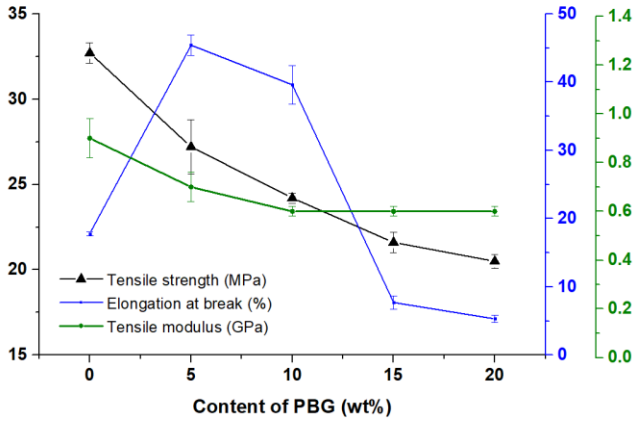

Figure 3. 4. Mechanical properties: tensile strength, tensile modulus, and % elongation at break for PHA/PBG blends with different PBG concentrations. The error bars represent standard deviations based on three repeated measurements.

8. *Processability in commercial extruder*

The objective of this experiment was to explore the processability and quality of the neat PHA filament and PHA/PBG filament that were melt processed using a commercial scale extruder. Based on the value of MFI and % elongation at break, the blend of 10% PBG with PHA was selected for this experiment. This concentration showed the best melt flow rate without compromising the % elongation at break. The other blends of PBG were not chosen because they were too brittle or had lower melt viscosity.

When the neat PHA was extruded without PBG in Leistriz, the pressure increased substantially. This intensely high melt pressure far exceeded the extruder's threshold level of 950 psi, which caused it to shut down in order to prevent damage to the extruder during the running process. However, when processing PHA with 10% PBG, the pressure was reduced to 500 psi and therefore PHA became possible to be extruded into a consistent filament. These results indicates that the PHA/PBG has lower viscosity than the neat PHA since its pressure decreases with polymer melt viscosity. The use of PBG not only can decrease the critical pressure in the extruder, but also can eliminate surface melt fracture (sharkskin) during extrusion. Figure 3.5. shows PHA filament made with and without PBG under the same condition. Clearly, sharkskin was observed on the filament without PBG.

a)

b)

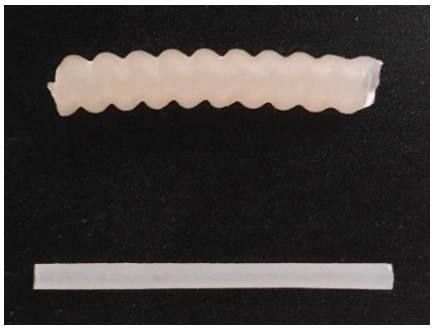

Figure 3.5. Filament extrudate without (a) and with PBG (b).

Conclusions

The extrusion of polymers is limited by flow instability which observed at high production rate. In order to overcome this problem, a processing aid is added to improve the processability of polymers. In this work, we reported the first study on the performance of PBG as a novel processing aid for PHA in hot-melt extruder. Under the processing conditions, high screw speeds and high melt temperatures in the lab-scale extruder led to thermo-mechanical degradation of PHA. The combination of a low screw speed at 30 rpm and low processing temperature at 150 °C had the least reduction of molecular weight. The wight percent ratio of PHA/PBG showed a significant influence in the rheology properties of the blends. With the increase in PBG concentration, the viscosity decreased, but the melt flow rate increased. Moreover, the DMA results showed a significant decrease in the E', E", and T_g of the samples with increasing PBG content. These results demonstrated that PBG enhanced the segmental mobility of PHA chains. In the DSC curves, PLA/PBG blends showed multiple melting peaks for each polymer which revealed the immiscible polymer blend system. The AFM measurements have confirmed the same fact. In addition, the tensile data showed that the % elongation at break of PHA/PBG blends was influenced by the concentration of PBG. For the blends containing >10 wt % PBG, the samples exhibited brittle failure in tensile testing, but there was a significant increase in % elongation at break when adding 5 wt% PBG.

References

1. Bhairav, B. A.; Kokane, P. A.; Saudagar, R. B., Hot Melt Extrusion Technique-A Review. *Research J. Science and Tech.* **2016,** *8* (3), 155-162.

2. Crowley, M. M.; Zhang, F.; Repka, M. A.; Thumma, S.; Upadhye, S. B.; Battu, S. K.; McGinity, J. W.; Martin, C., Pharmaceutical applications of hot-melt extrusion: part I. *Drug Dev Ind Pharm.* **2007,** *33* (9), 909-26.

3. Raquez, J.-M.; Narayan, R.; Dubois, P., Recent Advances in Reactive Extrusion Processing of Biodegradable Polymer-Based Compositions. *Macromol. Mater. Eng.* **2008,** *293* (6), 447-470.

4. Crawford, D. E., Extrusion - back to the future: Using an established technique to reform automated chemical synthesis. *Beilstein J. Org. Chem.* **2017,** *13*, 65-75.

5. Denn, M. M., Extrusion Instabiliies and Wall Slip. *Annu. Rev. Fluid Mech.* **2001,** *33* (1), 265-287.

6. Aarts, A. C. T. Analysis of the flow instabilities in the extrusion of polymeric melts. Ph.D. Dissertation, Eindhoven University of Technology, The Netherlands, 1997.

7. Ebnesajjad, S.; Morgan, R. A., 11 - Applications of Processing Aid Additives. In *Fluoropolymer Additives*, Ebnesajjad, S.; Morgan, R. A., Eds. William Andrew Publishing: Oxford, 2012; pp 193-209.

8. Achilleos, E. C.; Georgiou, G.; Hatzikiriakos, S. G., Role of Processing Aids in the Extrusion of Molten Polymers. *J. Vinyl Addit. Technol.* **2002,** *8* (1), 7-24.

9. Thompson, R. C.; Moore, C. J.; vom Saal, F. S.; Swan, S. H., Plastics, the environment and human health: current consensus and future trends. *Philos Trans R Soc Lond B Biol Sci* **2009,** *364* (1526), 2153-2166.

10. Song, J. H.; Murphy, R. J.; Narayan, R.; Davies, G. B. H., Biodegradable and compostable alternatives to conventional plastics. *Philos Trans R Soc Lond B Biol Sci* **2009,** *364* (1526), 2127-2139.

11. Holt, A.; Ke, Y.; Bramhall, J. A.; Crane, G.; Grubbs, J. B.; White, E. M.; Horn, J.; Locklin, J., Blends of Poly(butylene glutarate) and Poly(lactic acid) with Enhanced Ductility and Composting Performance. *ACS Applied Polymer Materials* **2021,** *3* (3), 1652-1663.

12. Muneer, F.; Rasul, I.; Azeem, F.; Siddique, M. H.; Zubair, M.; Nadeem, H., Microbial Polyhydroxyalkanoates (PHAs): Efficient Replacement of Synthetic Polymers. *J. Polym. Environ.* **2020,** *28* (9), 2301-2323.

13. Li, Z.; Yang, J.; Loh, X. J., Polyhydroxyalkanoates: opening doors for a sustainable future. *NPG Asia Mater.* **2016,** *8* (4), e265.

14. Meereboer, K. W.; Misra, M.; Mohanty, A. K., Review of recent advances in the biodegradability of polyhydroxyalkanoate (PHA) bioplastics and their composites. *Green Chem.* **2020,** *22* (17), 5519-5558.

15. Sharma, V.; Sehgal, R.; Gupta, R., Polyhydroxyalkanoate (PHA): Properties and Modifications. *Polymer* **2021,** *212*, 123161.

16. Bugnicourt, E.; Cinelli, P.; Lazzeri, A.; Alvarez, V., Polyhydroxyalkanoate (PHA): Review of synthesis, characteristics, processing and potential applications in packaging. *eXPRESS Polym. Lett.* **2014,** *8*, 791-808.

17. D638-14, Stardard Test Method for Tensile Properties of Plastics. ASTM International: West Conshohocken, PA, 2015.

18. Xu, X.; Chen, J.; An, L., Shear thinning behavior of linear polymer melts under shear flow via nonequilibrium molecular dynamics. *J. Chem. Phys.* **2014,** *140* (17), 174902.

CHAPTER 4

THE CRYSTALLIZATION AND MELTING BEHAVIORS OF POLY[(3-HYDROXYBUTYRATE)-CO-(3-HYDROXYHEXANOATE)] WITH POLY(3-HYDROXYBUTYRATE) AS A NUCLEATING AGENT[3]

[3] Holt, A.; White, E. M.; Horn, J.; Locklin, J. To be submitted to Journal of Applied Polymer Science.

Abstract

The effects of three kinds of nucleating agents: talc, boron nitride (BN) and poly(3-hydroxybutyrate) (PHB) on the crystallization of Poly[(3-hydroxybutyrate)-co-(3-hydroxyhexanoate)] (PHBHx) were studied. PHB is the most effective nucleating agent for the crystallization of PHBHx. The crystallization kinetics of neat PHBHx and PHBHx with various PHB concentration were studied by mean of differential scanning calorimetry (DSC) under the isothermal and non-isothermal crystallization process. The Avrami model was used to determine crystallization parameters such as crystallization half-time and Avrami exponent. Crystallization process of PHBHx was accelerated with the presence of PHB under both isothermal and non-isothermal condition. Modulated differential scanning calorimetry (MDSC) was used to characterize the melting behavior of the neat PHBHx and PHBHx/PHB. Multiple melting peaks were observed and identified as melting-recrystallization during the heating process. Crystal and spherulite morphology were investigated using polarized optical microscopy (POM) and atomic force microscopy (AFM). With the incorporation of PHB in PHBHx, the crystallization behavior exhibited two-crystal phases during the crystallization process. Moreover, spherulite numbers of PHBHx increase and the spherulite size was reduced with the addition of PHB. The high thermal treatment above the melting temperature of PHB does affect the nucleation efficiency. When PHB was totally melted, it will no longer nucleate PHBHx. Composting biodegradation of the neat PHBHx and PHBHx with 10wt% PHB were measured by gaseous carbon loss under aerobic conditions. The results of biodegradation in compost condition of the neat PHBHx and PHBHx with 10wt% PHB has exceeded 90% biodegradation within 90 days. Accordingly, PHB is a promising nucleating agent to create

biobased and biologically degradable alternatives to traditional inorganic nucleating agents.

Introduction

Polyhydroxyalkanoates (PHAs) are aliphatic polyesters that can be synthesized by biological fermentation from various microorganism using renewable carbon resources.[1] PHAs have received extensive study as potential substitutes for petroleum-based plastics due to their biological degradability which offer sustainable and environmental friendly alternatives.[2] There are now over 150 different types of monomers used as building blocks for PHA polymers that have been reported.[1] Based on their carbon-chain length in monomeric constituents, PHAs can be classified as short chain length PHA (sclPHA), medium-chain length PHA (mclPHA), and long-chain length PHA (lclPHA). The thermal and mechanical properties of PHAs depend on the distribution of monomer and comonomer unit composition.[3]

Poly(3-hydroxybutyrate) or PHB is the most well-studied homopolymer of these bacterial polyesters. Its monomer contains 4 carbon atoms (3-hydroxybutyrate, HB) and belongs to the sclPHA. The applications of PHB are limited due to its poor mechanical properties and lack of melt stability.[4] The high crystallinity and the effect of secondary crystallization cause a significant impact on PHB brittleness. In addition, the melting temperature (T_m) of PHB is very close to its thermal degradation temperature resulting narrow temperature window in melt processing technique. The random chain scission of PHB by internal cis elimination to yield crotonic acid is a critical drawback due to a decrease in molecular weight at processing temperature.[5]

It was found years ago that the introduction of 3-hydroxyhexanoate (Hx) comonomer unit containing 6 carbon atoms can reduce PHB high crystallinity and improve its elongation at break. Also, the increase of side chain length from HB to Hx can lower

the melting temperature. Poly[(3-hydroxybutyrate)-co-(3-hydroxyhexanoate)] or PHBHx that contained 10% of Hx has an increase of elongation at break from 5% to 400%, and the melting temperature decreases from 177°C to 127°C.[6] Unfortunately, the PHBHx containing Hx comonomer has a low crystallinity and a slow crystallization rate, and this problem become more serious with increasing Hx content.[7] The rate of crystallization is an important parameter for industrial process such as extrusion, injection molding, film blowing, and fiber production. If crystallization does not occur fast within the practical time frame, these commercial processes are unsuccessful. For instance, the polymer tends to stay soft, tacky and stick to itself even after long cooling times, making it difficult to be ejected without defect during extrusion, and thus extended injection molding cycle times are necessary.

To make PHBHx into a commercially processing material, usually nucleating agent is added to accelerate the crystallization rate. Inorganic compound such as talc and boron nitrile (BN) have been extensively investigated and found to be nucleating agents for many aliphatic polyesters such as poly(ethylene terephthalate), PET[8], poly(lactic acid), PLA[9], poly(1,4-butylene adipate), PBA[10], poly(3-hydroxybutyrate)-*co*-(3-hydroxyvalerate), PHBV[11], PHB[12], and PHBHx[7, 13] In the case of nucleation process, these small foreign particles are considered as heterogeneous nuclei which are responsible for the initiation of nucleation sites. It has been shown that talc and BN nucleate the crystallization of polymers through an epitaxial mechanism.[8, 13] The growing of polymer chain on the surface of heterogeneous nucleating agent is governed by the possible matching of the two lattices planes. Talc and BN show quite good lattice matched with PHBHx.[13] Although talc and BN are effective nucleating agents for many kinds of polyesters, they are inorganic

substances and therefore are not considered biologically degradable. The additional of talc and BN will restrict the applications of biologically degradable polymer which makes the fully environmentally friendly impossible.

From the point of view of the environment, biologically degradable nucleating agents are preferable, especially for the biologically degradable polymers. Considering PHB, it is a fully biobased and biologically degradable material. The usage of PHB as a nucleating agent can provide benefits over the conventional non-biologically degradable nucleating agents such as talc and BN. PHB has been used as nucleating agent for PLA[14] and PHBHV[15]. In the case of PHBHx, its unit cell lattice spacing is similar to the lattice parameters of PHB. This characteristic suggests that PHB serves as a proper nucleation seed for the epitaxial growth of PHBHx. The main objective of this study was to investigate the nucleation ability of PHB, and its effects on the crystallization and melting behavior of PHBHx. More importantly, crystallization kinetics of PHBHx with PHB were examined to describe crystallization behaviors and parameters. By understanding the crystallization process, one can select and control processing factors such as cooling rate and temperature.

In this study, the effect of PHB as nucleating agent on crystallization of PHBHx was first compared with two conventional inorganic nucleating agents, talc and BN. The isothermal and non-isothermal crystallization kinetics of PHBHx with the various concentration of PHB as a nucleator were investigated with differential scanning calorimeter (DSC). The kinetic parameters for all the samples were studied by mean of the Avrami model to explain the role of PHB on PHBHx crystallization. The effects of PHB on PHBHx melting behavior was analyzed by modulated differential scanning calorimetry (MDSC). Moreover, the crystalline growth was monitored by polarized optical microscopy

(POM) under isothermal conditions. Atomic Force Microscopy (AFM) was used to examine the spherulite morphology oriented in the thin films on silicon substrates. Finally, the composting biodegradation test under aerobic condition was investigated to determine the effect of PHB on biological degradability of PHBHx.

Experimental Section

1. Materials

PHBHx and PHB in powder form were provided by RWDC. Their respective characteristics in term of % Hx comonomer unit, % crystallinity, thermal properties, molecular weight, and polydispersity index are summarized in Table C.1. The powders of talc and BN were purchased from Imerys Talc America Inc. and Alfa Aesar, respectively. HPLC grade chloroform ($CHCl_3$) was purchased from JT Baker, U.S.A. All chemicals were used without further purification for the blends. Sigmacell cellulose (type 101) used as a positive control for composting biodegradation test was purchased from Sigma-Aldrich. Silicon wafers used as substrates were purchased from UniversityWafer Inc.

2. Sample Preparation

2.1 Preparation of Extrudates

All materials were pre-treated by drying in a vacuum oven at 60°C overnight to remove the moisture absorbed prior to extrusion. PHBHx and nucleating agents were pre-mixed and then melt blended by using a lab-scale co-rotating twin screws extruder with a backflow channel (MiniLab II HaakeTM Rheomex CTW 5). In all operations, the barrel temperature was set at 150°C, and the screw speed was 30 rpm. The total input of material approximately 7g was first loaded into the extruder within 2 minutes. Then it was recirculated in a backflow channel for 6 minutes to promote homogeneous mixing. The

extruded strands were collected through a die for a period of 4 minutes and then were cut into small pieces for further analysis. For evaluation of the nucleation efficiency, composition ratios of PHBHx and 5 wt% of nucleating agents (e.g. talc, BN, and PHB) were first prepared. For crystallization rate study, the blending weight ratios of PHBHx and PHB were 100/0, 99/1, 97/3, 95/5 and 90/0. Due to the high melting and low thermal stability of PHB, the neat PHB samples were not prepared under these extrusion conditions.

2.2 Preparation of Films on Silicon wafers

Thin films of PHBHx, PHBHx/PHB were prepared by spin coating onto silicon wafers coated with native oxide (UniversityWafer, Inc). The silicon wafers were cut into 2.5 cm × 2.5 cm squares and sonicated for 5 minutes with hexane, isopropyl alcohol, acetone, and water, respectively. Then the wafers were dried with a stream of nitrogen. PHBHx/PHB with various blend ratios (0-10%wt PHB) was dissolved in $CHCl_3$ at 60°C overnight to make 10 mg/mL solution. Prior to spin coating, the polymer solutions were filtered with 0.22 μm Millipore membrane. The spin coating was carried out by using 200 μL of the solution at 2000 rpm at room temperature. Film thickness was measured using spectroscopic ellipsometry (J.A. Woollam, M-2000V).

3. Characterization Method of PHA

3.1 Differential Scanning Calorimetry (DSC)

DSC measurements were performed on a DSC 250 (TA Instruments) under nitrogen atmosphere. The heat flow and temperature of DSC were calibrated with indium. Samples (approximately 5 to 6 mg) were sealed in aluminum pans and subjected to heating and cooling ramp. Three different experiments were conducted to investigate crystallization and melting behaviors of the blends. To analyze DSC crystallization

kinetics, the data was performed the Avrami fit with an Origin software. The Avrami plugin was developed by Muller et al.[16] The three experiments were as follows.

Isothermal

The samples were first melted at 180°C for 1 minute and cooled rapidly (60°C/min) to the various temperature (85-115°C) and maintained at that temperature for 25 minutes for completion of the crystallization process.

Non-isothermal

The samples were heated from 25°C to 180°C and held isothermally at 180°C for 1 minute to eliminate thermal history. They were then cooled to -20°C at various constant cooling rate and held isothermally for 1 minute to investigate the crystallization temperature (T_c). Finally, the sample were reheated again to 190°c to obtain glass transition temperature (T_g) and melting temperature (T_m). The heating rate was 10°C/min, while the cooling rate varied between 1, 5, 10, 20 and 40°C/min.

Modulated Differential Scanning Calorimetry (MDSC)

The samples were prepared in the same manner of non-isothermal crystallization experiment. After the completion of the non-isothermal crystallization, the samples were heated to the melt again (from -20°C to 190°C) to study the melting behavior by using MDSC. A standard modulation period of 60 s, modulation amplitude 0.32 °C and a heating ramp of 2°C/min were chosen based upon the recommended specifications from TA Instruments.[17]

3.2 Polarized Optical Microscope (POM)

The crystal morphologies of PHBHx and PHBHx/PHB were examined with a Nikon Eclipse LV100N POL microscope (Nikon Instruments) equipped with a Linkam

THMS 600 hot stage (Linkam Instruments). The samples were placed between two glass slides and were heated to the certain temperatures (180-200°C) with the heating rate of 100°C/min for 1 min. Then, they were cooled down to 120°C at 60°C/min to observe the crystal growth. The POM images were captured under crossed polarized light and an objective with 20X magnification was used.

3.3 Atomic Force Microscopy (AFM)

The AFM topographic images of the films of PHBHx and PHBHx/PHB were performed on a NanoIR3 system (Bruker) using contact mode. The tip type in the contact mode was PR-EX-nIR2-10 (Anasys Instruments Inc) with a resonance frequency of 13 ± 4kHz and a spring constant of 0.07-0.4 N/m. The height images were obtained in air at room temperature. The scan rate was adjusted in the range of 0.5-1 Hz with a scan size of 48 μm^2. All images were recorded with a resolution of 512 x 256 data points.

3.5 Composting Biodegradation Test

Composting biodegradation testing was carried out in a respirometer (ECHO instruments) under aerobic conditions at 58 °C for 90 days. Among all blends, the blend of 10% PHB and PHBHx was selected for evaluating the composting biodegradation compared with the neat PHBHx due to the highest amount of PHB using as a nucleator in this study. The extrudate samples of the neat PHBHx and PHBHx/PHB were crushed into powders and sieved using Sieve No. 4. The cellulose which was used to monitor microbial activities as a positive reference was used as received in powder form. In each experimental reactor, 5g of test material (such as PHBHx and PHBHx/PHB), and a 5 g of cellulose was prepared and well mixed in 250 g of compost. The reactors of the compost with no material were used as the blank controls. The preparation method and properties of the compost are

shown in Table C.2. Under aerobic conditions, oxygen gas (O_2) is consumed, and carbon (C) is converted to carbon dioxide gas (CO_2) by microorganisms in the compost. The method calculating biogas production and carbon loss from the samples are presented in the Supporting Information. The compost in all reactors was stirred weekly to prevent clumping and provide even distribution of moisture. Water was added into the reactors as necessary in order to maintain constant moisture level and prevent drying of the compost inoculum.

Results and Discussion

1. Nucleating Effects of Talc, BN and PHB on PHBHx Crystallization

The effect of nucleating agents on the crystallization behavior of PHBHx from the melt can be characterized by the crystallization peak. Generally, the addition of nucleating agents results in the crystallization peak shifts towards higher temperatures with a narrower slope which indicate faster crystallization. To study the effect of different nucleating agents (talc, BN, and PHB) on PHBHx, all samples were extruded with 5wt% of these nucleating agents at 150°C. Then, they were examined by means of DSC scanning from 180°C to -20°C after melted at 180°C for 1 minutes to erase the thermal history. Figure 4.1 shows the DSC thermograms of neat PHBHx, and their blends with the various nucleating agents at the cooling rate of 10°C/min.

During cooling, it is obvious that the additions of talc, BN or PHB into PHBHx enhanced the rate of crystallization. As shown in Figure 4.1, the T_c value of the neat PHBHx is 80.0°C and the crystallization proceeds in a broad temperature range. When adding the nucleating agents into PHBHx, the T_c peak shows a decrease in broadness and an increase in intensity and temperature. The T_c value of PHBHx/talc, PHBHx/BN, and PHBHx/PHB

is 87.9°C, 88.8°C, and 95.7°C, respectively. Clearly, PHBHx with talc or BN has a lower T_c than PHBHx with PHB. Among these three nucleating agents, the most effective nucleating agent is PHB which shifts the T_c of PHBHx to 95.7°C. This is almost 16°C higher than that of the neat PHBHx and thus, indicates the faster crystallization and better nucleating efficiency of PHB than talc or BN. Since PHB greatly enhances the nucleation and crystallization of the PHBHx, it was further explored to understand the effects of its various concentrations in PHBHx on the rate of crystallization.

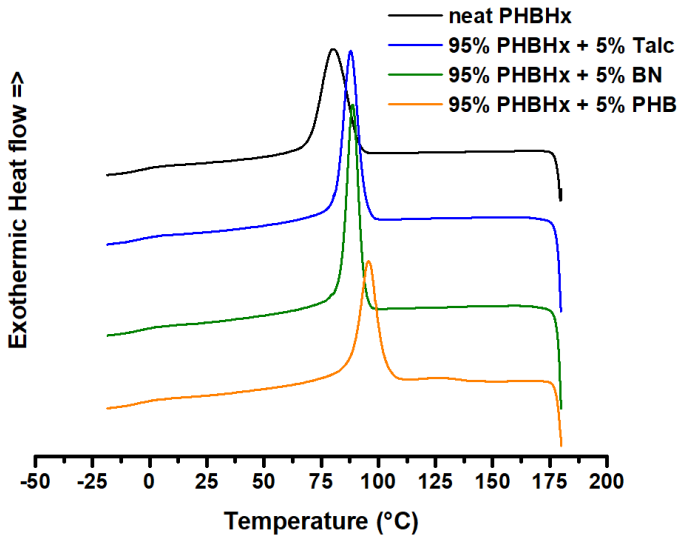

Figure 4.1. DSC thermograms of the neat PHBHx and PHBHx with various nucleators (talc, BN and PHB).

2. Effect of Isothermal Treatment on Crystallization Behavior of PHBHx/PHB

The crystallization kinetics of the neat PHBHx under isothermal condition were performed at temperature ranging from 85°C to 105°C. Because the crystallization rate of PHBHx/PHB is very fast, the range of isothermal crystallization temperature is limited from 95°C to 115°C under these experimental conditions. Figure C.1 show crystallization curves of neat PHBHx and PHBHx/PHB at various isothermal crystallization temperatures.

From the DSC curves, the crystallization peak shifts to a longer time and becomes more broad with increasing temperature. It is clearly seen that higher crystallization temperatures requires a longer time to complete crystallization. Figure C.2 show crystallization curves of PHBHx/PHB at various concentrations of PHB (0-10%wt) at 95°C, 100°C, and 105°C. As seen in these DSC curves, it is obvious that the crystallization peak sharpened, and crystallization time was shortened with increasing PHB content at all isothermal temperatures examined. This finding reveals that the amount of PHB has a positive influence on the crystallization behavior of PHBHx.

In this study, the relative crystallinity (X_t) was calculated according to the Equation C3 and have been plotted in Figure C.3 as a function of crystallization time. All these curves exhibit the sigmoidal shape suggesting that the X_t value increases with increasing crystallization time. Moreover, the corresponding crystallization time for the neat PHBHx and PHBHx/PHB was increase with increasing crystallization temperature, which means that the crystallization rate was decreasing. As for different PHB content, it can be seen from the plot that PHBHx with 10 wt% PHB had the fastest crystallization rate at 115°C. Avrami equation based on the guideline proposed by Muller et al.[16] was used to calculate the kinetics parameters of isothermal crystallization behavior (Equation C7). Figure 4.2 shows the plots of Avrami relations for the neat PHBHx and PHBHx/PHB at different crystallization time. As seen in these figures, all the curves are straight and parallel with one another indicating that the overall isothermal crystallization process can be described by the Avrami method.

Kinetics parameters such as the overall crystallization rate constant (k) and the Avrami exponent (n) can be determined from the intercept and slope of these Avrami plots.

The crystallization half time ($t_{1/2}$) defined as the time at which the relative crystallization reaches 50% which can be determined using the Equation C10. Detailed kinetic parameters are listed in Table 4.1. As can be seen, $t_{1/2}$ decreases and *k* increases apparently with increase in PHB content, implying that rate of crystallization increases with increase in PHB content. With incorporation of 1wt% and 10wt% PHB, the $t_{1/2}$ values at 105°C of PHBHx decrease from 5.9 to 2.3 and 0.9, respectively. Moreover, it was observed that the value of *k* and $t_{1/2}$ are strongly dependent on the crystallization temperature. With a decrease of crystallization temperature, the value of $t_{1/2}$ decreased, and the value of *k* increased continuously, which show gradually enhanced the rate of crystallization.

In this isothermal crystallization process, the n values of the neat PHBHx and PHBHx/PHB are in the range of 2.2 and 3.2 which demonstrates a two/three-dimensional spherulitic growth on heterogeneous nucleation. The value of n insignificantly decreased with increasing PHB, whereas it is almost insensitive to the addition of PHB as a nucleating agent. Also, the value of n did not decrease much with decreasing the crystallization temperature.

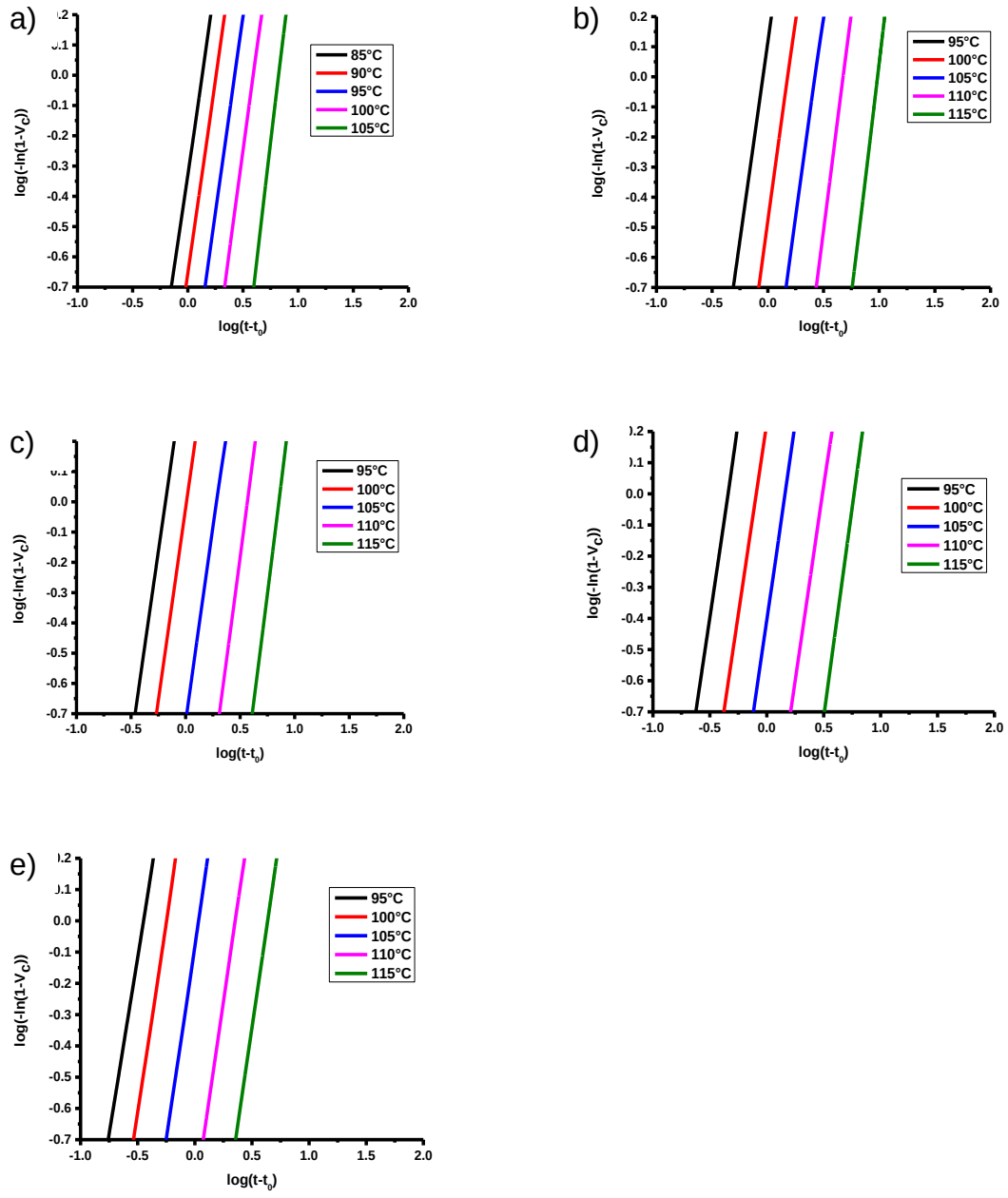

Figure 4.2. Avrami plot of log(-ln(1-V_c)) versus log (t-t_0) of PHBHx with various PHB content at different crystallization temperatures (a) 100% PHBHx, (b) 1% PHB+ 99% PHBHx, (c) 3% PHB+ 97% PHBHx, (d) 5% PHB+ 95% PHBHx, (e) 10% PHB+ 90% PHBHx.

Table 4.1. Kinetics parameters obtained from isothermal crystallization experiment and Avrami analysis of PHBHx and PHBHx/PHB.

Sample	Temperature, T_c (°C)	*n*	*k* (min^{-n})	$t_{1/2}$ (min)
100% PHBHx	85	2.5	4.7×10^{-1}	1.2
	90	2.6	2.2×10^{-1}	1.6
	95	2.8	7.5×10^{-2}	2.2
	100	3.0	2.0×10^{-2}	3.3
	105	3.2	2.6×10^{-3}	5.9
1% PHB+ 99% PHBHx	95	2.8	1.4	0.8
	100	2.8	3.4×10^{-1}	1.3
	105	2.8	6.9×10^{-2}	2.3
	110	2.9	1.1×10^{-2}	4.2
	115	3.1	9.6×10^{-4}	8.5
3% PHB+ 97% PHBHx	95	2.6	3.3	0.6
	100	2.6	9.7×10^{-1}	0.9
	105	2.7	1.9×10^{-1}	1.6
	110	2.8	2.7×10^{-2}	3.2
	115	2.8	3.7×10^{-3}	6.3
5% PHB+ 95% PHBHx	95	2.5	7.0	0.4
	100	2.5	1.8	0.7
	105	2.6	4.1×10^{-1}	1.2
	110	2.7	5.6×10^{-2}	2.6
	115	2.8	7.6×10^{-3}	5.0
10% PHB+ 90% PHBHx	95	2.2	9.4	0.3
	100	2.4	3.8	0.5
	105	2.6	8.9×10^{-1}	0.9
	110	2.7	1.3×10^{-1}	1.9
	115	2.7	2.2×10^{-2}	3.6

3. Effect of non-isothermal treatment on crystallization behavior of PHBHx/PHB

3.1 Crystallization behavior of PHBHx with PHB

Figure 4.3 shows DSC thermograms of the neat PHBHx and PHBHx/PHB at a constant cooling rate of 10°C/min. The amount of PHB as a nucleating agent varied between 1 and 10wt%. From these DSC curves, it shows that the crystallization peaks have shifted to higher temperature with the increasing amount of PHB as expected with an accelerated rate of crystallization. Comparing with the different amount of PHB in this study, the fastest crystallization rate was obtained with highest content of PHB which was 10wt%. By adding 1wt% of PHB, it causes a significant increase in T_c from 80.0°C to 91.2°C. However, when the PHB loading increased above 1wt%, the crystallization peaks were slightly higher than the PHBHx with 1wt% PHB. This result suggested that 1 wt % PHB is a sufficient concentration to enhance the crystallization rate of PHBHx. Additionally, it is seen in Figure 4.3 that the nucleated PHBHx exhibited a narrower exothermic peak than the neat PHBHx indicating faster crystallization. However, with increasing concentration of PHB, a decrease in the absolute height of the peak but an increase in the height of shoulder around 120°C was observed.

The non-isothermal crystallization behavior of PHBHx and PHBHx/PHB was further explored by varying the cooling rate between 1 and 40°C/min. The values of T_c are shown in Figure 4.4 and Table C.4. As shown in Figure 4.4, the T_c of PHBHx and PHBHx/PHB is dependent on the cooling condition. With increasing cooling rate, the crystallization peak is shifted toward lower temperature. This behavior can be explained to the fact that the polymer chain did not have enough time to compete its whole crystallization during the cooling scan.

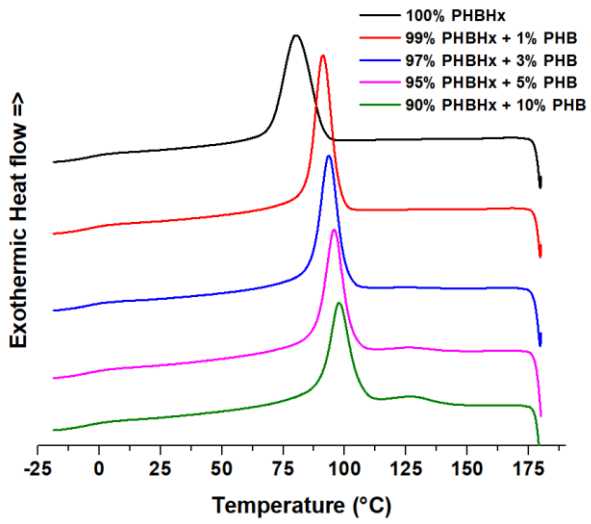

Figure 4.3. DSC thermograms of PHBHx/PHB at different concentration at cooling rate of 10°C/min.

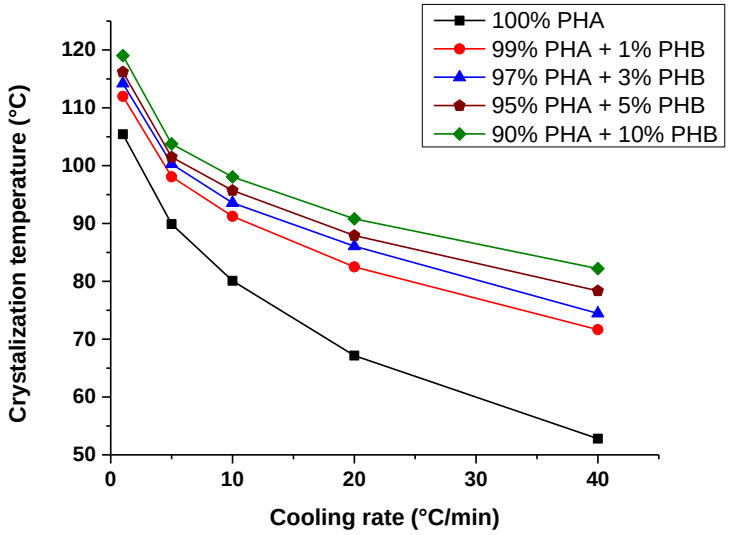

Figure 4.4. Crystallization temperature (T_c) as a function of the amount of PHB and cooling rate.

In all industrial manufacturing processes, the methods of extrusion and injection molding operate under non-isothermal crystallization conditions. It is important to evaluate or predict the non-isothermal crystallization kinetics to achieve the optimum condition for commercial processing. Figure C.4 shows an overlay of relative crystallinity (%) as a function of temperature of the neat PHBHx and PHBHx/PHB at different cooling rates. By using the relationship between the crystallization time (t), the crystallization temperature (T), and the constant cooling rate (equation C5), the relative crystallinity plots can be converted from temperature to time dependent data (Figure C.5). From these results, at any PHB concentration, it is obvious that the time required to complete the crystallization decrease as the cooling rate increased.

It is well known that Avrami equation is often used to analyze the isothermal crystallization kinetics. However, Avrami analysis can also be applied to study the non-isothermal kinetics experiments. The modified Avrami model proposed by Jeziorny[18] was employed to describe the non-isothermal crystallization kinetics of the neat PHBHx and PHBHx/PHB in this study. Jeziorny suggested that the crystallization rate constant (k) should be corrected with factor of constant cooling rate (ϕ) because temperature changes immediately in non-isothermal crystallization. The kinetics of the non-isothermal crystallization was given as follows:

$$\ln(k_c) = \ln(k)/\phi \qquad (1)$$

The non-isothermal Avrami plots of $\log(-\ln(1-V_c))$ versus $\log(t-t_0)$ for each cooling rate are given in Figure 4.5. A series of nearly straight lines with linear slope were obtained, which indicated that the Avrami model can be used to describe the primary stage of non-isothermal crystallization kinetics of PHBHx and PHBHx/PHB. However, these Avrami

plots were found to deviate from the linearity at the late stages, especially at lower cooling rate, indicative of the occurrence of the secondary crystallization.

The parameters of *n* and *k* can be obtained from the slopes and intercepts of these Avrami linear lines. The value of *n*, *k*, and modified ln (k_c) with ϕ are shown in Table C.5. As can be seen, the *n* value, and $t_{1/2}$ decreased, but *k* value increase with the increasing cooling rate. The decreasing in the value of n means the decrease in the dimensionality of spherulite growth. Generally, low values of *n* and $t_{1/2}$ and high value of k imply that the crystallization rate increase with a more instantaneous nucleation process which leads to smaller spherulite dimension. From Table C.5, it can be seen that the n values are slightly larger than the postulated value for a maximum crystal dimensionality (n>4) when using the slow cooling rate.

3.2 Melting behavior of PHBHx with PHB

Figure 4.6 illustrates the second melting endotherm of PHBHx/PHB at different concentration of PHB on heating rate of 10°C/min. This DSC results were analyzed after cooling PHBHx/PHB from 180°C to -20°C with a cooling rate of 10°C/min. In Figure 4.6, the multiple endotherm peaks were labeled as T1, T2 and T3 starting with the lowest temperature. These values were taken as the melt peak temperatures. The multiple components of melting behavior of PHB and PHBHx/PHB have been further examine by using MDSC. In this technique, two simultaneous heating rates composed of a linear heating rate and a sinusoidal or modulated heating rate were applied to the samples. The results from MDSC can be distinguished thermodynamic (reversing heat flow) and kinetic (non-reversing heat flow) events that occur under the heating conditions.

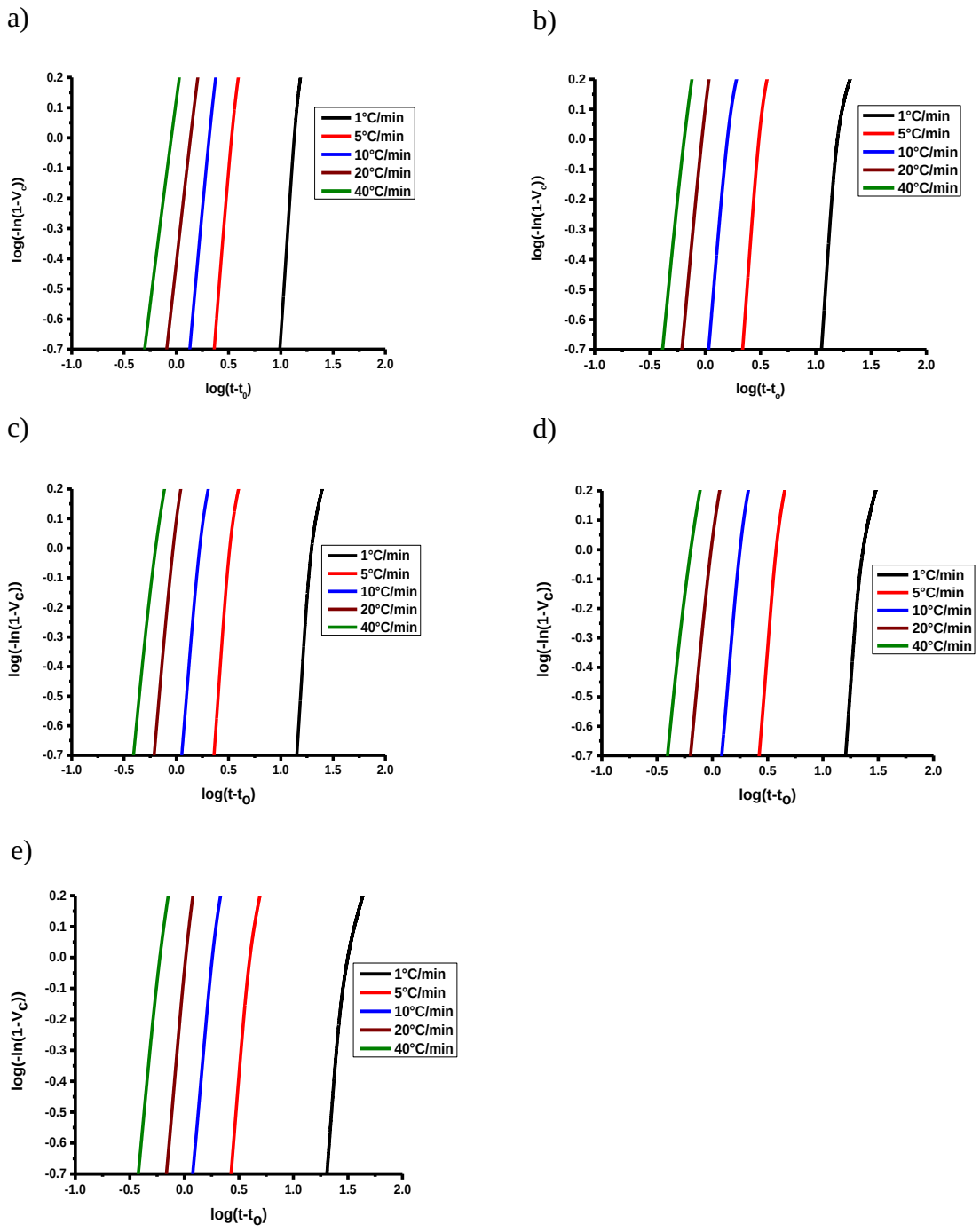

Figure 4. 5. Avrami plot of log(-ln(1-V_c)) versus log (t-t_0) of PHBHx with various PHB content at different cooling rates (a) 100% PHBHx, (b) 1% PHB+ 99% PHBHx, (c) 3% PHB+ 97% PHBHx, (d) 5% PHB+ 95% PHBHx, (e) 10% PHB+ 90% PHBHx.

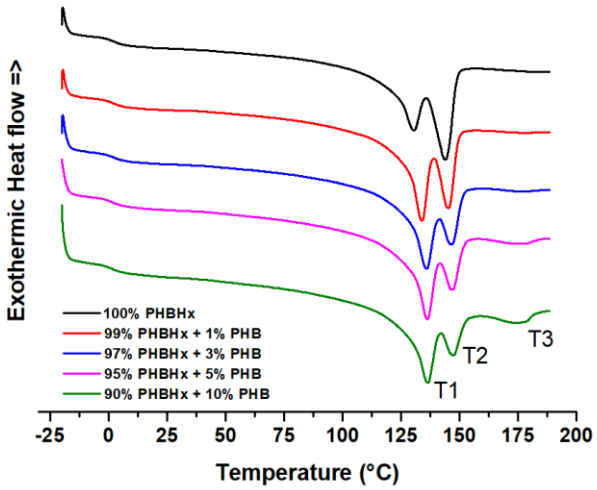

Figure 4.6. DSC thermograms of PHBHx/PHBs at different concentration at heating rate of 10°C/min.

Figure C.6 shows the modulated DSC results of the neat PHB and PHBHx/PHB. From MDSC curves, the total heat flow was separated into reversing and non- reversing heat flow. The MDSC total heat flow is similar to the conventional DSC curves, showing two melting endoderm with a shoulder when PHB content increasing. The reversing melting curves exhibited an overlapped melting endotherm and exotherm at T1 and T2. In the non-reversing curve, the exotherm was found close to T1 and the endotherm was found close to T2 and T3, suggesting the presence of melting recrystallization and remelting processes. In other words, the peak with the lowest melting temperature (T1) is attributed to the imperfect crystals that experience melting and recrystallization during the DSC heat scan. The T2 is related to the melting of the crystal formed from the result of recrystallization. The temperature of T3 was detected around 173°C which is close to the melting temperature of pure PHB (174.2°C). Similar to the crystallization peaks, it is

observed that PHBHx with 10%wt of PHB exhibits the most pronounce T3 melting peak. This result suggested that the immiscibility of PHBHx and PHB causing a phase separation. The melting temperatures are a direct result from the crystallization condition that occurs in the DSC. To investigate the influence of DSC crystallization condition, the subsequent melting behavior of PHBHx and PHBHx/PHB were determined after the samples had finished non-isothermal crystallization from the melt at various cooling rates. The melting temperatures (T1, and T2), enthalpy of melting, and % crystallinity are listed in Table C.6, C.7 and C.8. The % crystallinity was calculated during this heating scan by using Equation S11. By comparing the results obtained for the neat PHBHx and PHBHx/PHB, it is obvious that their melting behaviors depend on the concentration of PHB and cooling rate. Table C.6 shows the T1 and T2 melting endotherm increase with the increasing amount of PHB. Moreover, it has been seen that the enthalpy of melting and % crystallinity of the PHBHx/PHB increase with the PHB content.

Considering the effect of cooling rate summarized in Table C.6, the lower melting endotherm (T1) and higher melting endotherm (T2) of the neat PHB and PHBHx/PHB decrease when the cooling rate increase from 1°C/min to 40°C/min. As seen in Table C.7-8, the enthalpy of melting and % crystallinity decrease remarkably with increase in cooling rate due to the samples not having enough time for complete crystallization under the fast cooling. According to the multiple melting peaks in Figure 4.6, it was observed that the area ratio of peak T1 to peak T2 increase drastically with the addition of PHB. As a result, the presence of PHB as a nucleating agent has an effect on the crystal imperfection.

4. Limitation of using the PHB as a nucleating agent.

For heterogeneous nucleation, the melting point of nucleating agents is generally higher than the melting point of polymer. In order to be able to nucleate, nucleating agents should remain as discrete particles in the melt polymer. In other words, nucleating agents are not melted at the processing temperature, but remains as a crystalline solid upon cooling of the polymer melt and subsequently facilitate the formation of crystallization sites. Both talc and BN are inorganic nucleating agents which have a very high melting temperature around 1500°C[19] and 2973°C,[20] respectively. These materials can provide wider processing windows for the melt polymers than PHB which has the melting point around 174°C. PHB can promote the nucleation of PHBHx and its acceleration effectiveness is better than talc and BN. However, PHB is sensitive to the high melting temperature and when PHB is fully melted, it no longer nucleates PHBHx.

Figure 4.7a shows the crystallization peaks of PHBHx and PHBHx/PHB which were cooled from the melt state that reached the temperature of 190°C. Without PHB, PHBHx could not crystallize after melting at 190°C. However, the results of DSC analysis show a delay of the crystallization peak of PHBHx after adding a high content of PHB. The crystallization ability increased significantly with an increase in the PHB content. This behavior could be attributed to partial melting of PHB due to the DSC condition. Although the melting temperature was higher than the melting point of PHB (~174 °C), the insufficient time to completely melt the material can be a result of partially melted polymer. In order to completely melt the PHB in a short period of time, it is necessary to heat this material at a temperature higher than 192°C.[21] As increase in the temperature of melting to 200°C, no crystallization peak of PHBHx with 10 wt % PHB is seen during the cooling

process (Figure 4.7b). In this case, PHBHx could not be nucleated due to the absence of heterogenous particles of PHB.

a)

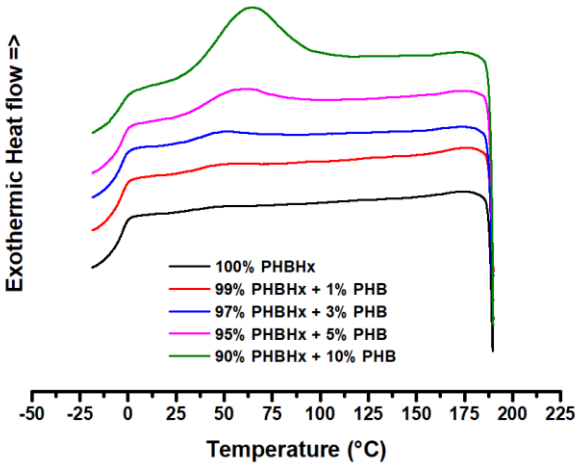

b)

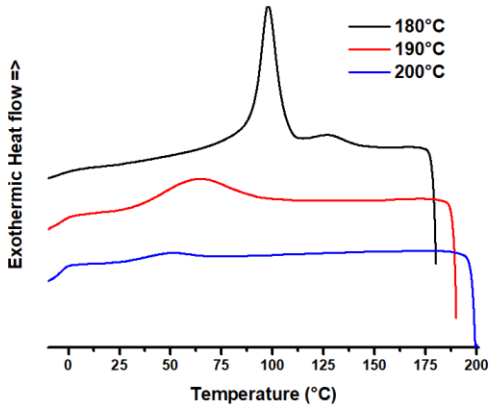

Figure 4.7. Crystallization peaks (a) PHBHx/PHB at various PHB content after treatment at 190°C (b) 90wt% PHBHx + 10wt% PHB after treatment at 180, 190, and 200°C.

5. Crystal morphology observation by POM

Figure 4.8 shows the results of POM studies of the effect of PHB nucleating agent on the crystallization of PHBHx. At first, the samples were heated to 180°C for 1 min

followed by quenching to 120°C. Then, they were heated to 190°C for 1 min followed by quenching to 120°C. As seen in Figure 4.8, when the pretreatment temperature is 180°C, all samples exhibited a spherulite morphology after isothermal at 120°C, but variation in crystallization rate and crystalline content. The crystal growth rate and % crystallinity of the samples increases rapidly with increasing PHB content. PHBHx with 10wt% PHB was the most fully covered with the crystallites after isothermal at 120°C for 180 seconds. These results are thus consistent with the previous observations with DSC.

It is important to note that PHBHx with the addition of PHB showed two-crystal phases during the cooling process. Crystallization of large micrometer sized crystals appeared first at the beginning of isothermal process, while small micrometer sized crystals occurred later. With further increase of PHB content, the amounts of the large crystals appeared more. This is well in agreement with above DSC discussions about the exhibition of the shoulder on the crystallization peaks. Obviously, the large crystals are corresponding to crystallization of PHB, while the small crystals are corresponding to crystallization of PHBHx.

When the pretreatment temperature is 190°C, no crystallites are seen in the neat PHBHx at 120°C. However, with the addition of PHB, PHBHx could be partially crystallized. The increase of melting temperature results in a lower density of nucleation and a corresponding delay of crystallization process (Figure C.7). To evaluate the effect of melting temperature on crystallization peak, PHBHx with 10wt% PHB sample was further heated to 195, 197 and 200°C. As shown in Figure C.8, there is no formation of any crystals at 120°C as a result of completely melted PHB. This POM observation agrees well with DSC data.

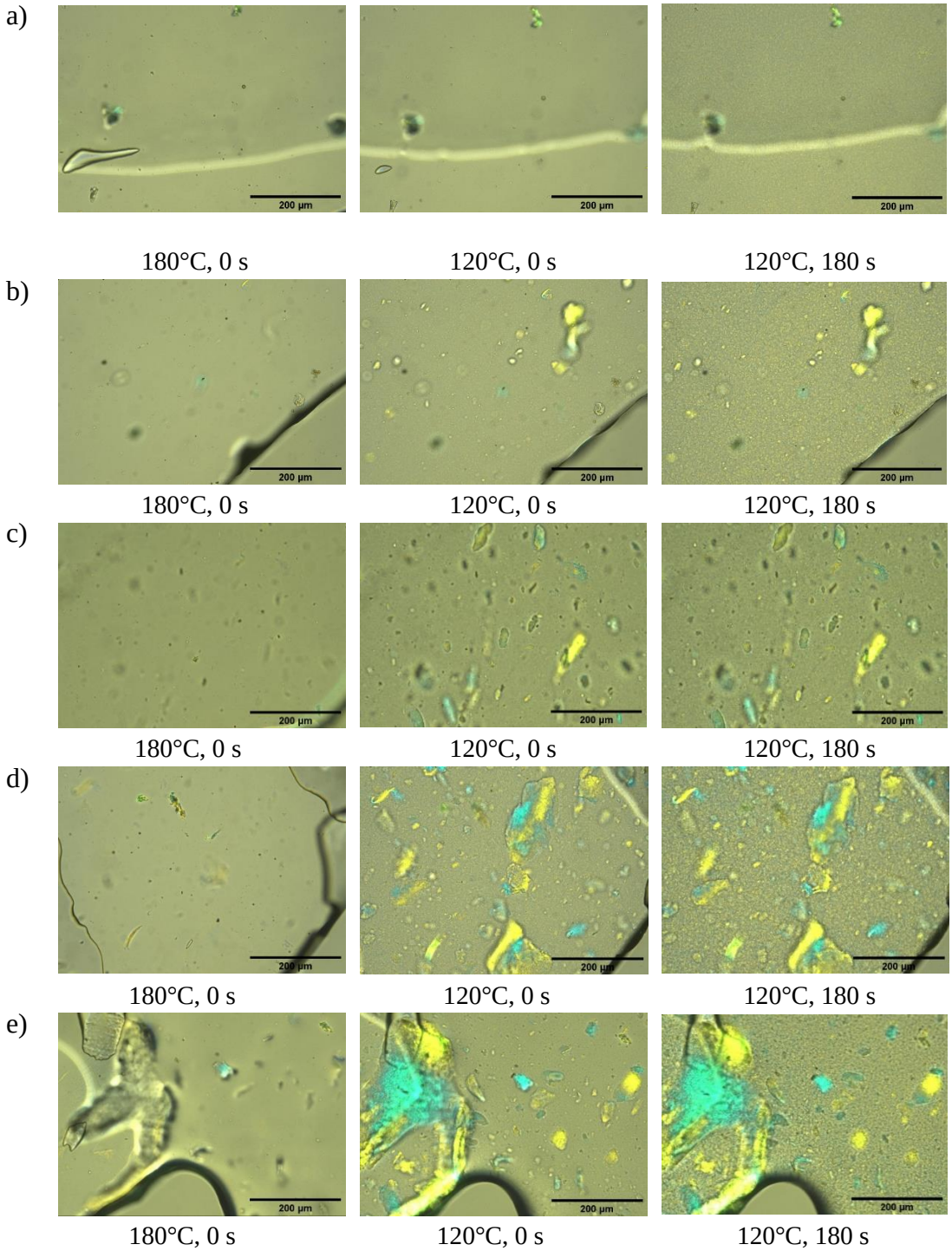

Figure 4.8. POM images of PHBHx/PHB at various PHB content, isothermal crystallized at 120°C after melting at 180°C for 1 min. (a) 100% PHBHx, (b) 1% PHB+ 99% PHBHx, (c) 3% PHB+ 97% PHBHx, (d) 5% PHB+ 95% PHBHx, (e) 10% PHB+ 90% PHBHx.

6. Spherulitic Morphology observation by AFM.

AFM was used to study the size and number of the spherulites of the neat PHBHx and PHBHx/PHB. Figure 4.9 shows contact-mode AFM height images of spin-coated films of the varying the concentration of PHB. The film thickness was 150-180 nm (Table C.9). As shown in Figure 4.9, the spherulite size of neat PHBHx sample is larger than that of PHBHx nucleated by PHB. Upon addition of PHB, the size of spherulite is decreased, but the number of spherulite has increased, thus promoting the nucleation rate of PHBHx. This result can be explained to the fact that the numbers of nuclei sites in polymer matrix increase in proportion to the loading levels of PHB. The increase nuclei would induce more spherulite formation. The high density of spherulites continue to grow until they impinge on adjacent spherulites leading to the smaller spherulites size. Clearly, the polygonal shape of the spherulites was formed as seen in these AFM images.

7. Aerobic composting biological degradability of PHBHx/PHB blends.

In order to investigate the effect of PHB addition on composting biodegradation of PHBHx, 90wt% PHBHx + 10wt% PHB was compared with the neat PHBHx in the respirometer. Due to the space limitation in the respirometer, this blend was selected for evaluating the composting degradation since it has the fastest rate of crystallization in the isothermal condition and has the highest content of PHB in this study. The carbon and nitrogen contents of the neat PHBHx were 61.0% and 0.04%, and for the 10wt% PHB + PHBHx were 60.6 % and 0.02 %, respectively. All the emitted CO_2 was monitored and quantified during the composting degradation test. The percent of composting biodegradation can be calculated by using Equation C1 and C2.

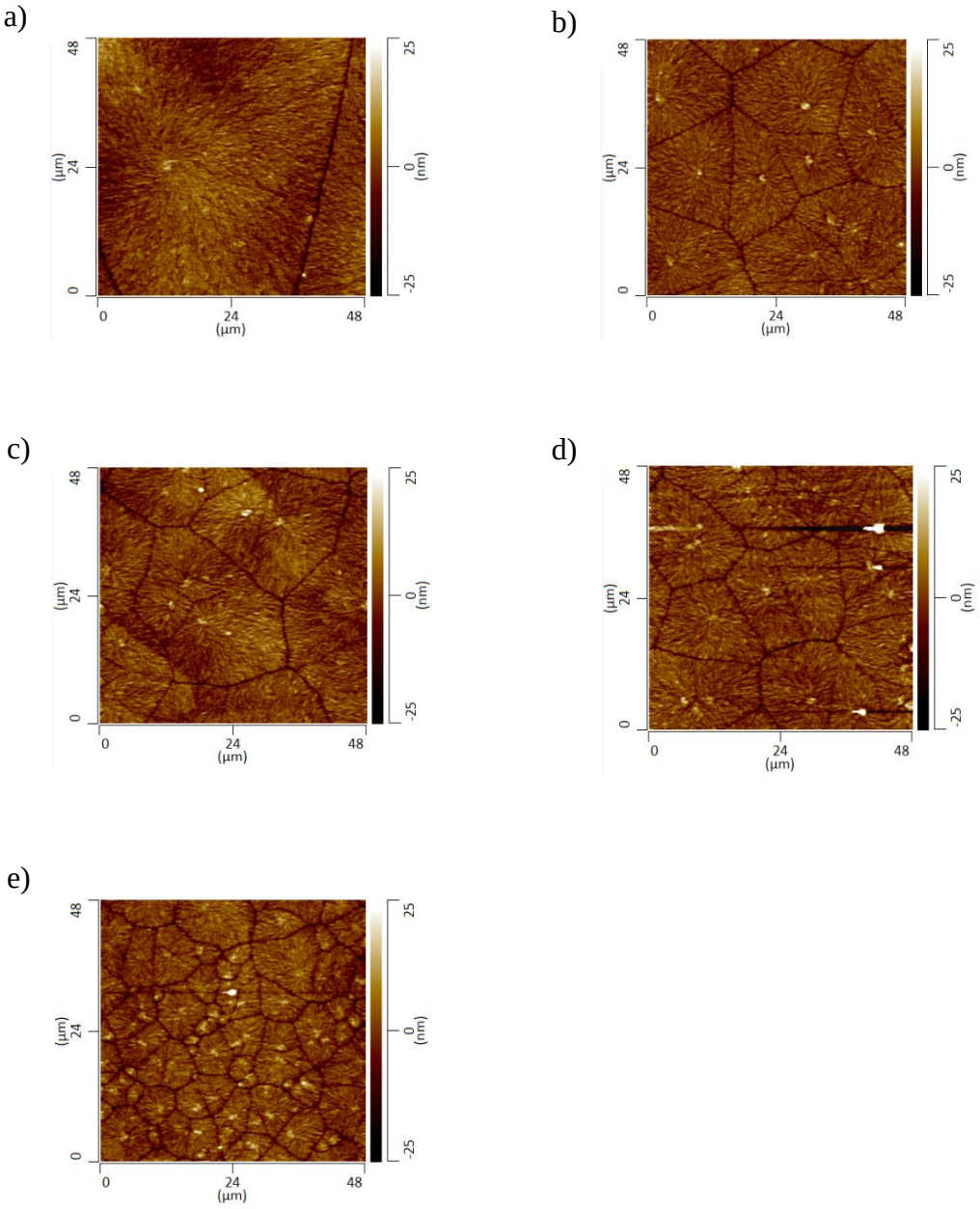

Figure 4.9. Contact-mode AFM height images of (a) 100% PHBHx, (b) 1% PHB + 99% PHBHx, (c) 3% PHB + 97% PHBHx, (d) 5%PHB + 95% PHBHxx, (e) 10% PHB + 90% PHBHx.

Results of the composting biodegradation test are shown in Figure 4.10. After 90 days of incubation at 58°C, the % absolute biodegradation of PHBHx has reached 97.5 %, while 10 wt% PHB + 90 wt% PHBHx has reached 103.6 %. It was found the degradation of both samples were comparable.

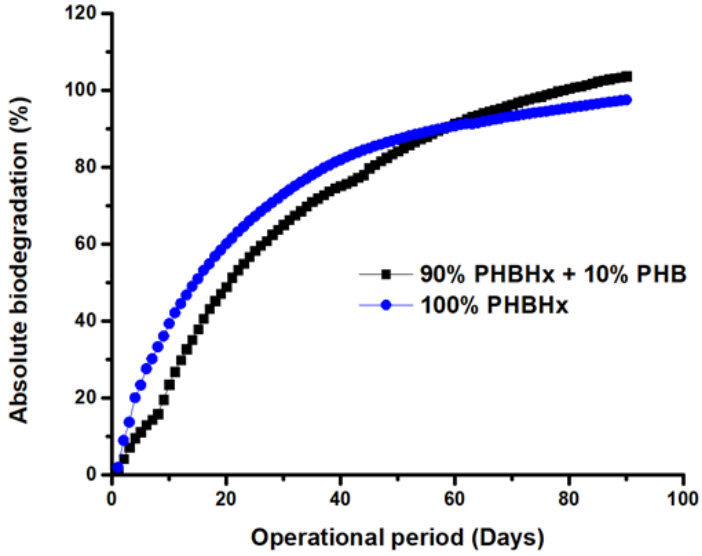

Figure 4.10. Absolute composting biodegradation of 100% PHBHx and 90% PHBHx + 10% PHB.

Conclusions

PHBHx was melt mixed with three different nucleating agents (talc, BN, and PHB) in order to study their effects on the crystallization of PHBHx. Among these three kinds of nucleating agents, PHB showed the most efficient nucleating effect on PHBHx. Under both isothermal and non-isothermal crystallization conditions, the slow crystallization process of PHBHx has been accelerated by PHB. The parameters of the isothermal and the non-isothermal crystallization kinetics were obtained through Avrami equation. It was found that the presence of multiple melting peaks of PHBHx upon heating was attributed to the melt-recrystallization mechanism. Recrystallization occurred due to the melting of the imperfect crystals to form more perfect crystals. The incorporation of PHB as a nucleating agent in PHBHx not only increased the imperfect crystals, but also increased % crystallinity. Upon addition of PHB, the spherulite size of PHBHx decreased and the spherulite number was much higher than that of neat PHBHx. During the crystallization process, PHBHx with high loading of PHB showed behavior characteristic of two-crystal phases, where crystallization peak at higher temperature corresponds to PHB and crystallization peak at lower temperature corresponds to PHBHx. It is important to note that PHB can act as a heterogeneous nucleating agent and provide crystallization sites when it remains as crystalline solid (discrete particles) upon processing temperature.

References

1. Braunegg, G.; Lefebvre, G.; Genser, K. F., Polyhydroxyalkanoates, biopolyesters from renewable resources: physiological and engineering aspects. *Journal of biotechnology* **1998,** *65* (2-3), 127-161.

2. Meereboer, K. W.; Misra, M.; Mohanty, A. K., Review of recent advances in the biodegradability of polyhydroxyalkanoate (PHA) bioplastics and their composites. *Green Chem.* **2020,** *22* (17), 5519-5558.

3. Noda, I.; Green, P. R.; Satkowski, M. M.; Schechtman, L. A., Preparation and Properties of a Novel Class of Polyhydroxyalkanoate Copolymers. *Biomacromolecules* **2005,** *6* (2), 580-586.

4. Li, Z.; Yang, J.; Loh, X. J., Polyhydroxyalkanoates: opening doors for a sustainable future. *NPG Asia Materials* **2016,** *8* (4), e265.

5. Bugnicourt, E.; Cinelli, P.; Lazzeri, A.; Alvarez, V., Polyhydroxyalkanoate (PHA): Review of synthesis, characteristics, processing and potential applications in packaging. *eXPRESS Polym. Lett.* **2014,** *8* (11), 791-808.

6. Doi, Y.; Kitamura, S.; Abe, H., Microbial Synthesis and Characterization of Poly(3-hydroxybutyrate-co-3-hydroxyhexanoate). *Macromolecules* **1995,** *28* (14), 4822-4828.

7. Jacquel, N.; Tajima, K.; Nakamura, N.; Miyagawa, T.; Pan, P.; Inoue, Y., Effect of Orotic Acid as a Nucleating Agent on the Crystallization of Bacterial poly(3-hydroxybutyrate-co-3-hydroxyhexanoate) Copolymers. *J. Appl. Polym. Sci.* **2009,** *114* (2), 1287-1294.

8. Haubruge, H. G.; Daussin, R.; Jonas, A. M.; Legras, R.; Wittmann, J. C.; Lotz, B., Epitaxial Nucleation of Poly(ethylene terephthalate) by Talc: Structure at the Lattice and Lamellar Scales. *Macromolecules* **2003,** *36* (12), 4452-4456.

9. Shakoor, A.; Thomas, N. L.; Science, Talc as a Nucleating Agent and Reinforcing Filler in Poly (lactic acid) Composites. *Polym. Eng. Sci.* **2014,** *54* (1), 64-70.

10. Kai, W.; Zhu, B.; He, Y.; Inoue, Y., Crystallization of Poly(butylene adipate) in the Presence of Nucleating agents. *J. Polym. Sci., Part B: Polym. Phys.* **2005,** *43* (17), 2340-2351.

11. Liu, W. J.; Yang, H. L.; Wang, Z.; Dong, L. S.; Liu, J. J., Effect of Nucleating Agents on the Crystallization of Poly(3-Hydroxybutyrate-co-3-Hydroxyvalerate). *J. Appl. Polym. Sci.* **2002,** *86* (9), 2145-2152.

12. Puente, J. A. S.; Esposito, A.; Chivrac, F.; Dargent, E., Effect of Boron Nitride as a Nucleating agent on the Crystallization of Bacterial Poly (3-hydroxybutyrate). *J. Appl. Polym. Sci.* **2013,** *128* (5), 2586-2594.

13. Jacquel, N.; Tajima, K.; Nakamura, N.; Kawachi, H.; Pan, P.; Inoue, Y., Nucleation Mechanism of Polyhydroxybutyrate and Poly(hydroxybutyrate-co-hydroxyhexanoate) Crystallized by Orotic acid as a Nucleating agent. *J. Appl. Polym. Sci.* **2010,** *115* (2), 709-715.

14. Ohkoshi, I.; Abe, H.; Doi, Y., Miscibility and solid-state structures for blends of poly[(S)-lactide] with atactic poly[(R,S)-3-hydroxybutyrate]. *Polymer* **2000,** *41* (15), 5985-5992.

15. Withey, R. E.; Hay, J. N., The effect of seeding on the crystallisation of poly(hydroxybutyrate), and co-poly(hydroxybutyrate-co-valerate). *Polymer* **1999,** *40* (18), 5147-5152.

16. Lorenzo, A. T.; Arnal, M. L.; Albuerne, J.; Müller, A. J., DSC isothermal polymer crystallization kinetics measurements and the use of the Avrami equation to fit the data: Guidelines to avoid common problems. *Polym. Test.* **2007,** *26* (2), 222-231.

17. Thomas, L. C. *Modulated DSC® Paper# 3 Modulated DSC® Basics; Optimization of MDSC® Experimental Conditions*; TA Instruments: 2005; pp 1-10.

18. Jeziorny, A., Parameters characterizing the kinetics of the non-isothermal crystallization of poly(ethylene terephthalate) determined by d.s.c. *Polymer* **1978,** *19* (10), 1142-1144.

19. Karian, H., *Handbook of polypropylene and polypropylene composites, revised and expanded*. CRC press: 2003.

20. Kiran, K. U. V.; Arora, A.; Sunil, B. R.; Dumpala, R., Effect of heat treatment on the temperature dependent wear characteristics of electroless Ni–P–BN(h) composite coatings. *SN Appl. Sci.* **2020,** *2* (6), 1101.

21. Di Lorenzo, M. L.; Sajkiewicz, P.; Gradys, A.; La Pietra, P., Optimization of melting conditions for the analysis of crystallization kinetics of poly(3-hydroxybutyrate). *e-Polymers* **2009,** *9* (1), 1-12.

CHAPTER 5

CONCLUSIONS AND FINAL REMARKS

Conclusions

The continuously growing concern for environmental issues has provoked efforts to replace fossil-based materials with bio-based or (industrially or naturally) biodegradable materials. In this dissertation, commercial aliphatic polyesters such as PLA and PHA have been studied and modified by adding some additives to improve their properties for industrial applications. The blends of PLA/PBG, PHA/PBG, and PHA/PHB were prepared by solution casting or melt extrusion process. Thermal and mechanical properties of the blends along with their morphology were investigated using a variety of analytical techniques. The effects of adding these additives as a plasticizer, processing aid, and nucleating agent on composting biodegradation have also been described.

In chapter 1, a literature review of structure and properties of PLA and PHAs was presented. The concepts of polymer additives such as plasticizer, processing aid, and nucleating agent have been discussed. In addition, the process of mixing polymers including solution casting and hot-melt blending was described in this chapter.

Chapter 2 investigated the use of PBG as a plasticizer for PLA. PBG was synthesized through polycondensation reaction between 1,4-butanediol and glutaric acid. PBG degraded faster than PBS under a controlled composting aerobic condition at 58 °C due to the effect of the odd carbon atom number in the dicarboxylic acid monomer. The results demonstrated that the ductility and composting performance of PLA can be

improved by blending PLA with PBG. Also, PLA/PBG blends exhibited higher % elongation at break than PLA/PBS blends. Morphology of the PLA/PBG blends were observed and found that they were immiscible exhibited phase separation above 3 wt% PBG.

Chapter 3 addressed the importance of processing aid as an additive in hot-melt extrusion of PHA. It was shown that PBG is a useful additive which eliminated the flow instability (melt fracture) when extruding PHA in the commercial scale extruder. Various composition of PHA/PBG blends were prepared by lab-scale extruder and studied their rheological properties. It was found that the addition of PBG reduced the viscosity of the blends. Evidently, the MFI values increased with increasing PBG content. As a result of blending PHA and PBG, two phases are formed with PBG dispersed in the PHA matrix.

Chapter 4 described the effects of PHB as a nucleating agent on the rate of crystallization of PHA. Crystallization and melting behaviors of PHA/PHB blends were discussed. Crystallization kinetics and parameters of the blends were examined and described by Avrami model under the isothermal and non-isothermal crystallization process. The crystallization rate constant and crystallization half-time showed that PHB greatly increased the crystallization rate of PHA. By the incorporation of PHB, the crystallization behaviors exhibited two-crystal phases during the cooling process. In addition, multiples melting peaks were also observed during the heating process. These results can be attributed to melt-recrystallization mechanism. The composting biodegradation measurement of PHA blended with 10% PHB were evaluated and the resulted showed the blend has exceeded 90% biodegradation within 90 days.

Future Outlook

In this dissertation, PLA and PHA have been blended with various additives such as PBG and PHB. Polymer blending is a practical and less expensive method to modify the polymer properties. The new materials can be developed and created a new combination of properties, depending on the composition and level of compatibility. The major challenge of polymer blends is they are immiscible which affects the overall properties of the blends. In this study, three polymer mixtures in binary blends such as PLA/PBG, PHA/PBG, and PHA/PHB are incompatible. Their morphology showed a unique phase separation due to weak interfacial adhesion between their phases.

The interfacial adhesion between the blended components can be enhanced through the addition of compatibilizers. Compatibilizing agents can be either reactive or nonreactive. The most commonly used non-reactive compatibilizers are block copolymer which one block can be miscible with one blend component, and a second block miscible with the other blend component. In the case of reactive compatibilizers, polymers with reactive functional group can be used as compatibilizers. The compatibilization of two polymers can be done by grafting their functional group with the two polymer components. In order to achieve better final properties, it is necessary to solve the problem of phase separation. Further studies related to improve the compatibility between the blends should be explored. The selection of an appropriate compatibilizer to enhance the compatibilization is still needed.

Final Remarks

Although PLA and PHA are valuable environmentally friendly bio-based materials which can be used to replace fossil-based plastics, they exhibit a number of limitations for

specific applications, such as low toughness, slow biodegradation rate, and slow crystallization. The modification of these polymers can be achieved by using blending techniques such as solution casting or melt compounding. By blending polymers with additives, new materials can be developed and tailored with the suitable properties for different applications. This dissertation has described a few types of additives including PBG and PHB, and the properties that can be modified. The results presented here provide an insight of functional additives such as plasticizer, processing aid, and nucleating agent, for the end-use applications of plastics in industry.

APPENDIX A

Supporting Information for PLA/PBG blends

Determination of acid value for prepolymer poly(butylene glutarate), PBG

The acid numbers were determined by standard titrimetric methods with potassium hydroxide and phenolphthalein as indicator. Approximately, 0.4 g of the sample was added into 20 mL of dioxolane. The mixture was slowly heated until all solid is dissolved in the solvent, and 3-4 drops of phenolphthalein was added. Then, titrate the sample with 0.03 M aqueous solution of potassium hydroxide (KOH) until the color changes from colorless to pink. The titration was conducted in three replications and the result is an average of these titers. The acid number was calculated using Equation A1.

$$AN = \left(\frac{V*56.1*M}{m}\right) * 100 \quad \text{(A1)}$$

Where: AN is the acid number, V is the volume of KOH (mL) used to titrate the sample, M is the molarity of KOH (0.03 M) and m is the mass of the sample (g).

Sample preparation for SEM

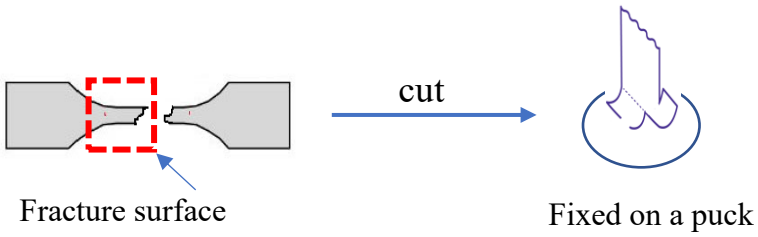

Figure A.1. The three-dimensional image of sample geometry fixed on puck for SEM imaging.

Characteristics of the two compost sets and samples

Table A.1. Carbon and nitrogen content of samples.

Name	Carbon (%)	Nitrogen (%)
Compost 1st set	11.5	0.8
Compost 2nd set	25.7	1.3
PBS	59.7	0.02
PBG	60.1	0.02
PLA	52.5	0.03
90%PLA+15%PBG	53.3	0.01

Biogas production calculations

The evolved biogas of each sample was calculated daily by the difference in CO_2 production (in mg) of each sample compared to the daily average CO_2 contribution from blank controls as described by Equation A2.

$$Sample_{CO_2} = Reactor_{CO_2} - Blank_{CO_2} \quad \text{(A2)}$$

The sample mass and the percent organic carbon content was used to determine the carbon contributions to CO_2 for each sample. The dimensionless value of 44/12 was used to account for the carbon mass of the mass of CO_2 generated from each reactor for each day. The calculated evolved CO_2 for each sample was then used to calculate the daily absolute biodegradation according to Equation A3.

$$Absolute\ Biodegradation\ (\%) = \left(\frac{Sample_{CO_2}}{Sample\ Mass\ X\ Carbon\ Content\ (\%) X\ 44/12}\right) * 100 \quad \text{(A3)}$$

Table A.2. Cumulative CO_2, % composting biodegradation, and % relative Biodegradation of PBS and PBG[a]

Name	Cumulative CO_2 (g)			% Composting biodegradation			% Relative biodegradation		
	30 days	60 days	90 days	30 days	60 days	90 days	30 days	60 days	90 days
1. Blank	6.9	9.7	12.1	-	-	-	-	-	-
2. Cellulose	12.6	16.2	19.0	72.1	83.6	87.4	-	-	-
3. PBS	11.9	17.9	22.0	45.1	74.1	90.6	62.5	88.6	103.7
4. PBG	15.5	19.5	22.5	77.7	89.0	94.0	107.7	106.4	107.6

[a]The results of blank, cellulose, PBS and PBG are from three replicated reactors.

Modified Gompertz kinetics

To investigate the composting degradation kinetics of materials, the experimental data of carbon loss in aerobic biodegradation were modeled using a modified Gompertz equation (Equation A4) as shown in previous studies. Cumulative CO_2 evolution for all samples, including the cellulose positive control were fitting using a Modified Gompertz.

$$V_{nCO_2} = P_m \times \exp\left(-\exp\left[\frac{R_m \times e}{P_m}(\lambda - t) + 1\right]\right) \quad \text{(A4)}$$

Where V_{nCO_2} is the net cumulative CO_2 production from tested samples on the nth day (mL). P_m is the CO_2 production potential ($mL\ CO_2 \cdot g^{-1}\ sample$); R_m is the maximum specific CO_2 production rate (mL $CO_2 \cdot day^{-1}$); e is 2.718282; λ is the lag phase time (days); and t is the nth day of operation.

Structural Analysis and thermal properties of Poly(butylene glutarate)

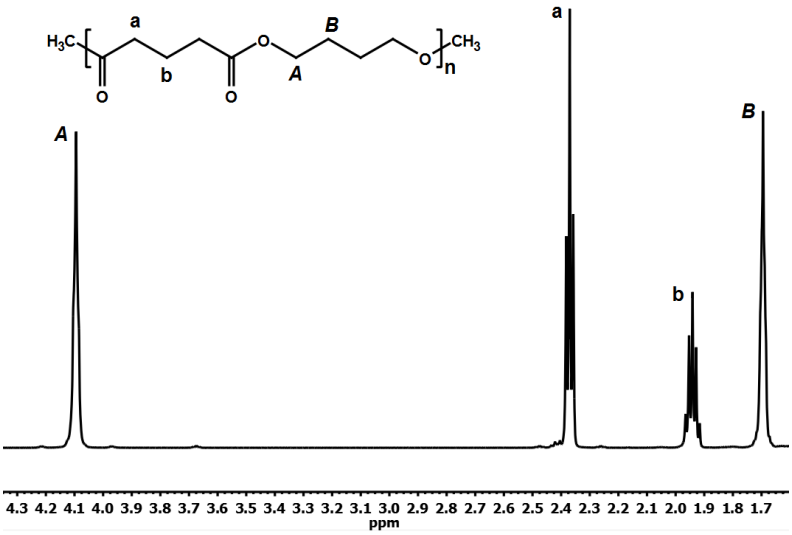

Figure A.2. ^{1}H NMR spectra of PBG, where *A* and *B* protons are the butylene sub-unit resonance signals and a and b protons are the glutarate sub-unit resonance signals.

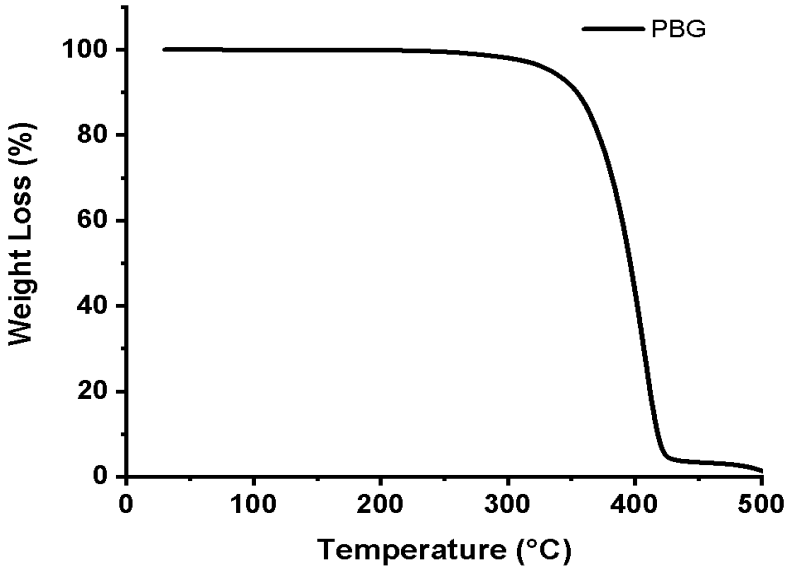

Figure A.3. TGA thermogram of PBG.

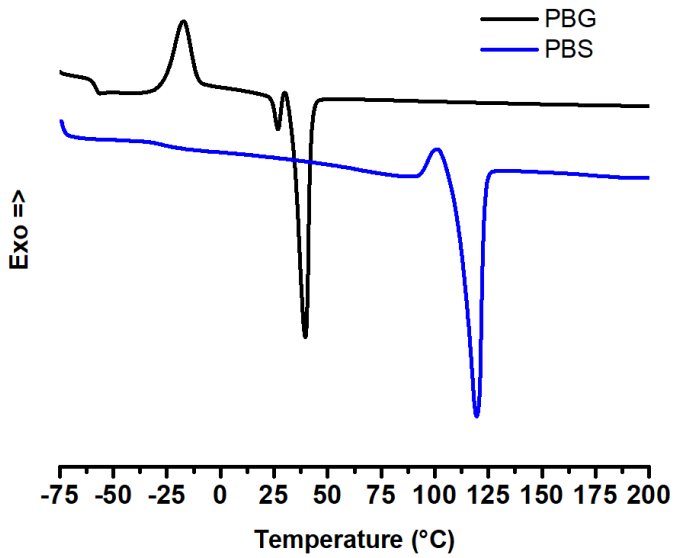

Figure A.4. DSC thermograms of the melting curve of PBG and PBS.

Thermal properties of PLA/PBG blends

Table A.3. DSC data of PLA/ PBG blends.

Sample	PLA/PBG content (wt%)	T_g (°C)	T_{cc} (°C)	ΔH_{cc} (J/g)	T_m (°C)	ΔH_m (J/g)	X_C % of PLA
1	100/0	57.5	105.9	37.9	169.0	40.8	3.1
2	99/1	57.2	99.9	35.0	168.4	38.9	4.3
3	97/3	56.8	96.8	34.1	168.4	38.7	5.1
4	95/5	56.7	95.7	31.8	168.2	37.3	6.3
5	90/10	55.4	94.6	29.4	168.0	35.1	6.8
6	85/15	54.9	94.3	27.2	167.7	33.0	7.5

Thermal history of PLA and PLA/PBG blends

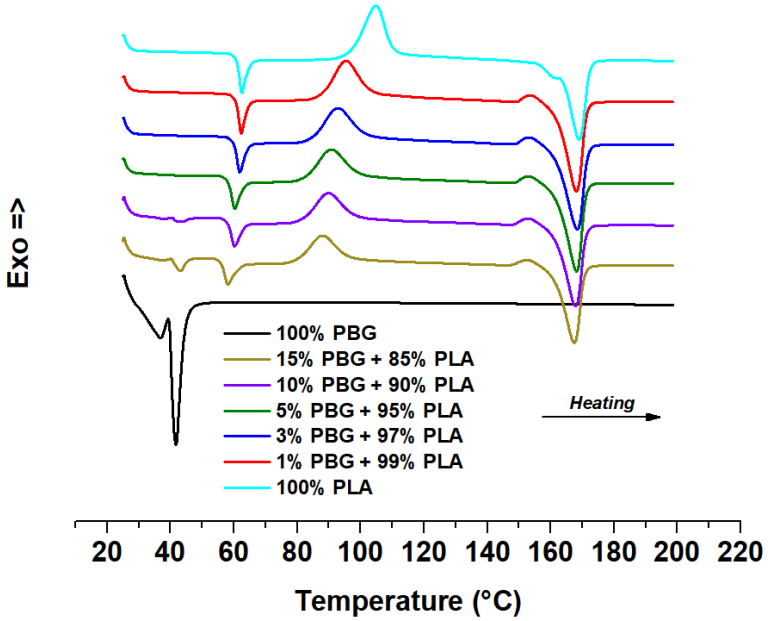

Figure A.5. DSC thermograms of first heating cycle of PLA and PLA/PBG blends.

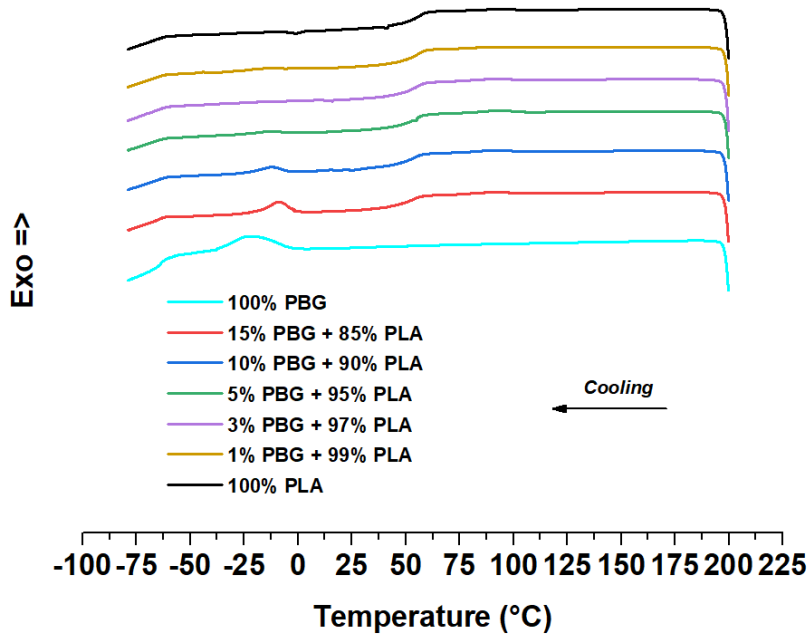

Figure A.6. DSC thermograms of first cooling cycle of PLA and PLA/PBG blends.

Viscoelastic behavior of PLA/PBG blends

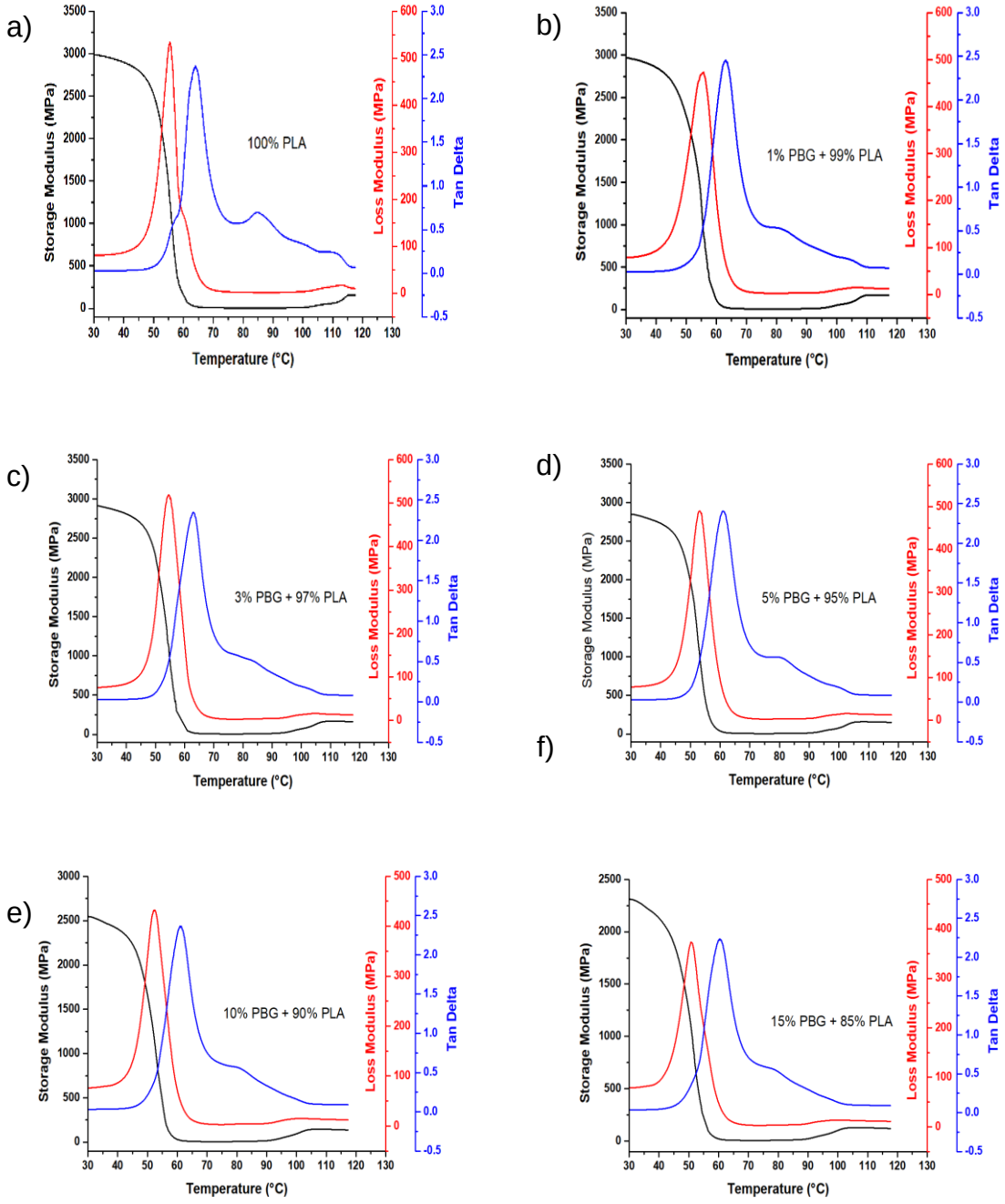

Figure A.7. Dynamic mechanical curves of storage modulus, loss modulus, and tan delta of (a) neat PLA, (b) 1% PBG + 99% PLA, (c) 3% PBG + 97% PLA, (d) 5% PBG + 95% PLA, (e) 10% PBG + 90% PLA, (f) 15% PBG + 85% PLA.

Miscibility of PLA/PBG blends

Table A.4. Surface characterizations of PLA and PLA/PBG blends.

Sample	PLA/PBG content (wt%)	Thickness (nm)	Mean Diameter (nm)	Mean Height (nm)
1	100/0	191.1	N/A	N/A
2	99/1	186.1	N/A	N/A
3	97/3	186.6	N/A	N/A
4	95/5	186.1	29.3	-1.3
5	90/10	186.3	43.2	-4.2
6	85/15	177.0	60.8	-7.8

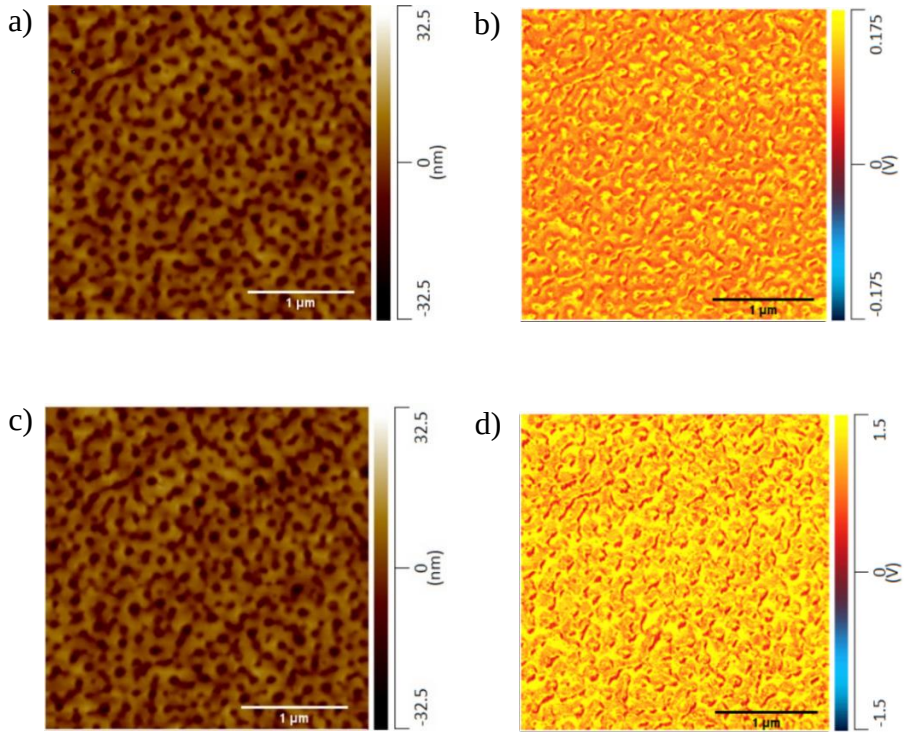

Figure A.8. AFM height images of 15% PBG + 85% PLA (a and c) with the corresponding AFM-IR images at 1730 cm^{-1} (b) and 1760 cm^{-1} (d).

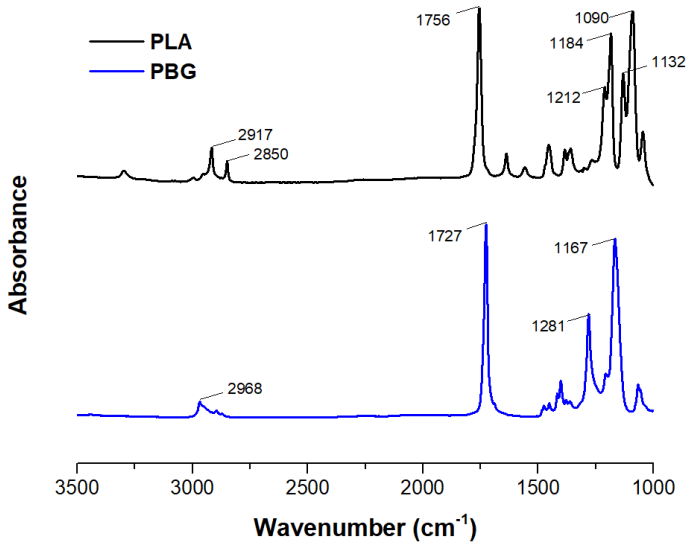

Figure A.9. FTIR spectra of PLA and PBG.

Tensile properties of PLA/PBG blends

Table A.5. Tensile data of PLA/ PBG blends and PLA/PBS blends.

Sample	Content (wt%)	Tensile Modulus (GPa)	Tensile strength (MPa)	Elongation at break (%)
1	PLA	3.4 ± 0.1	46.1 ± 1.6	2.5 ± 0.3
2	PLA + PBG (99:1)	3.0 ± 0.3	41.8 ± 0.8	3.2 ± 0.4
3	PLA + PBG (99:3)	2.9 ± 0.0	40.9 ± 1.2	10.1 ± 1.4
4	PLA + PBG (99:5)	2.9 ± 0.1	32.4 ± 2.9	14.9 ± 1.3
5	PLA + PBG (99:10)	2.6 ± 0.0	31.6 ± 0.1	18.9 ± 0.9
6	PLA + PBG (99:15)	2.3 ± 0.2	26.9 ± 1.4	21.6 ± 1.2
7	PLA + PBS (99:1)	3.0 ± 0.2	50.2 ± 2.1	3.9 ± 0.2
8	PLA + PBS (99:3)	2.7 ± 0.2	49.7 ± 2.0	4.9 ± 0.6
9	PLA + PBS (99:5)	2.7 ± 0.2	48.6 ± 1.8	5.0 ± 0.5
10	PLA + PBS (99:10)	2.6 ± 0.0	47.6 ± 1.0	7.9 ± 0.9
11	PLA + PBS (99:15)	2.3 ± 0.1	41.4 ± 4.7	13.2 ± 1.6

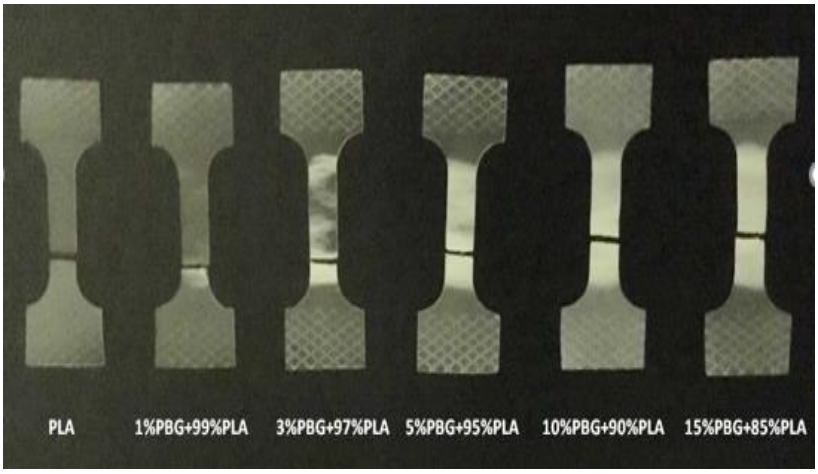

Figure A.10. Fractured tensile bars of PLA and PLA/PBG blends after stress-strain analysis.

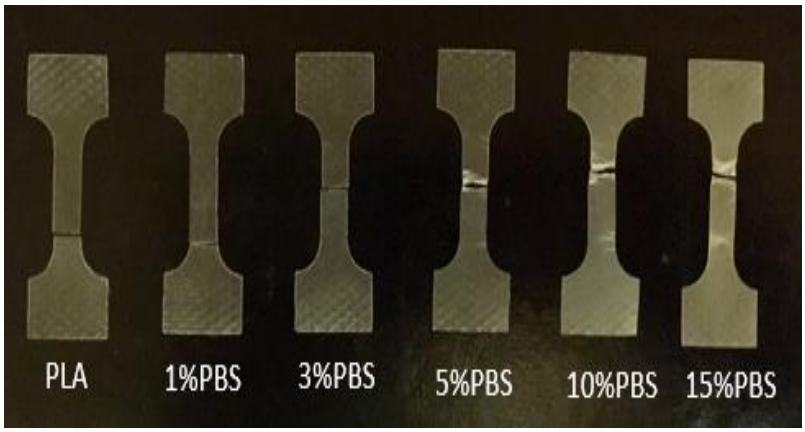

Figure A.11. Fractured tensile bars of PLA and PLA/PBS blends after stress-strain analysis.

Morphology of PLA/PBG blends

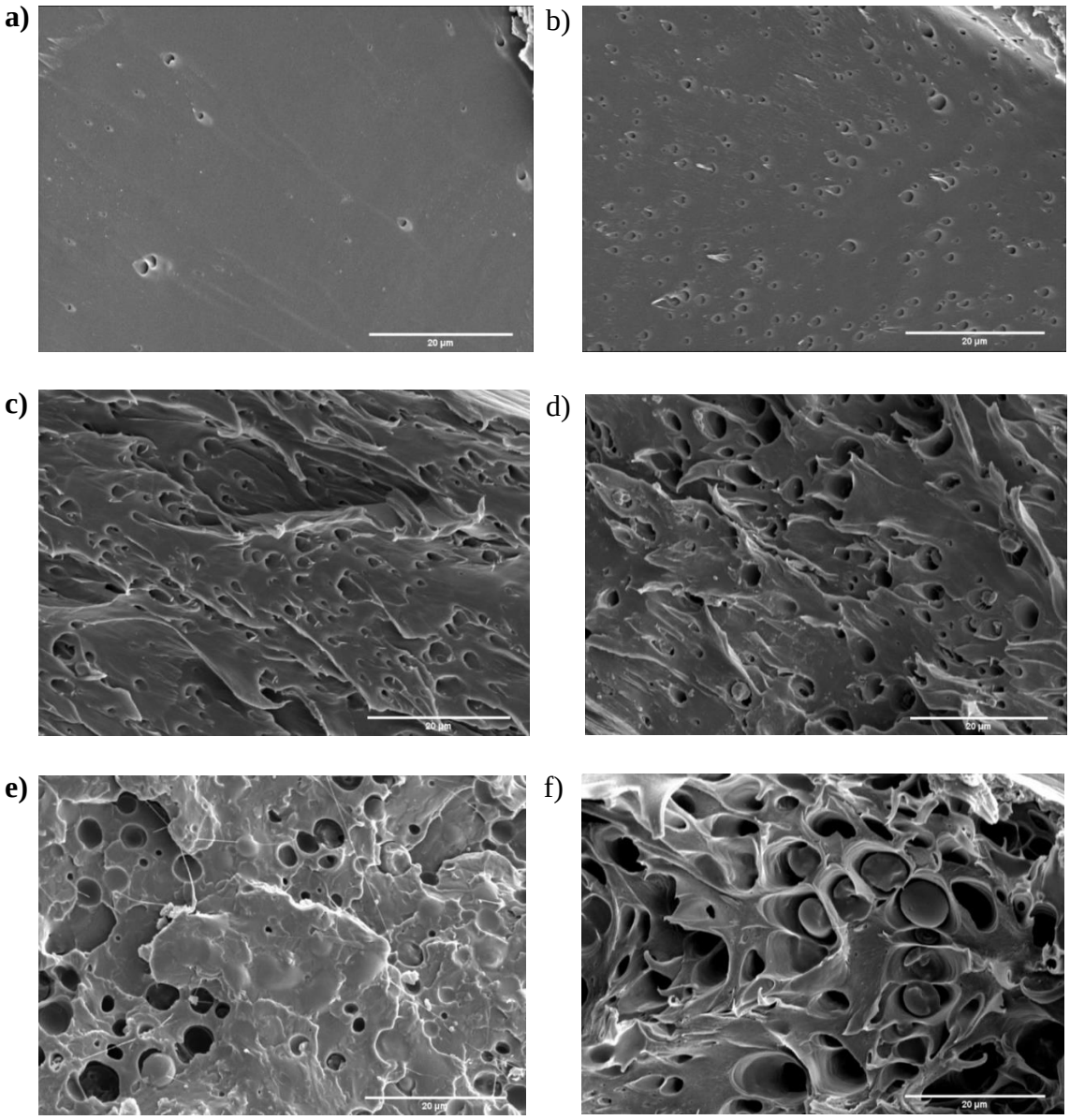

Figure A.12. SEM cross-section images of the fracture surface of tensile bars of PLA and PLA/PBG blends (a) neat PLA, (b) 1% PBG + 99% PLA, (c) 3% PBG + 97% PLA, (d) 5% PBG + 95% PLA, (e) 10% PBG + 90% PLA, (f) 15% PBG + 85% PLA.

APPENDIX B

Supporting Information for PHA/PBG blends

Rheological test

Viscosity was measured directly in the MiniLab. The backflow (recirculating) channel equipped with two pressure sensors allows to obtain the rheological information. Shear stress (τ) can be calculated form the pressure drop by using Equation B1.

$$\tau = \left(\frac{h}{2\Delta l}\right) * \Delta P \quad \text{(B1)}$$

Where: h is the depth of the flow channel (mm), Δl is the distance between the pressure sensors (mm), ΔP is the pressure drop (Pa).

By using the geometry of the backflow channel, the screw speed (n) and the calibration constant (c), the shear rate (γ) can be calculated as.

$$\gamma = \left(\frac{6}{w.h^2}\right) * c * n \quad \text{(B2)}$$

Where: w is the width of the flow channel (mm), c is equal to 8 x 10^{-7} (According to the manufacture)

The calculated τ and γ values were then used to calculate the viscosity (η) according to Equation B3.

$$\eta = \left(\frac{\tau}{\gamma}\right) \quad \text{(B3)}$$

Viscoelastic properties

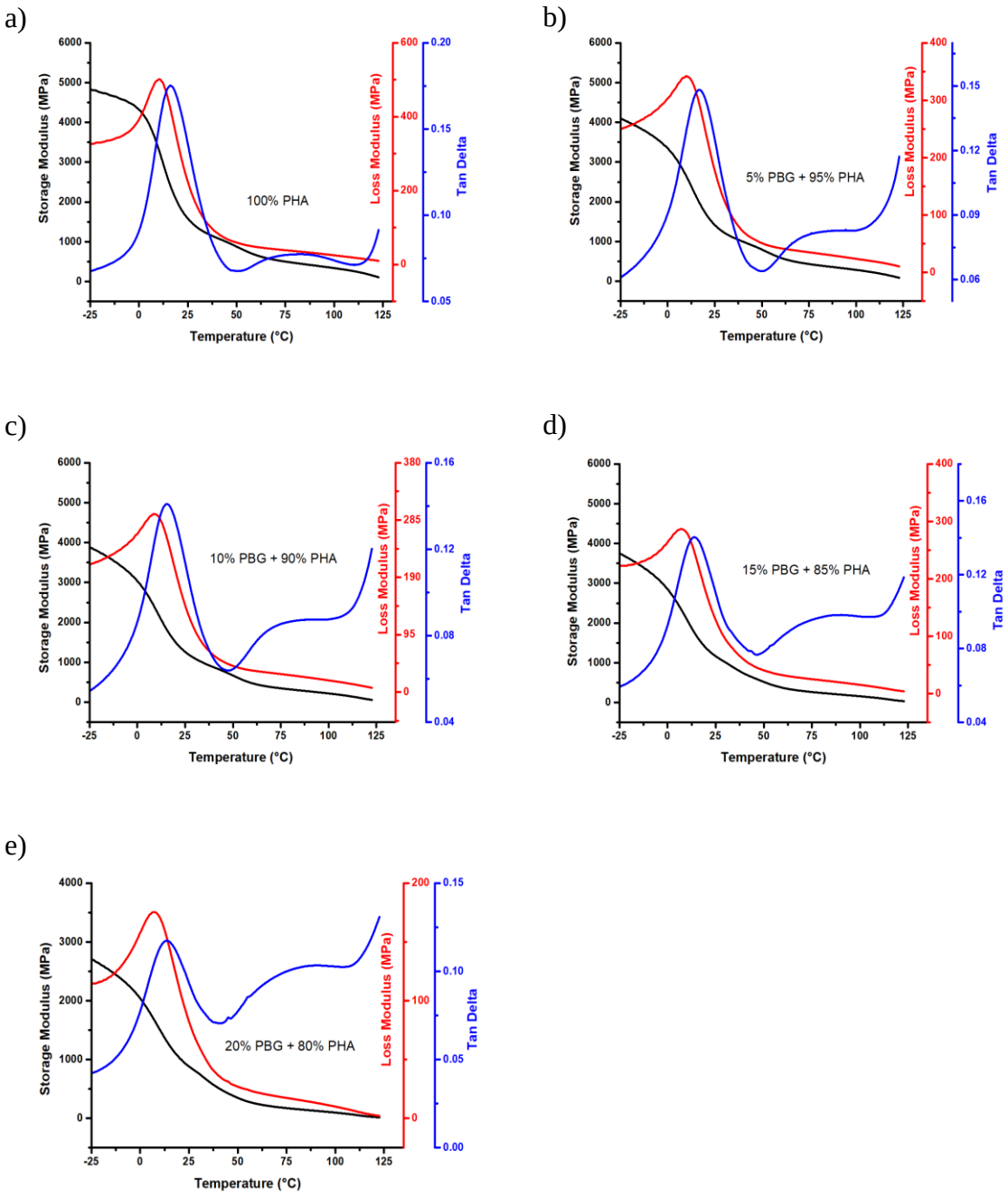

Figure B.1. Dynamic mechanical curves of storage modulus, loss modulus, and tan delta of (a) neat PLA, (b) 5% PBG + 95% PHA, (c) 10% PBG + 90% PHA, (d) 15% PBG + 85% PLA, (e) 20% PBG + 80% PHA.

Thermal properties

Table B.1. Glass transition temperatures (T_g), crystallization temperatures (T_c), and melting temperatures (T_m) of PHA/PBG blends.

Sample	T_g (°C)	T_c (°C)		T_m (°C)			
PHA	2.7		79.7			129.2	142.7
PHA + PBG (95:5)	2.2		87.5		37.2	131.4	143.8
PHA + PBG (90:10)	1.6		88.8		37.3	131.5	144.1
PHA + PBG (85:15)	1.0	-16.5	87.5	26.5	37.3	131.6	143.5
PHA + PBG (80:20)	0.5	-16.4	86.7	26.5	37.4	131.4	143.3

Phase morphology

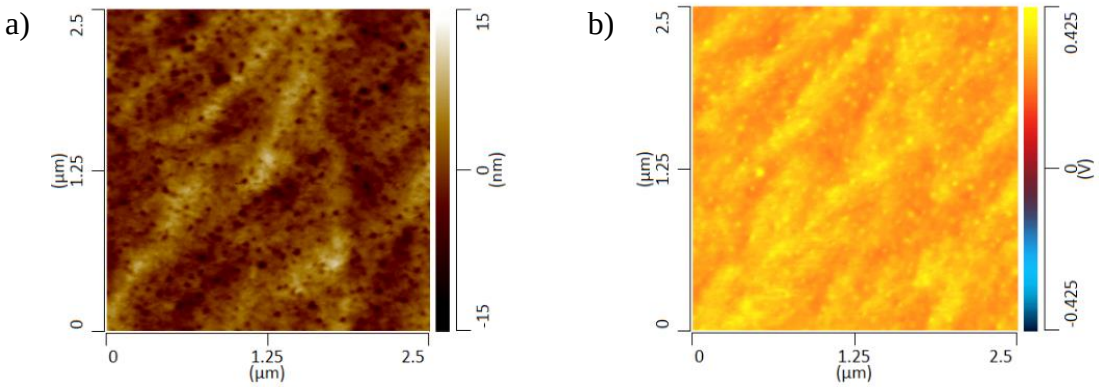

Figure B.2. AFM height images (a) of 15% PBG + 85% PHA with the corresponding AFM-IR images at 1730 cm^{-1} (b)

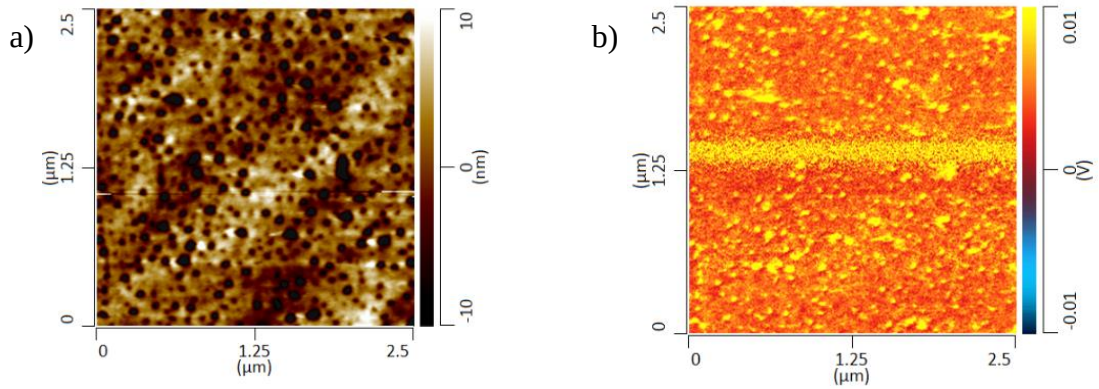

Figure B.3. AFM height images (a) of 20% PBG + 85% PHA with the corresponding AFM-IR images at 1170 cm^{-1} (b)

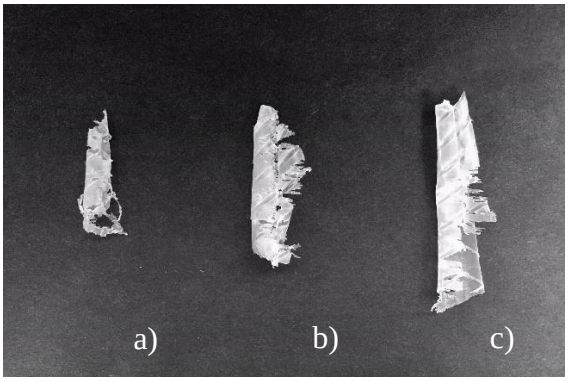

Figure B.4. Accumulation of films on the extruder wall during the extrusion of (a) 10% PBG + 90% PHA, (b) 15%PBG + 85% PHA, (c) 20% PBG + 80% PHA.

Tensile testing

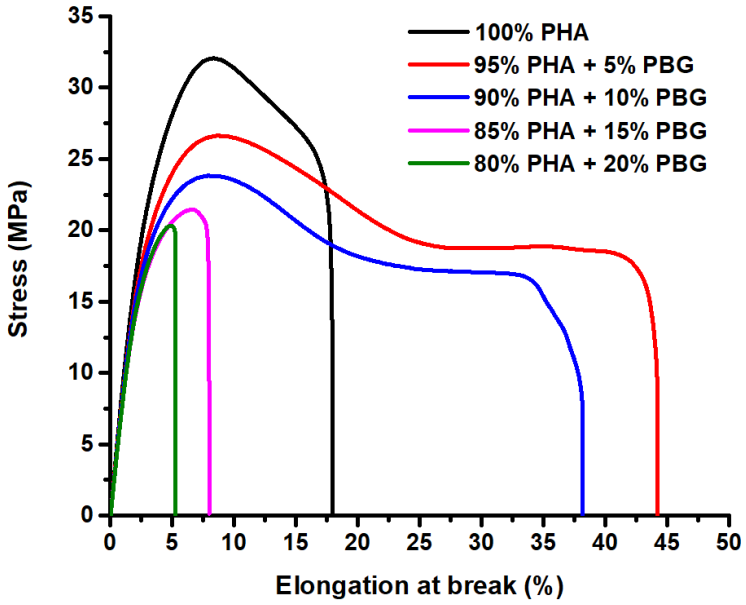

Figure B.5. Stress-strain curves for PHA/PBG blends.

Table B.2. Tensile data of PHA/ PBG blends.

Sample	Content (wt%)	Tensile Modulus (GPa)	Tensile strength (MPa)	Elongation at break (%)
1	PHA	0.9 ± 0.08	32.7 ± 0.6	17.8 ± 0.3
2	PHA + PBG (95:5)	0.7 ± 0.06	26.5 ± 1.6	45.4 ± 1.5
3	PHA + PBG (90:10)	0.6 ± 0.02	24.2 ± 0.3	39.6 ± 2.8
4	PHA + PBG (85:15)	0.6 ± 0.02	21.6 ± 0.6	7.7 ± 1.0
5	PHA + PBG (80:20)	0.6 ± 0.02	20.5 ± 0.4	5.3 ± 0.5

APPENDIX C

Supporting Information for PHA/PHB blends

Material characterizations

Table C.1. Characteristics of the neat PHBHx and PHB.

Characteristics	PHBHx	PHB
% Hx comonomer unit	5.6	0.07
T_c (°C)	80.0	121.5
T_m (°C)	130.3, 143.9	174.2
Enthalpy (J/g)	53.6	94.4
% Crystallinity	36.7	64.7
Weight average molecular weight, M_w (kg/mol)	1,253.0	1,436.5
Number average molecular weight, M_n (kg/mol)	902.6	866.0
Polydispersity index	1.4	1.7

Preparation method of compost

The compost was collected from industrial-scale compost facility located at the University of Georgia, Athens, GA. This compost was about 4-5 months old derived from composting the organic fraction of green waste, forest residue, food waste, and livestock manure. The temperature in the composting pile (50 cm depth) while collecting was 58°C. The collected compost was sieved using a 4.75 mm screen (Sieve No.4) to discard any large items such as stone, wood, and glass. The properties of fine and homogeneous

compost such as pH, volatiles and total solids were measured by pH probe and thermogravimetric analysis. Carbon and nitrogen content of the compost were measured using the method described in Kristen.[1]

Table C.2. Properties of compost.

Properties	Value
Total dry solid (%)	43.3
Volatile solid (%)	19.8
pH of compost	8.0
Total carbon amount	12.6
Total nitrogen amount	0.7
C/N ratio	18

Biogas production calculations

The evolved biogas of each sample was calculated daily by the difference in CO_2 production (in mg) of each sample compared to the daily average CO_2 contribution from blank controls as described by Equation C1.

$$Sample_{CO_2} = Reactor_{CO_2} - Blank_{CO_2} \quad \text{(C1)}$$

The sample mass and the percent organic carbon content was used to determine the carbon contributions to CO_2 for each sample. The dimensionless value of 44/12 was used to account for the carbon mass of the mass of CO_2 generated from each reactor for each day. The calculated evolved CO_2 for each sample was then used to calculate the daily absolute biodegradation according to Equation C2.

$$Absolute\ Biodegradation\ (\%) = \left(\frac{Sample_{CO_2}}{Sample\ Mass\ X\ Carbon\ Content\ (\%) X\ 44/12}\right) * 100 \qquad \text{(C2)}$$

The isothermal and non-isothermal crystallization kinetics

In both isothermal and non-isothermal crystallization experiment, crystallinity occurred during the cooling process from the polymer melt. The degree of crystallinity is related to the amount of heat flow which releases during the transition process from liquid to solid. Crystallization is an exothermic process which has often been recorded as a function of time or temperature by DSC. In the isothermal crystallization process, the crystallinity at time t can be expressed as relative crystallinity (X_t). This X_t value is calculated based on experimental data according to Equation C3 which explains the fractional area of crystallization exotherm normalized to the entire exotherm area.

$$X_t = \frac{\int_{t_0}^{t}\left(\frac{dH_c}{dt}\right)dt}{\int_{t_0}^{t\infty}\left(\frac{dH_c}{dt}\right)dt} = \frac{\int_{t_0}^{t}\left(\frac{dH_c}{dt}\right)dt}{\Delta H_c} \qquad \text{(C3)}$$

Where X_t is relative crystallinity at time t. dH_C/dt is the enthalpy measured by the DSC as a function of time. ΔH_C is the total enthalpy of crystallization process. t_0 and t_∞ are the onset and the end crystallization time. t is the time during crystallization process.

On the other hand, in the non-isothemal crystallization experiment, the crystallization ocurred at a set cooling rate and can be rewrited as Equation C4. The crystallinity at temperature T can be expressed as relative crystallinity (X_T).

$$X_T = \frac{\int_{T_0}^{T}\left(\frac{dH_c}{dT}\right)dT}{\int_{T_0}^{T\infty}\left(\frac{dH_c}{dT}\right)dT} = \frac{\int_{T_0}^{T}\left(\frac{dH_c}{dT}\right)dT}{\Delta H_c} \qquad \text{(C4)}$$

Where X_T is relative crystallinity at temperature T. dH_C/dT is the enthalpy mesured by the DSC as a function of temperature. T_0 and T_∞ are the onset and the end crystallization temperature. T is the temperture(s) during crystallization process. This relative crystallinity (X_T) as a function of temperature can be convert to relative crystallinity (X_t) as a function of time by using the following relationship:

$$t = \frac{T_0 - T}{\emptyset} \tag{C5}$$

Where ϕ is a cooling rate in °C /min.

The crystallization kinetics of polymer under isothermal and non-isothermal conditions can be well described by the Avrami equation (Equation C6). This equation has been derived for the specific description of primary crystallization occurred under constant temperature. Primary crystallization involves a constant nucleation rate and a linear growth of lamellae with time. It assumes that the development of X_t increases with increasing crystallization time. The Avrami equation is defined as.

$$1 - X_t = \exp(-kt^n) \tag{C6}$$

Where k is the overall crystallization rate constant involving both nucleation and growth rate of the crystals. n is the Avrami exponent describing the growth geometry of the crystals summarized in Table C.3.

Table C.3. Simplified Avrami exponent interpretation.

Avrami exponent	Growth geometry
1<n<2	One-dimensional, rod-like
2<n<3	Two-dimensional, disc-like
3<n<4	Three-dimensional, spherulitic-like

Since no polymers undergo complete crystallization to achieved 100% crystallinity, Muller et al.[2] modified the Avrami equation by describing as a two-phase model and considered the densities of the crystalline and amorphous phases which can be expressed by Equation C7.

$$1 - V_c = \exp(-kt^n) \tag{C7}$$

Where V_c is the relative volumetric fraction and can be calculated as.

$$V_c = \frac{X_t}{X_t + (\frac{\rho_c}{\rho_a})(1 - X_t)} \tag{C8}$$

Where ρ_c is the fully crystalline polymer density and ρ_a is the fully amorphous polymer density. The crystalline PHB has a density of 1.25 g/mL and the amorphous PHB has a density of 1.17 g/mL.[3]

By applying logarithmic properties to both sides and rearranging of equation C7, the linear from of the Modified Avrami equation can be obtained as follows.

$$\log(-\ln(1 - V_c)) = \log k + n \log t \tag{C9}$$

From the slope and intercept of this linear equation, the value of *n* and *k* and can be determined, respectively. Another important parameter is the crystallization half-time ($t_{1/2}$) which is the time at which the crystallization process reaches 50% completion. The value of $t_{1/2}$ can be calculated from n and k using Equation C10.

$$t_{1/2} = \left(\frac{\ln 2}{k}\right)^{1/n} \tag{C10}$$

Effect of isothermal treatment on crystallization behavior of PHBHx/PHB

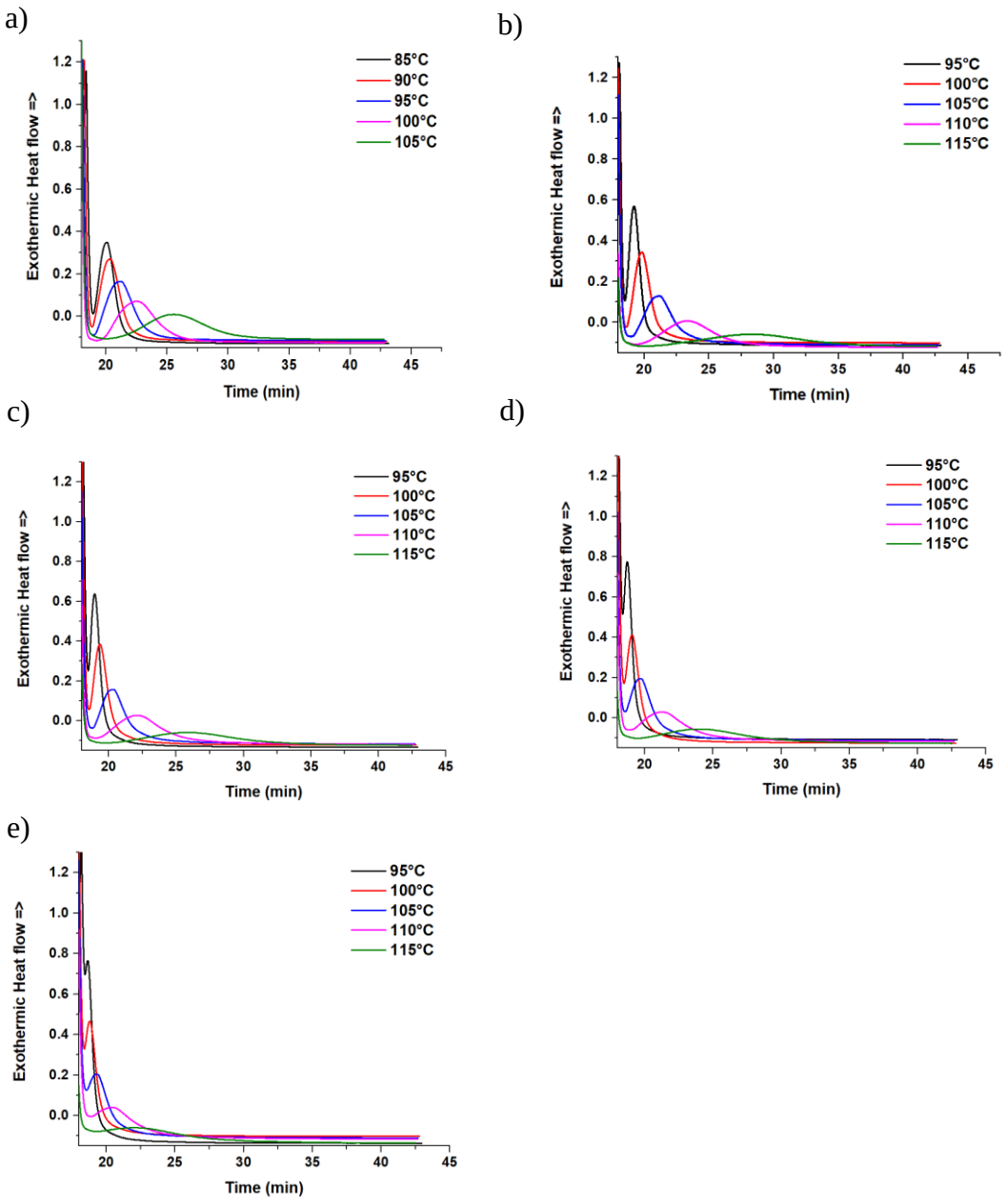

Figure C.1. Isothermal DSC cooling curves at various crystallization temperatures (a) 100% PHBHx, (b) 1% PHB + 99% PHBHx, (c) 3% PHB + 97% PHBHx, (d) 5%PHB + 95% PHBHx, (e) 10% PHB + 90% PHBHx.

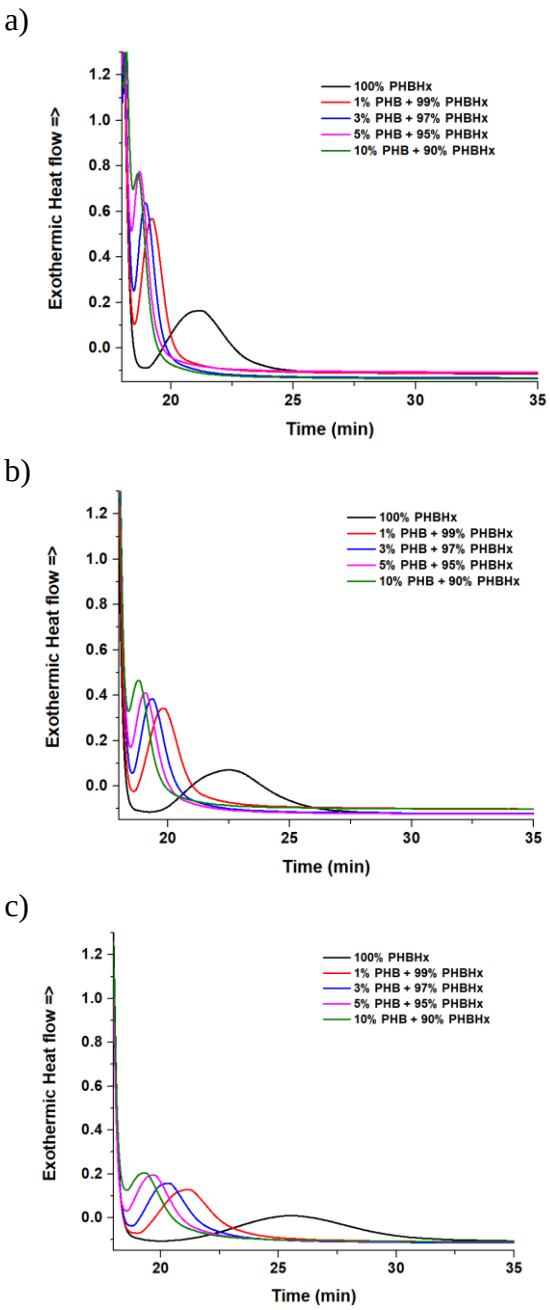

Figure C.2. Isothermal DSC cooling curves at various concentrations of PHB (a) crystallization temperature at 95 °C, (b) crystallization temperature at 100 °C, (c) crystallization temperature at 105 °C.

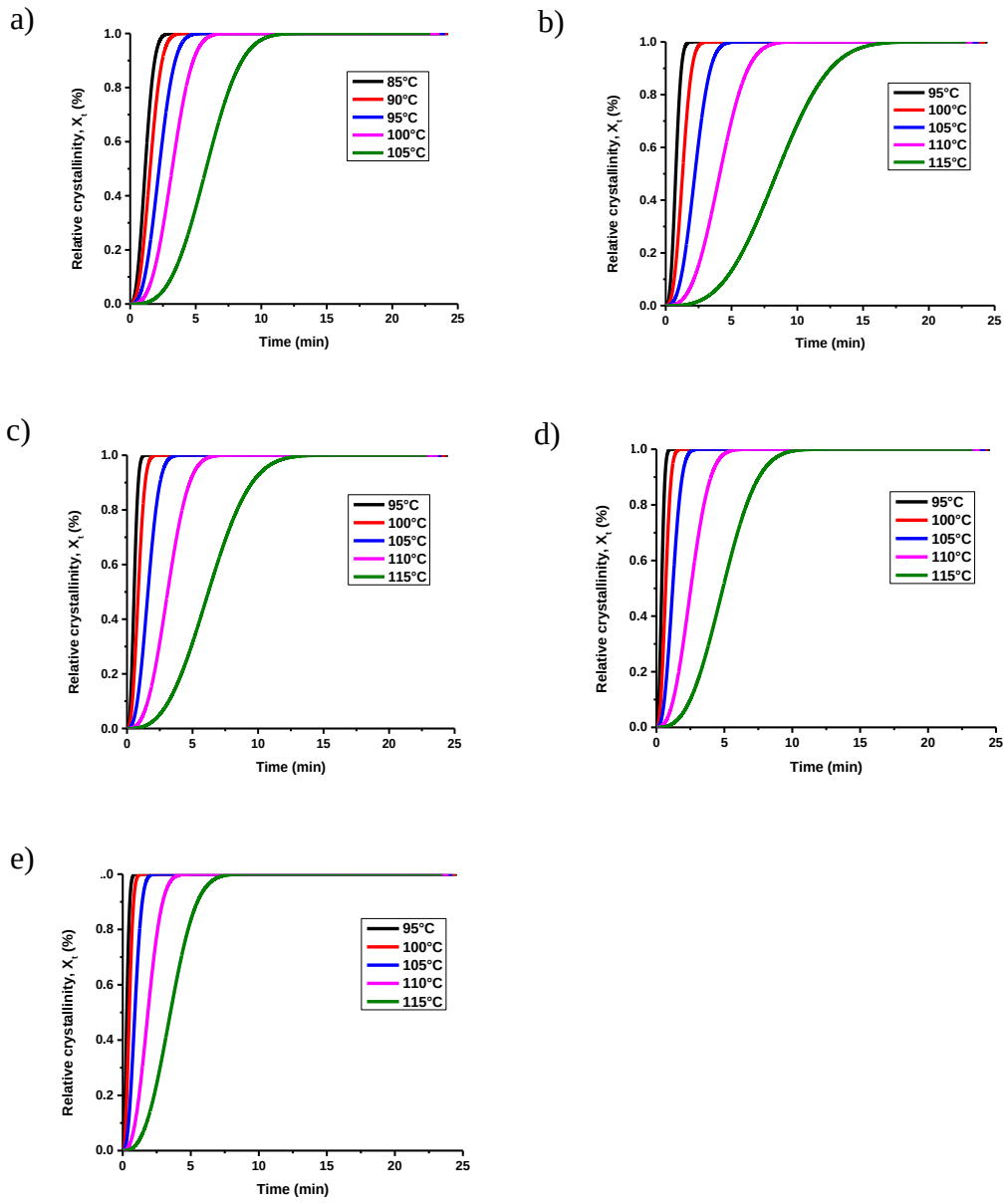

Figure C.3. Relative Crystallinity (X_t) versus crystallization time (t) curves of different crystallization temperature and content of PHB (a) 100% PHBHx, (b) 1% PHB + 99% PHBHx, (c) 3% PHB + 97% PHBHx, (d) 5%PHB + 95% PHBHxx, (e) 10% PHB + 90% PHBHx.

Effect of non-isothermal treatment on crystallization behavior of PHBHx/PHB

Table C.4. Crystallization Temperature at different concentration PHB and cooling rate.

Names	Crystallization temperature, T_C (°C) at cooling rate of				
	1°C/min	5°C/min	10°C/min	20°C/min	40°C/min
100% PHBHx	105.4	89.9	80.1	67.2	52.8
1% PHB+ 99% PHBHx	112.0	98.1	91.2	82.5	71.7
3% PHB+ 97% PHBHx	114.2	100.3	93.6	86.1	74.4
5% PHB+ 95% PHBHx	116.2	101.5	95.7	87.9	78.4
10% PHB+ 90% PHBHx	119.0	103.8	98.1	90.8	82.2

Table C.5. Kinetics parameters obtained from non-isothermal crystallization experiment and Avrami analysis of PHBHx and PHBHx/PHB.

Sample	Cooling rate, ϕ (°C/min)	n	k (min^{-n})	ln k_c (min^{-n})	$t_{1/2}$ (min)
100% PHBHx	1	4.5	6.3×10^{-6}	-12.0	12.9
	5	4.4	4.8×10^{-3}	-1.1	3.1
	10	4.1	5.9×10^{-2}	-0.3	1.8
	20	3.1	3.9×10^{-1}	-0.05	1.2
	40	2.8	1.4	0.01	0.8
1% PHB+ 99% PHBHx	1	4.7	2.1×10^{-6}	-13.1	14.8
	5	4.5	5.9×10^{-3}	-1.0	2.9
	10	4.2	1.5×10^{-1}	-0.2	1.5
	20	3.9	1.3	0.01	0.9
	40	3.7	5.3	0.04	0.6
3% PHB+ 97% PHBHx	1	4.6	8.5×10^{-7}	-14.0	18.8
	5	4.4	5.1×10^{-3}	-1.1	3.1
	10	3.9	1.2×10^{-1}	-0.2	1.6
	20	3.8	1.3	0.01	0.9
	40	3.5	5.4	0.04	0.6
5% PHB+ 95% PHBHx	1	4.5	8.2×10^{-7}	-14.0	21.3
	5	4.0	3.9×10^{-3}	-1.1	3.6
	10	3.8	9.2×10^{-2}	-0.2	1.7
	20	3.6	9.8×10^{-1}	-0.001	0.9
	40	3.5	5.2	0.04	0.7
10% PHB+ 90% PHBHx	1	4.2	6.9×10^{-7}	-14.2	27.6
	5	4.0	3.6×10^{-3}	-1.1	3.7
	10	3.4	1.1×10^{-1}	-0.2	1.7
	20	3.4	6.9×10^{-1}	-0.02	1.0
	40	3.3	4.8	0.04	0.6

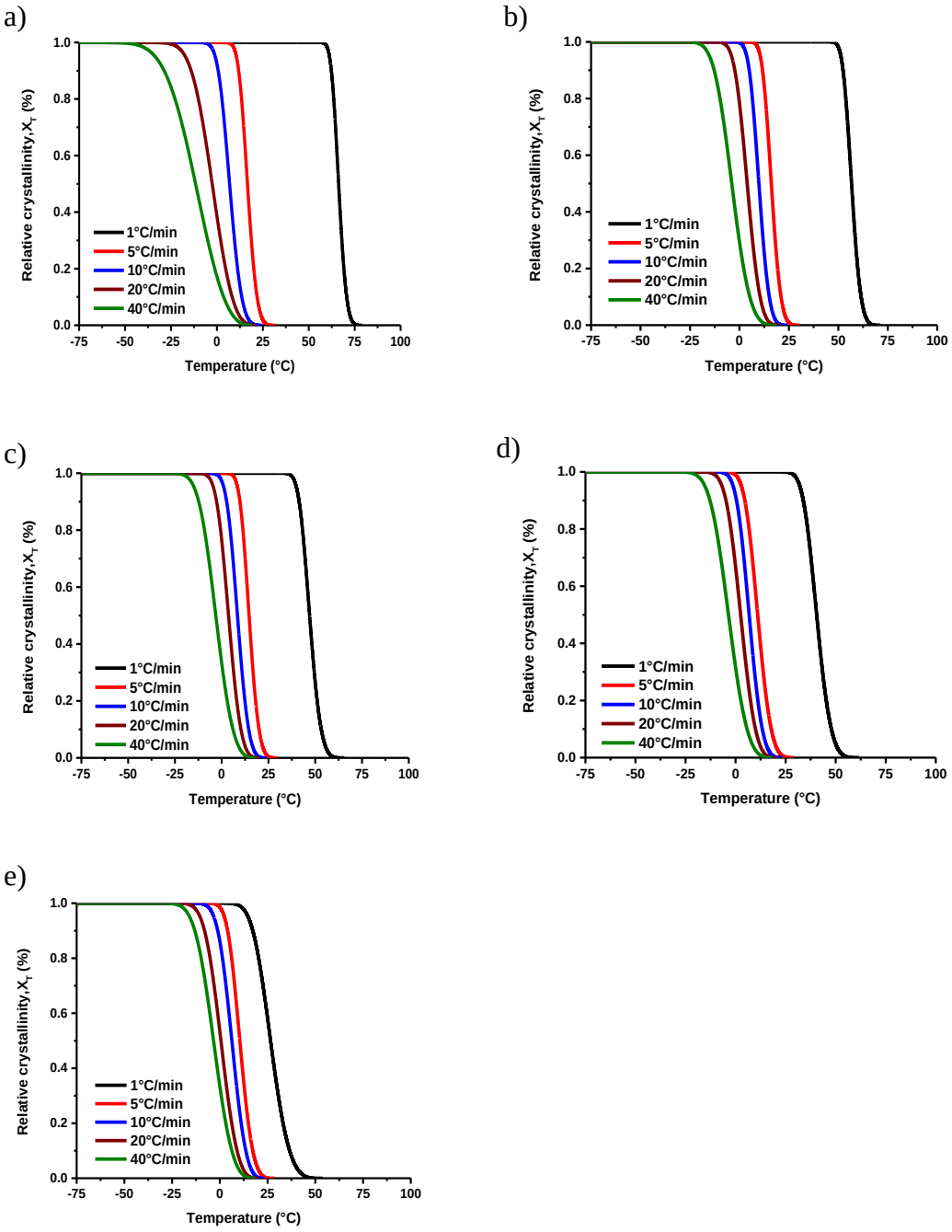

Figure C.4. Relative Crystallinity, X_T versus crystallization temperature, T curves of different cooling rate and content of PHB (a) 100% PHBHx, (b) 1% PHB + 99% PHBHx, (c) 3% PHB + 97% PHBHx, (d) 5%PHB + 95% PHBHxx, (e) 10% PHB + 90% PHBHx.

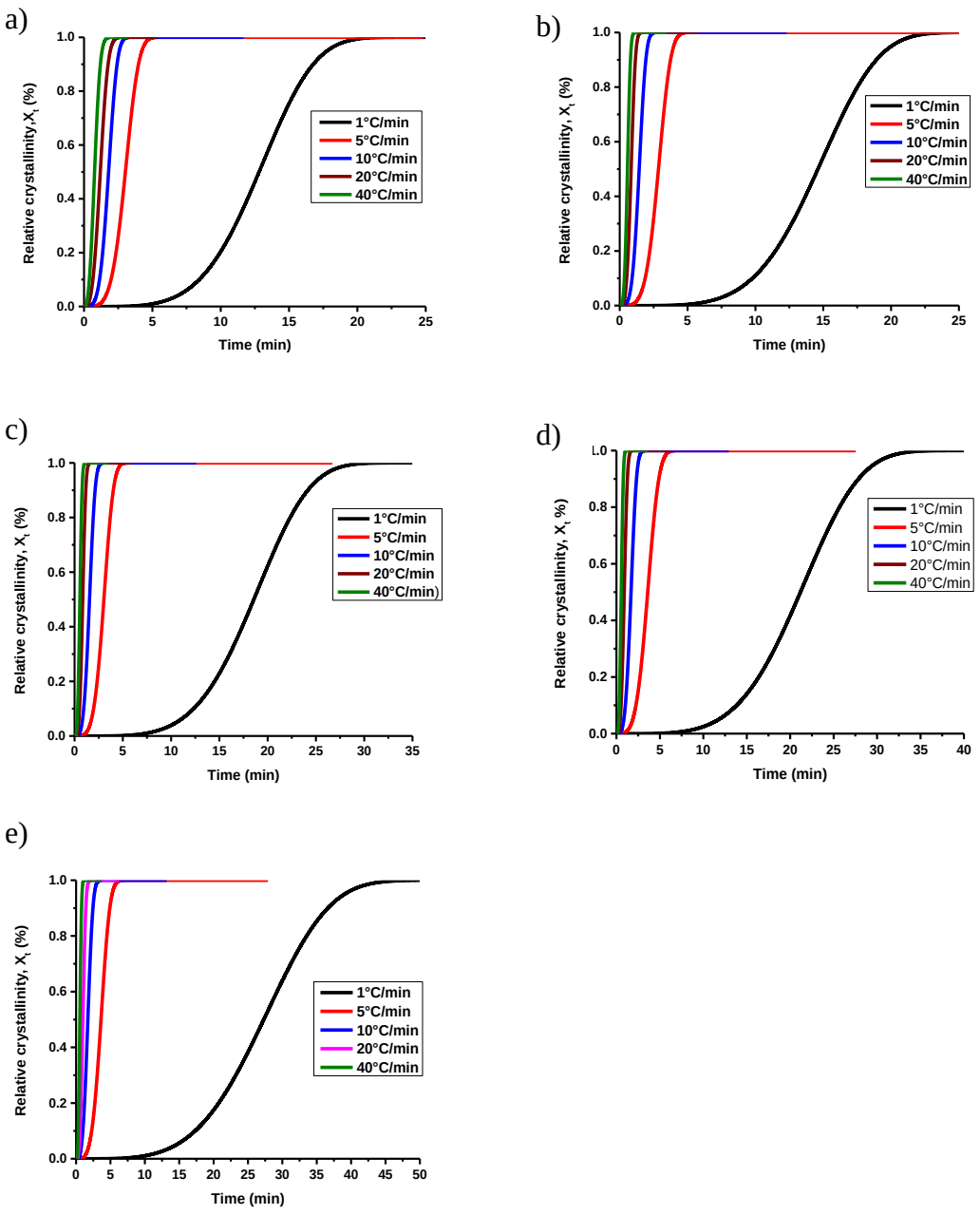

Figure C.5. Relative Crystallinity, X_t versus crystallization time, t curves of different cooling rate and content of PHB (a) 100% PHBHx, (b) 1% PHB + 99% PHBHx, (c) 3% PHB + 97% PHBHx, (d) 5%PHB + 95% PHBHxx, (e) 10% PHB + 90% PHBHx.

Modulated Differential Scanning Calorimetry (MDSC)

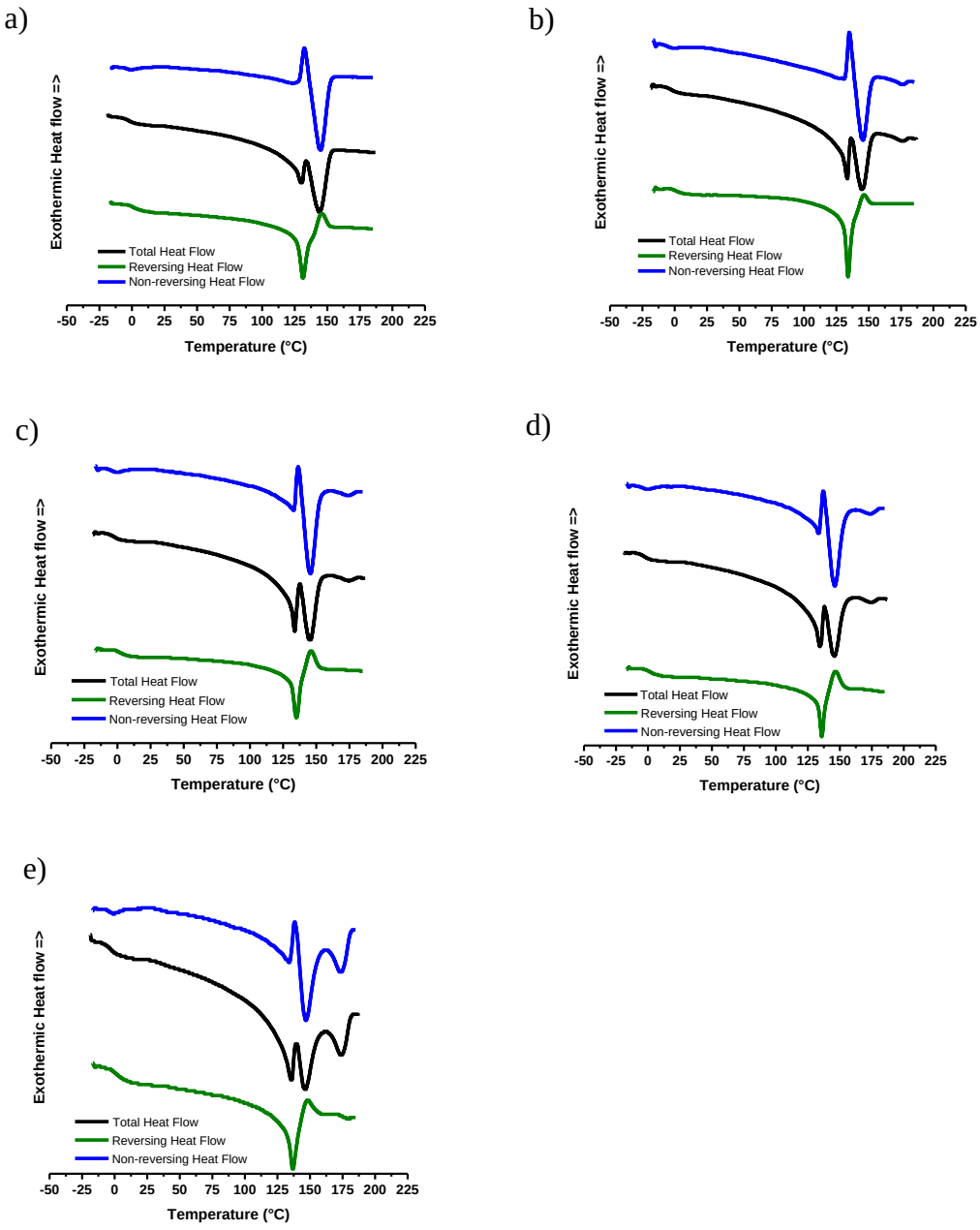

Figure C.6. MDSC thermograms of (a) 100% PHBHx, (b) 1% PHB + 99% PHBHx, (c) 3% PHB + 97% PHBHx, (d) 5%PHB + 95% PHBHxx, (e) 10% PHB + 90% PHBHx.

Determination of crystallinity

The crystallinity of PHBHx (X_C%) was calculated from DSC curves using the following equation:

$$X_C\% = (\Delta H_m / \Delta H^0_m) \times 100 \quad \text{(C11)}$$

where ΔH_m was the enthalpy of melting, ΔH^0_m was the melting enthalpy of 100% crystalline PHB, which is 146 J/g.[4]

Table C.6. Values of T_1 and T_2 during the second heating DSC of the neat PHBHx and PHBHx/PHB.

Cooling rate (°C/min)	100%PHBHx		1% PHB + 99% PHBHx		3% PHB + 97% PHBHx		5% PHB + 95% PHBHx		10% PHB + 90% PHBHx	
	T_1(°C)	T_2(°C)	T_1(°C)	T_2(°C)	T_1(°C)	T_2(°C)	T_1(°C)	T_2(°C)	T_1(°C)	T_2(°C)
1	138.5	148.5	141.7	150.7	142.9	152.7	143.8	155.1	144.4	158.9
5	132.9	145.0	135.8	146.2	137.1	146.9	137.8	147.7	139.0	149.4
10	130.3	143.9	133.9	145.0	135.9	146.3	136.3	146.7	136.4	147.2
20	127.5	143.5	131.8	144.5	133.3	145.1	134.5	145.9	135.1	146.1
40	124.5	143.1	128.8	143.4	131.6	144.7	132.0	144.9	132.6	145.3

Table C.7. Values of ΔH_m during the second heating DSC of the neat PHBHx and PHBHx/PHB.

Cooling rate (°C/min)	Enthalpy (J/g)				
	100% PHBHx	1% PHB + 99% PHBHx	3% PHB + 97% PHBHx	5% PHB + 95% PHBHx	10% PHB + 90% PHBHx
1	61.4	61.4	62.6	63.1	64.5
5	55.6	55.8	60.6	61.1	64.4
10	53.6	54.4	55.8	59.0	61.6
20	50.0	53.0	54.6	55.6	60.9
40	18.8	49.6	53.1	54.7	58.1

Table C.8. Values of % crystallinity during the second heating DSC of the neat PHBHx and PHBHx/PHB.

Cooling rate (°C/min)	% Crystallinity				
	100% PHBHx	1% PHB + 99% PHBHx	3% PHB + 97% PHBHx	5% PHB + 95% PHBHx	10% PHB + 90% PHBHx
1	42.1	42.1	42.9	43.2	44.2
5	38.1	38.2	41.5	41.8	44.1
10	36.7	37.3	38.2	40.4	42.2
20	34.2	36.3	37.4	38.1	41.7
40	12.9	34.0	36.4	37.5	39.8

Crystal morphology observation by POM

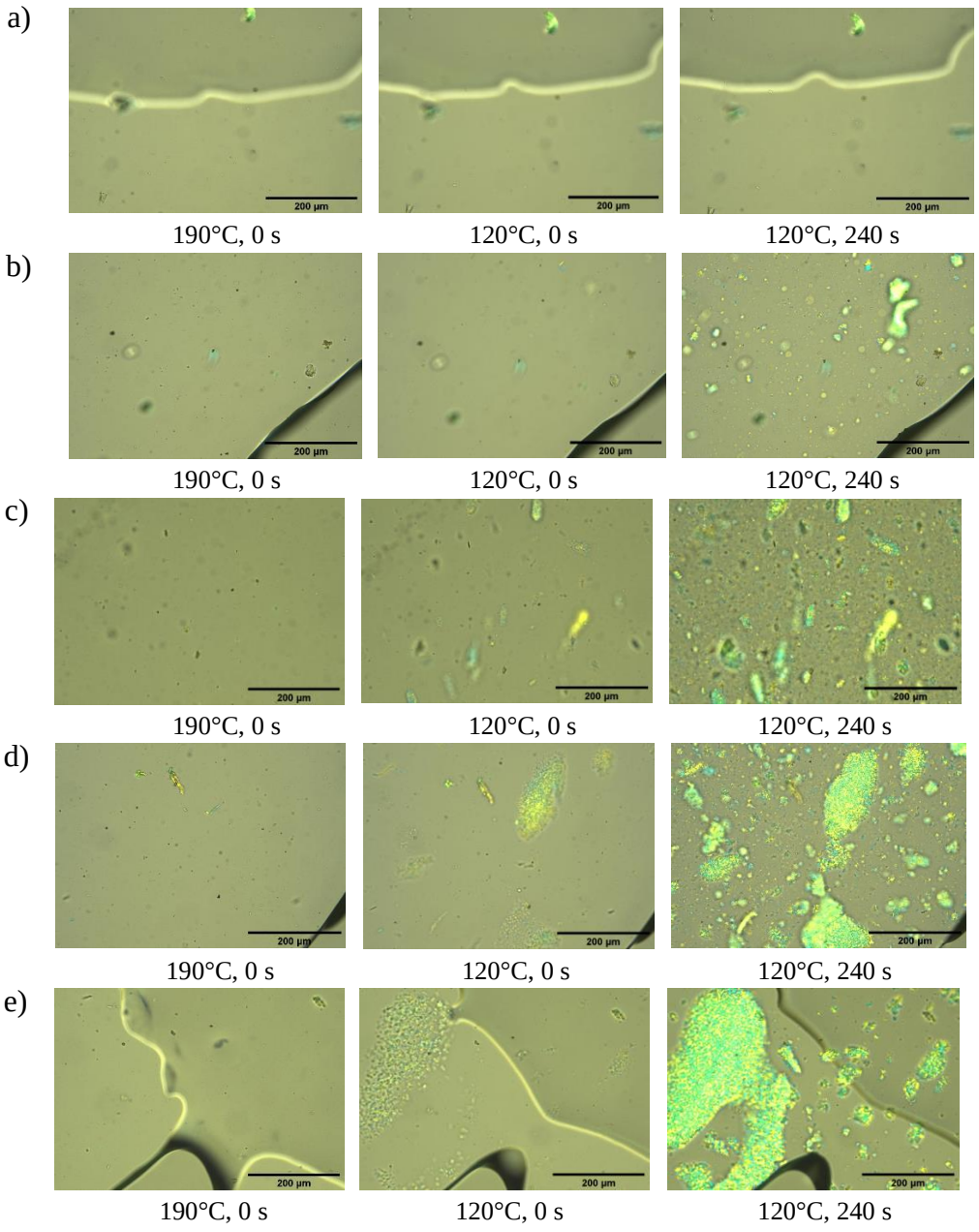

Figure C.7. POM images of PHBHx/PHB at various PHB content, isothermal crystallized at 120°C after melting at 190°C for 1 min. (a) 100% PHBHx, (b) 1% PHB+ 99% PHBHx, (c) 3% PHB+ 97% PHBHx, (d) 5% PHB+ 95% PHBHx, (e) 10% PHB+ 90% PHBHx.

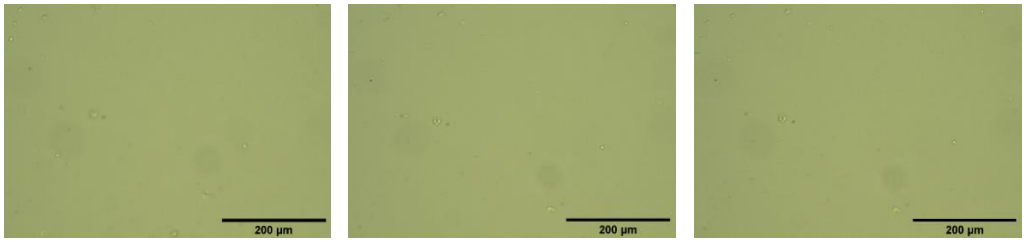

200°C, 0 s 120°C, 0 s 120°C, 300 s

Figure C.8. POM images of 10% PHB+ 90% PHBHx, isothermal crystallized at 120°C after melting at 200°C for 1 min.

Spherulitic Morphology observation by AFM

Table C.9. Film thickness of PHBHx/PHB at various PHB content.

Samples	Thickness (nm)
100% PHBHx	183.6
1% PHB+ 99% PHBHx	156.4
3% PHB+ 97% PHBHx	169.2
5% PHB+ 95% PHBHx	167.8
10% PHB+ 90% PHBHx	148.9

References

1. Kirsten, W. J., Automatic Methods for the Simultaneous Determination of Carbon, Hydrogen, Nitrogen, and Sulfur, and for Sulfur Alone in Organic and Inorganic materials. *Analytical Chemistry* **1979,** *51* (8), 1173-1179.

2. Lorenzo, A. T.; Arnal, M. L.; Albuerne, J.; Müller, A. J., DSC isothermal polymer crystallization kinetics measurements and the use of the Avrami equation to fit the data: Guidelines to avoid common problems. *Polym. Test.* **2007,** *26* (2), 222-231.

3. Martin, D. P.; Gerngross, T. U. In *Aspects of PHB granule formation in vitro*, 1996 International Symposium on Bacterial Polyhydroxyalkanoates, NRC Research Press: Ottawa: 1997; pp 28-35.

4. Wei, L.; McDonald, A. G., Thermophysical properties of bacterial poly(3-hydroxybutyrate): Characterized by TMA, DSC, and TMDSC. *J. Appl. Polym. Sci.* **2015,** *132* (34), 42412.